R/V METEOR

CRUISE REPORT M67/1

CHILE-MARGIN-SURVEY

Talcahuano (Chile) – Balboa (Panama)
20 February - 13 March 2006

Edited by:
Wilhelm Weinrebe and Silke Schenck
with contributions of cruise participants

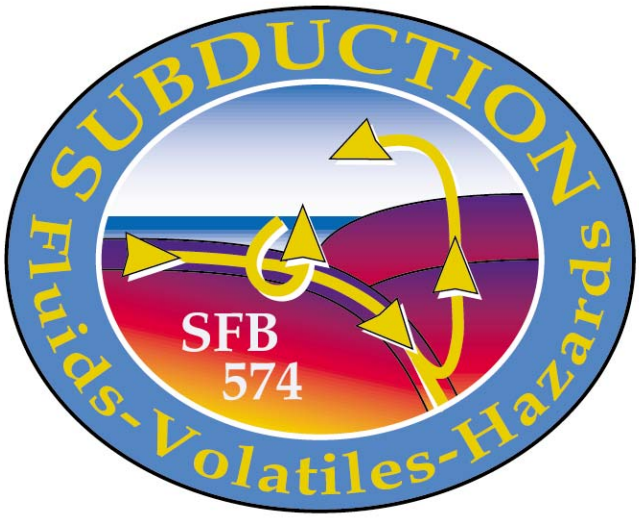

Table of Contents

1. Summary

Cruise M67/1 of RV METEOR was undertaken to gain a better understanding of the relationship between active tectonic processes and fluid venting at convergent continental margins. The role of volatiles and fluids in subduction zones is of great interest as it has major influence on short-term and long-term climate change and on the geochemical evolution of hydrosphere and atmosphere, and it may constitute a major trigger mechanism for natural hazards. The transport of volatiles and fluids through the subduction zone is influenced by tectonic processes, which, again, are modified by fluids and volatiles.

Active tectonic processes dominate the accretionary Chilean continental margin between 33°S and 37°S, particularly on the incoming oceanic plate and the lower and middle continental slope. Tectonic processes shape the morphology of the ocean floor. The morphology can be mapped by bathymetric measurements. The focus of cruise M67/1 was therefore on conducting a detailed bathymetric survey of the continental margin of the area to reveal a high-resolution image of the morphology. In addition, the results of this survey will constitute an essential prerequisite for any further investigations. They may also help in finding manifestations of fluid venting on the ocean floor. Possible venting sites were sampled during the cruise using a gravity corer to reveal indications of active fluid expulsion.

2. Objectives of the Cruise and Current State of Investigation

2.1 Objectives of Cruise M67/1

At subduction zones material is transferred intensively between the lithosphere and the asthenosphere as well as between the lithosphere, the hydrosphere and the atmosphere. The transfer and exchange of volatiles and fluids between these regimes has been in the focus of research in the recent years. Sediments have been identified as a major player in material transfer. Pelagic and hemipelagic sediments on the oceanic plate as well as terrigeneous sediments on the continental margin carry large amounts of volatiles and fluids. Of key interest is the question of what happens to the sediments in the subduction zone. Tectonic processes control if and how sediments are subducted. At the same time, tectonic processes are influenced by volatiles released from sediments. These complex interactions are not yet fully understood. However, they have fundamental implications on the climatic variability on different time scales. The geochemical development of the hydrosphere and atmosphere may act as a trigger for natural disasters. Thus, they are of fundamental scientific and economic importance. A variety of factors control the complex interacting system. In order to understand which factors are relevant and how they act it is important to study subduction zones in different settings. A key difference between ocean-continent margins is whether sediments are accreted or subducted. The first leads to growing accretionary wedges of off-scraped sediments. The latter may lead not only to the complete subduction of sediments but to erosion of the upper plate resulting in shortening and subsidence as can be found along the Central American margin.

The convergent continental margin of Chile display several various segments with different tectonic characteristics. The northern part is clearly dominated by subduction erosion. The central part around 33°S is controlled by the subduction of the Juan Fernandez Ridge. The area south of 33°S is predominantly accretionary, however, the accretionary prisms are quite small in many areas. Seismic images indicate that in the region between 36°S and 40°S a subduction channel is well developed, which transports most of the sediments in the trench with the downgoing plate. Within the CONDOR, SPOC and TIPTEQ projects large areas of the Chilean continental margin have been bathymetrically mapped. This data displays the different segments quite well. Yet, a major part of the margin between 36°S and 33°S has not been mapped before. To survey this area was the main objective of the cruise M67/1.

Bathymetric surveys reveal the morphology of the continental margin and yield information on tectonic processes shaping the morphology. In particular, the following topics are addressed by the mapping survey of M67/1:

- the structure of the oceanic plate before subduction: pattern, size, directions of the horst-and-graben structures created by the bending of the downgoing oceanic lithosphere
- width and sediment infill in the trench
- structure of the central turbidite channel in the trench
- size and structure of the accretionary wedge
- shape and size of the small ridges close to the deformation front
- faults as possible pathways for uprising fluids
- canyons on the upper and middle slope, deposition of terrigeneous sediments into the trench
- manifestations of fluid venting on the continental slope
- mass-wasting structures along the margin

2.2 Tectonic Domains along the Chile Convergent Margin

Ranero, C.R. and Weinrebe, W.

The Chile convergent margin is ideal to study, along a single plate boundary, the factors that govern the interplay between tectonic and fluid flow processes at convergent margins. The Chile subduction zone spans more than 3500 km providing a continuum of tectonic settings from the end-member sector dominated by long-term subduction erosion to accretionary sectors with large accretionary prism (>60 km).

At large scale, the topography of the Chile trench is divided in segments by the subduction of two large positive topography features of the oceanic plate: the Chile Rise, an active spreading centre, and the Juan Fernández Ridge formed by hot spot activity. In addition, the extreme climatic change from the Atacama Desert north of ~26°S, to the glacially influenced (on the tens of thousands of years average) southern latitudes, south of ~42°S, produces a dramatic variability in the amount of terrigenous sediment supplied to the trench from the continent (Fisher and Raitt, 1962; Scholl et al., 1970; Schweller et al., 1981; Bourgois et al., 2000; Yañez et al., 2002). The distribution of sediment along the trench is further influenced by the high relief gradients of the segmented oceanic lithosphere.

Most of central and south Chile, where the trench contains thick turbidite infill, accretionary prisms, some 50-60 km wide, have developed. These prisms, however, are ephemeral (on the millions-of-years scale) and can be rapidly removed by high-relief morphological features on the incoming oceanic plate. Where topographic barriers stop the transport of turbidites along the trench, sediment infill abruptly decreases to less than 1 km in thickness and is confined to a narrow trench axis. There, all sediment is subducted; the margin is extending by normal faulting and collapsing due to basal tectonic erosion. The transition from accretion to tectonic erosion occurs over short distances (a few tens of km) along the trench.

In this introduction to the different tectonic settings of the Chile margin we summarize the recent review of previous marine studies (Fig 2.2.1) by Ranero et al (in press. a), with a special focus on three tectonic settings: 1) the effect of spreading centre subduction and subsequent margin evolution, 2) the collision of the Juan Férnandez Ridge, and 3) the contrasting tectonic processes between heavily sedimented and starved segments of the trench. The study area of METEOR 67-1 is located just south of the Juan Fernández Ridge; across the ridge occurs the transition from subduction erosion to sediment accretion and subduction. The METEOR 67-1 area presents a typical Chilean accretionary margin structure with a series of margin-parallel accretionary ridges in the lower-middle slope that give way upslope to a smooth upper slope cut by large canyons that supply Andean terrigenous sediment to the trench.

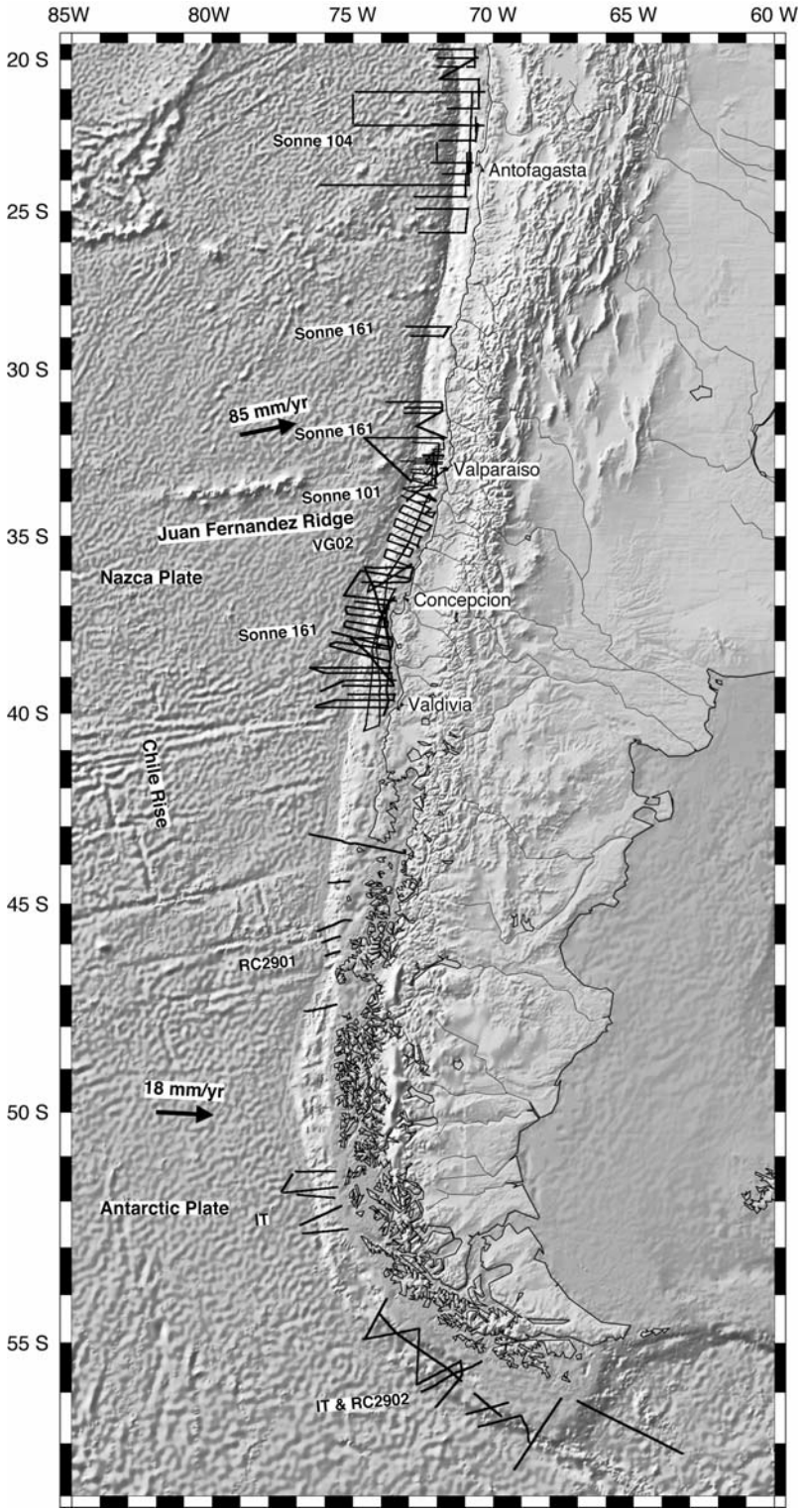

Figure 2.2.1: *Shaded relief map of the Nazca and Antarctica plates and South America continent (Smith and Sandwell, 1994). Convergence vectors are after DeMets et al., (1990). Black lines are tracks of most of the seismic reflection data collected along the continental margin in the past ~15 years. Bold tracks are multichannel seismic reflection (MCS) lines, and thin track, high-resolution MCS lines. Sonne 104 tracks are offshore from Antofagasta. Sonne 101 (thin) and Sonne 104 and Sonne 161 (bold) tracks are offshore and north of Valparaiso. Offshore from Valparaiso to Valdivia are Vidal Gormaz (VG02, thin) and Conrad and Sonne 161 (bold) tracks. Near the triple junction are Conrad RC2901 tracks. Along southernmost Chile are RC2902 and OGS-Explora IT95 & IT97 tracks. (Ranero et al., in press, a).*

2.2.1. The Tectonic Evolution of the Margin after Spreading Centre Subduction in South Chile

The subduction of the Chile Rise has been widely associated with tectonic erosion and the destruction of the frontal part of the margin in the collision area (Cande et al., 1987; Bangs et al., 1992; Behrmann et al., 1994; Bourgois et al., 1996; 2000; Bangs and Cande 1997; Behrmann and Kopf, 2001; Lagabrielle et al., 2000). Here we discuss the rebuilding of the margin after the subduction of the spreading centre.

Southernmost Chile

In southernmost Chile, where the Chile Rise collided with the margin at ~14 Ma; line RC2902-790 crosses the trench, the continental slope and the shelf (Fig. 2.2.2). The accretionary prism and fore-arc basin are clearly imaged and have also been imaged in other seismic lines across the margin (Fig 2.2.1; e.g. Polonia et al., 1999; Polonia et al., 2001).

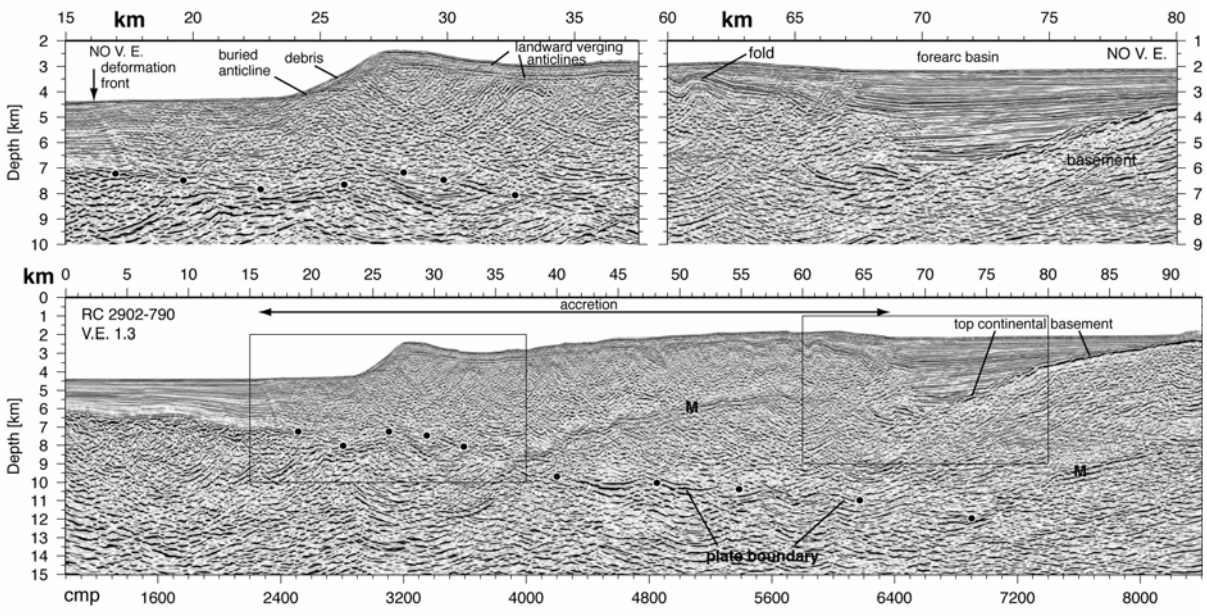

Figure 2.2.2: *Pre-stack depth migration of RC2902 line 790. The lower panel shows the profile with a 1.3 vertical exaggeration (V.E.) and the two close-ups with no vertical exaggeration. The reflections marking the plate boundary are delineated by the black-filled circles. Note the shallow angle of the subducting plate and the ~40 km wide, 5-8 km thick, accretionary prism. Accretion involves an area ~10 km wide across the trench, that is filled with ~2.5 km of sediment. The upper strata of the fore-arc basin onlap the accretionary prism and are folded, indicating recent deformation. The continental basement has a smooth top surface onlapped by undeformed sediment of the fore-arc basin. cmp: common mid point gather. (Ranero et al., in press, a)*

From the frontal thrust to the fore-arc basin, the accretionary prism is about 50 km wide (km ~16-66, Fig. 2.2.2). The area of accretion has similar dimensions in other seismic profiles across the lower density body (Polonia et al., 2001). In the trench, strata thicken slightly landwards indicating gradual tectonic thickening. Even though the deformation at the front indicates thickening of the accretionary prism over a short distance, this shortening may not explain the 6 to 8 km thickness of most of the older part of the prism. The internal structure of the older prism is generally not well imaged deeper than about 1 km below the seafloor, but a series of deeper discrete reflections indicate a broad tectonic structure. Folded strata are imaged in the upper 1 km of the prism, and the flanks of some of anticlines can be locally

followed for a few kilometres depth into the prism. Several of these thrust anticlines have a landward vergence (e.g. ~ km 30-45, Fig. 2.2.3). Several landward-dipping reflections seem to cut across the prism probably representing out-of-sequence thrusts thickening the prism to the 6-8 km total thickness across most of the prism.

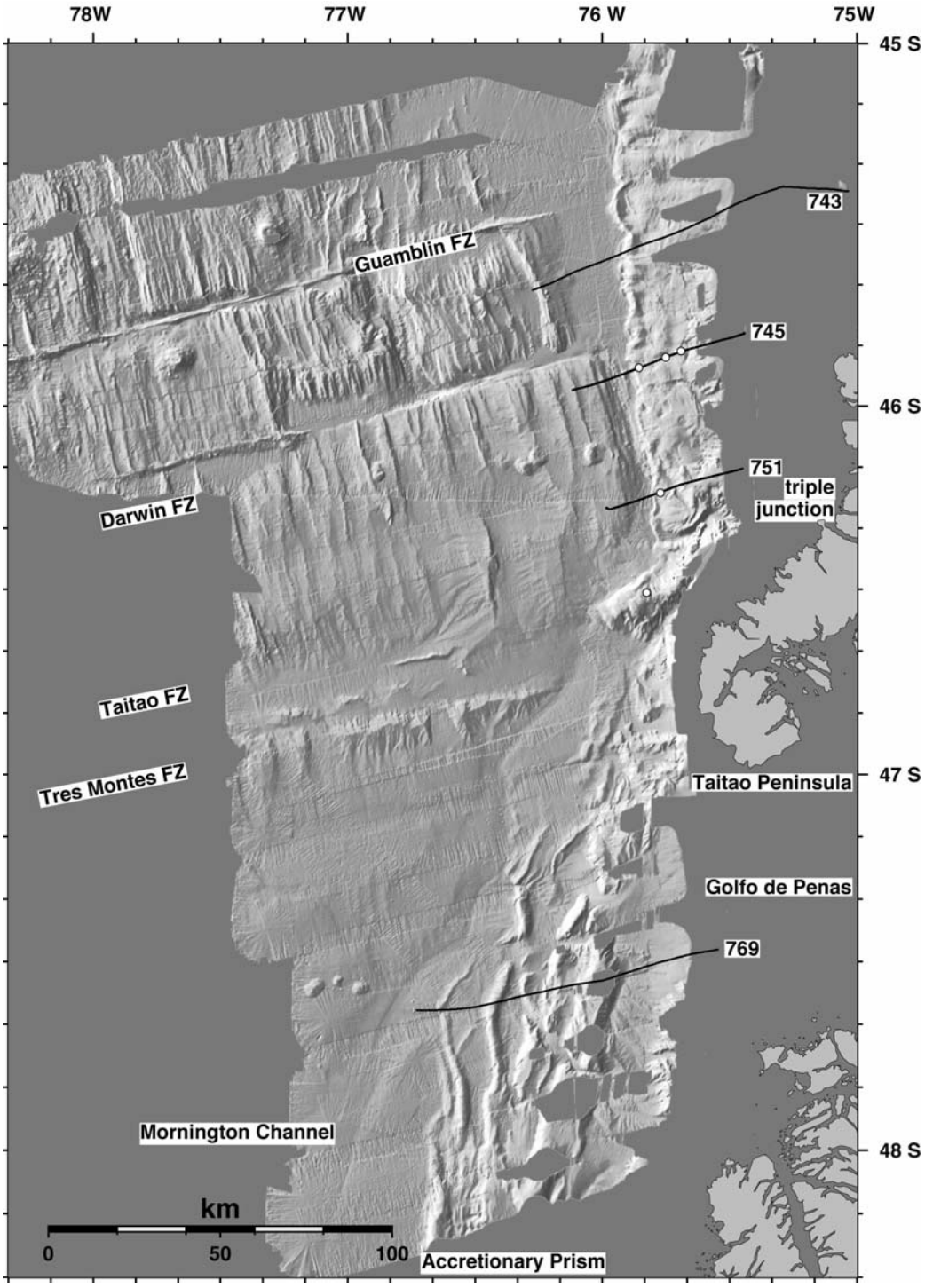

Figure 2.2.3: *Shaded relief map from a compilation of multibeam bathymetry data of the area around the triple junction. Most of the data were collected with RV Atlalante using the SIMRAD EM12 system (Bourgois et al., 2000). Some coverage gaps have been filled with data collected with a Seabeam system by R/V R. Conrad (Bangs et al., 1992). Black lines are tracks of seismic reflection profiles collected during cruise RC2902. Filled circles are ODP-141 sites (Behrmann et al., 1992). FZ: fracture zone. (Ranero et al., in press, a)*

Structure near the Chile triple junction

Most multibeam bathymetry data around the triple junction (Fig. 2.2.3) were collected with Research Vessel (R/V) L'Atalante (Bourgois et al. 2000) and gaps in coverage were filled around the Taitao Ridge with older data collected with R/V R. Conrad (Bangs et al., 1992).

Line RC2901-769, located about 100 km south of the triple junction, shows the structure of the margin where the Chile Rise collided with the continent at ~3-6 Ma (Fig. 2.2.4). It can be compared with the structure of line 790 (Fig.2.2.2) to understand the effect of spreading centre subduction and the subsequent evolution of the margin.

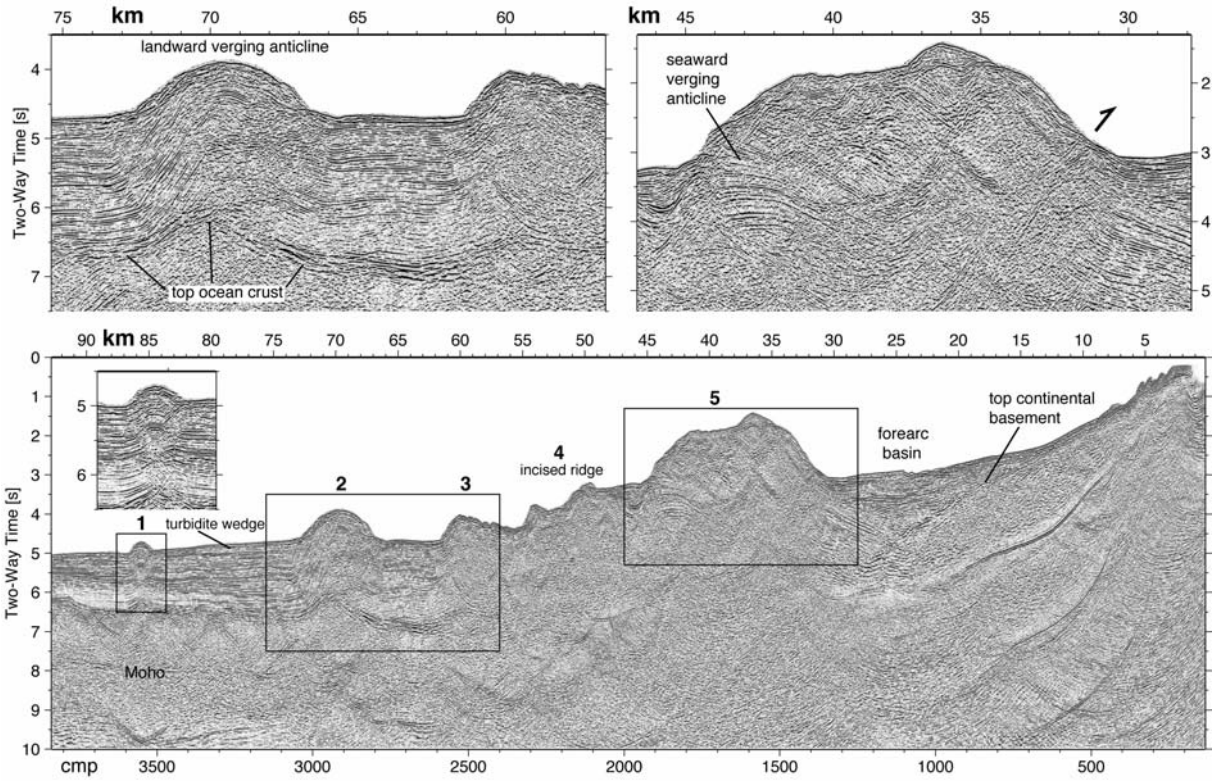

Figure 2.2.4: *Post-stack time migration of RC2902 line 769 across the Golfo de Penas accretionary prism (see Fig. 2.2.3 for location). The area of accretion is ~60 km wide. Note the general landward increase in dimension of the accretionary ridges. Ridges 1 and 2 display a clear, landward vergence. Ridge 5 seems to have overthrusted the older sediment of the fore-arc basin and then back-thrust by out-of-sequence faulting, thus thickening the prism. The fore-arc basin has a configuration similar to that imaged for southernmost Chile in Figure2.2.3. cmp: common mid point gather. (Ranero et al., in press, a)*

Seafloor morphology shows the marked difference in structure north and south of the triple junction (Fig. 2.2.3, Bourgois et al., 2000). Turbidite supply is diverted north and south from the collision point owing to topographic gradients. North of the triple junction, the margin is fronted by a small, Plio-Quaternary, sediment prism with much of the older material removed by tectonic erosion (Bangs et al., 1992; Behrmann et al., 1992; 1994; Bourgois et al., 2000). South of the triple junction, the trench is flooded with turbidites where the Golfo de Penas accretionary prism is developing (Bourgois et al., 2000). The prism broadens abruptly to the south as the deformation front migrates seawards and a broader zone of turbidites is accreted (Cande and Leslie, 1986; Bourgois et al., 2000).

Line 769 runs from the trench axis to the edge of the continental shelf, across the area where the deformation zone widens. The seismic image provides a snapshot of the ongoing rebuil-

ding of the accretionary prism after the subduction of the Chile Rise (Fig. 2.2.4). This line images some 92 km across the margin, about the same length as line 790 in southernmost Chile. The same bsic tectonic units are present in both line 769 and line 790, however, the seafloor relief is markedly different and the internal structure indicates a different stage of margin development.

Accretion has occurred across some 57 km (~ km 30-87, Fig. 2.2.4), from the landward-most accreted sediment to the current deformation front. Two accretionary ridges are currently developing at km 70 and km 86, and with little intervening vertical deformation (1 and 2 in Fig. 2.2.4). The small ridge (km 86) shows incipient thrusting. The anticline is towards the northern end of a bathymetric ridge that progressively decreases in size from south to north (Figs. 2.2.3 and 2.2.4). Thus, the image shows the area where thrusting is propagating northwards. The second ridge, centred at about km 70, displays 3 to 4 kilometres of shortening and landward vergence, similar to some anticlines in line 790. Landwards of ridges 1 and 2 are three increasingly higher and broader, margin-parallel ridges cut by large canyons (ridges 3 to 5, ~ km 30-62 in Fig. 2.2.4). Both the width and height of the older ridges progressively increase landwards, a pattern observed across the entire accretionary prism (Fig. 2.2.4). This gradual thickening seems to be a result of accretion suggesting that it may eventually lead to the formation of structures similar to that observed in southernmost Chile along line 790.

2.2.2 Tectonics Related to the Subduction of the Juan Fernández Ridge

The subduction of the Juan Fernández Ridge has fundamentally influenced margin tectonics for at least the past 20 million years (Yañez et al., 2001, 2002). The chain of seamounts trends ~85˚E, with a gap between volcanic edifices, some 250 km wide, separating the younger seamounts from seamounts near the trench, where the ridge changes strike to a NE direction (Figs. 2.2.1 and 2.2.5). The Juan Fernández Ridge influences margin tectonics in two fundamental ways. Firstly, the ridge produces locally extensive deformation where it collides with the continent (von Huene et al., 1997). Secondly, the ridge is a topographic barrier at the trench inhibiting the transport of sediment. The ridge separates a trench with several-km-thick sediment to the south that extends close to the triple junction, from a trench north of ~32.5˚S with less than 1-km-thick turbidite infill (Schweller et al., 1981). The volume of trench infill away from ridges seems to primarily govern tectonic style along the margin.

Multibeam bathymetry across the incoming plate and continental margin shows the morphotectonic and sedimentary structure of the different tectonic domains resulting from ridge subduction (Fig 2.2.5). Two seismic profiles (Figs. 2.2.6 and 2.2.7) show the structure under the continental slope and trench axis in areas that have been affected by the collision of the southward migrating Juan Fernández Ridge. The changes in topography of the incoming plate and trench infill are paralleled by the pattern of tectonic structures along the continental margin. The continental slope topography shows 4 main areas with different morphotectonic structure: (1) the depressed continental slope north of the Punta Salinas Ridge; (2) tectonic uplift over the ridge; (3) the lower slope seawards of the Valparaiso Basin; and (4) the elevated margin south of the Topocalma knoll.

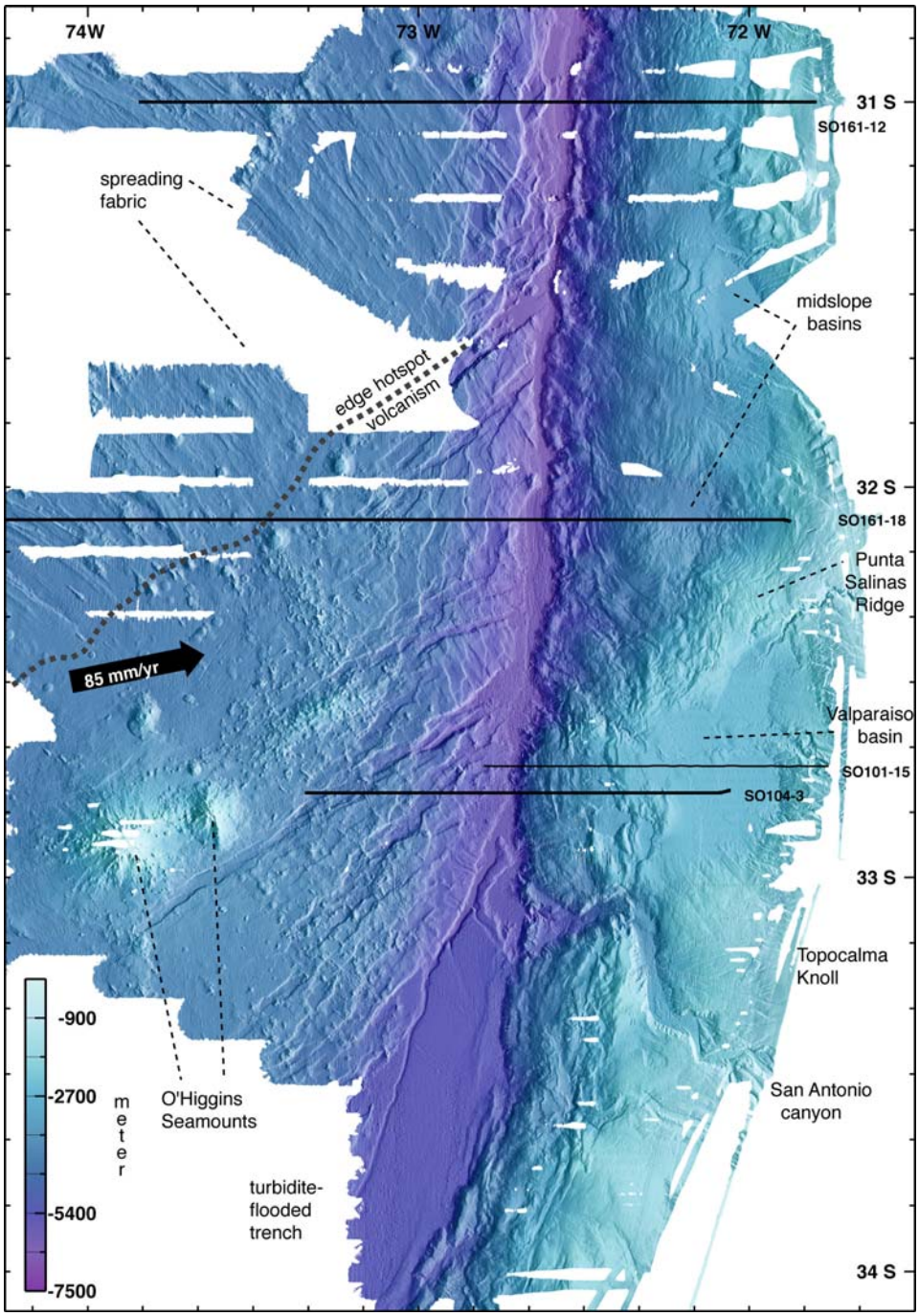

Figure 2.2.5: *Shaded-relief bathymetry from central Chile illuminated from the east. Black lines are seismic tracks. The Juan Fernández Ridge is a wide (~150 km), gentle swell crested by the O'Higgins seamounts and spotted by many small volcanoes. As it bends, it breaks along NE-trending faults. The plate unaffected by the hot spot has a seafloor-spreading fabric of narrow NW-SE ridges and breaks along trench-parallel faulting. The trench south of the ridge is flooded with turbidites and starved northwards. The flooded and starved trenches face, respectively, an accretionary prism and a depressed continental slope cut by normal faults. The Valparaiso Basin is bounded seawards by an extending, inactive, accretionary prism. The Punta Salinas Ridge is formed by uplift over large subducting seamounts. The ridge trends ~20˚ to the convergence vector (black arrow, DeMets et al., 1990) and is slowly migrating southwards. (Ranero et al., in press, a)*

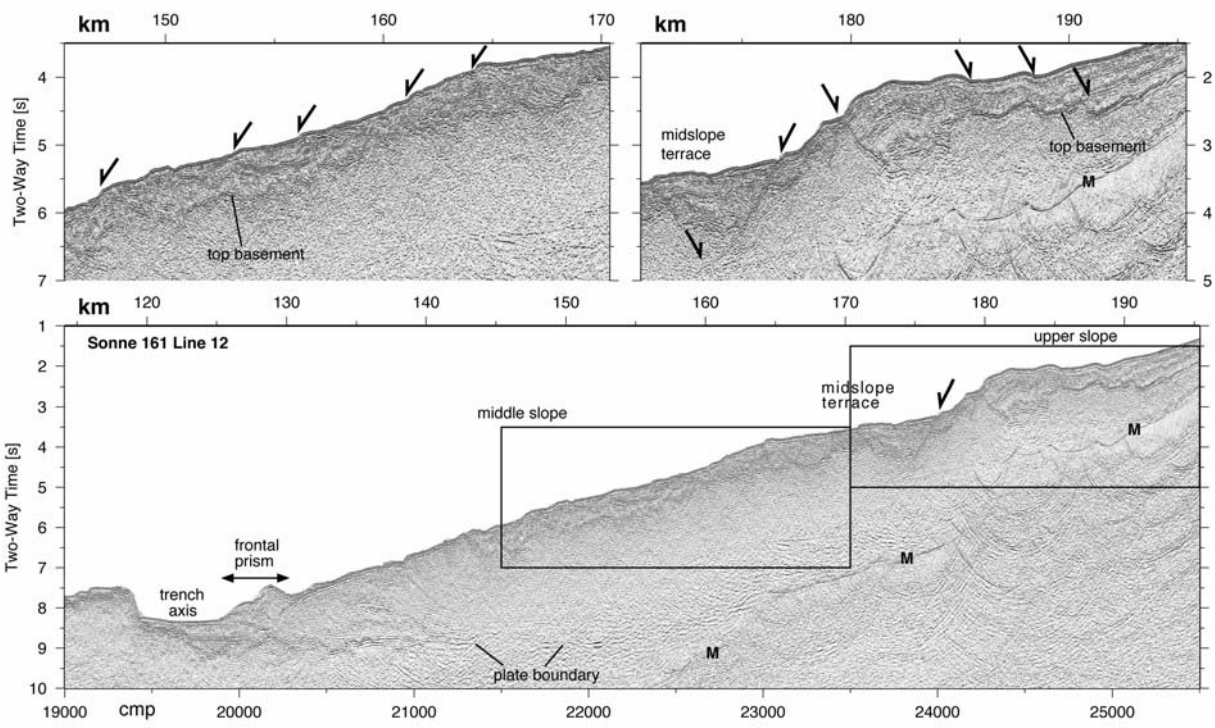

Figure 2.2.6: *Post-stack time migration of Sonne 161 line 12 (see Fig. 2.2.5 for location). The line images the northern part of the depressed continental slope where the Juan Fernández Ridge collided ~0.5 Ma, but where normal oceanic lithosphere currently subducts. The margin is fronted by a sediment prism ~5 km wide. The middle slope is covered by ~500 m of deformed sediment cut by numerous seaward-dipping faults. The change from middle to upper slope occurs abruptly across a scarp of a large seaward-dipping fault forming the mid-slope terrace. The upper slope is a less deformed terrain cut by landward-dipping faults. cmp: common mid point gather. (Ranero et al., in press, a)*

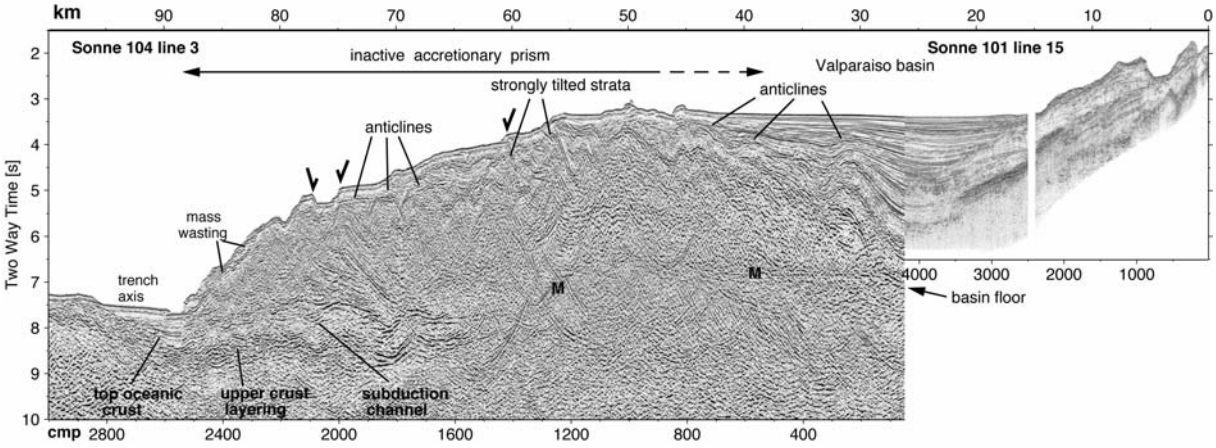

Figure 2.2.7: *Post-stack time migration of Sonne 101 line 15 and Sonne 104 line 3 (see Figs. 2.2.5 and 2.2.8 for location). The image shows the structure across the Valparaiso Basin and the inactive accretionary prism. The basin contains a large, fault-propagating anticline that documents, along with several smaller anticlines and a syncline forming the depocentre, shortening and the long-term uplift of the seaward flank of the basin. The frontal part of the margin shows accreted sediment in thrust slices. However, the seaward-sloping prism, cut by normal faults, indicates that accretion is not active and the prism is extending and collapsing owing to basal erosion that supplies material to a thick subduction channel. cmp: common mid point gather. (Ranero et al., in press, a)*

The depressed continental slope

North of the Punta Salinas Ridge a narrow trench axis occurs opposite a steep continental slope divided into three margin-parallel distinct morphological domains: The base of the lower slope is formed by narrow ridges; a generally steeper middle slope that contains a terrace in the shallower area; and an upper slope more coherently structured (Figs. 2.2.5 and 2.2.6). One or two narrow ridges meander along the base-of-slope, only locally disrupted by subducting, high topography on the oceanic plate. Seismic line SO161-12 shows a narrow trench axis filled with turbidites some 500-800 m thick underthrust beneath the ridges under the slope (Fig. 2.2.6). A locally bright décollement reflection occurring beneath the ridges at the base of slope continues updip to the trench seafloor, indicating that little, if any, turbidite is frontally accreted (Fig. 2.2.6). The narrow ridges may have formed either by limited accretion and/or by the reworking of slope debris. Resembling ridges at the slope toe have been imaged in other thinly sedimented trenches, such as the Middle America Trench (Ranero et al., 2000; Ranero and von Huene, 2000; von Huene et al., 2000; Ranero et al., in press. b), where drilling documented that the frontal prism is formed by reworked slope material, and all incoming sediment is subducted (Kimura et al 1997). The character of the frontal ridges changes little in the ~180 km from the northern SO161-12 line to just north of the Punta Salinas Ridge where the Juan Fernández Ridge currently subducts, further supporting little, if any, accretion along this segment. The middle slope is characterized by smoother topography disrupted by small-offset, normal fault scarps (Figs. 2.2.5 and 2.2.6). The transition from the middle to the upper slope occurs across a terrace. The terrain of the upper slope is cut by landward-dipping faults that have offsets of up to several hundred metres, much larger than the seaward-dipping faults in the mid slope (Fig. 2.2.6). An abrupt topographic transition from the upper to the middle slope occurs across a scarp of some 700 m, formed by a large, seaward-dipping fault that marks a sudden change in the dominant fault dip (~ km 177, Fig. 2.2.10). Although the upper to middle slope transition is only partially mapped in this area, the abrupt seafloor scarps indicate a ubiquitous, fault-controlled transition (Figs. 2.2.8 and 2.2.9).

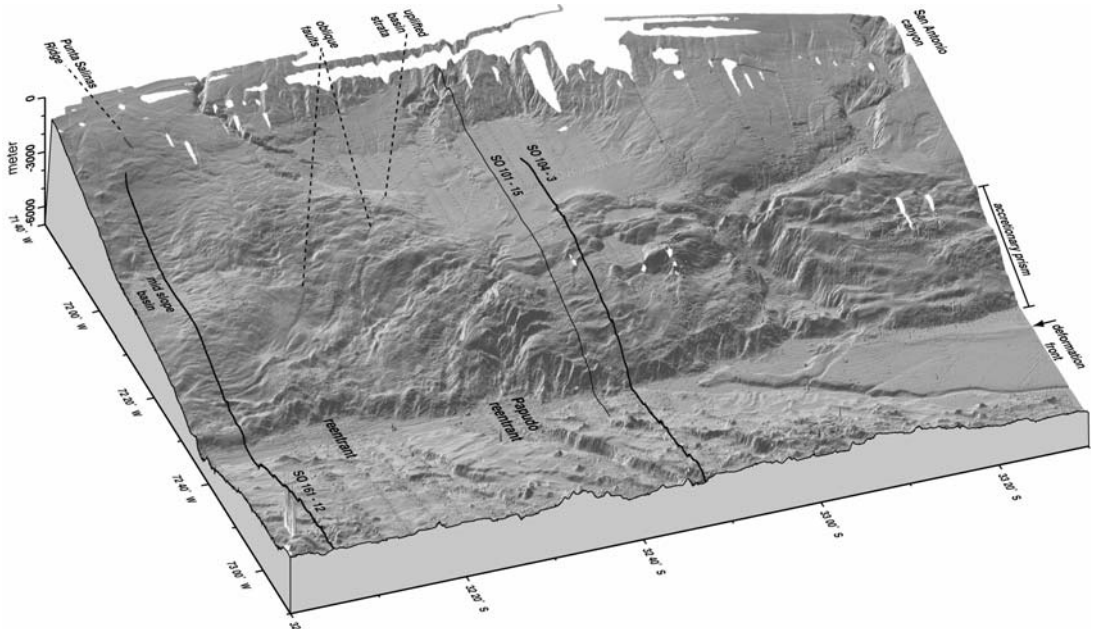

Figure 2.2.8: *Perspective view from 290˚ azimuth and 38˚ elevation of shaded-relief bathymetry illuminated from 45˚N. The data shows the area where the crest of the Juan Fernández Ridge has recently begun subducting. Note the deformed accretionary prism seawards of the Valparaiso Basin and the undisturbed accretionary prism south of the San Antonio canyon, where the trench is flooded with turbidites. (Ranero et al., in press, a)*

The structure of the depressed margin segment, characterized by a tectonically extending upper plate, is both the result of the progressive, southward migration of the Juan Fernández Ridge and subduction erosion where the thickness of turbidite infill is reduced to less than 1000 m and confined to a narrow axial zone. The observations described above indicate that subduction erosion affects the entire continental slope. The tectonic style of this region resembles that of Central America offshore Costa Rica, Nicaragua, El Salvador and Guatemala (Ranero et al., 2000, Ranero and von Huene, 2000; von Huene et al., 2000; Ranero et al., in press. b) were the SFB has worked during the past years. We now discuss ridge subduction and margin evolution along a trench axis that is both thinly and heavily sedimented.

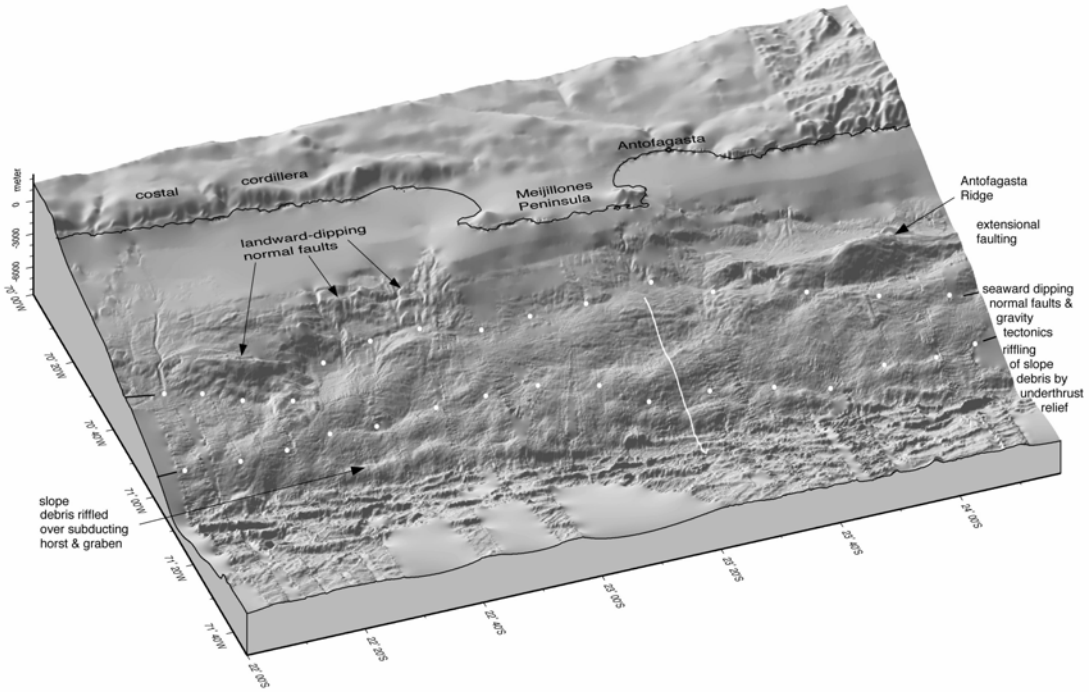

Figure 2.2.9: *Perspective view of shaded-relief bathymetry and topography from the sediment-starved trench of the northern Chile margin offshore Antofagasta. White line is Sonne 104 line 13 shown in Figure 10. White-filled diamonds bound the upper, middle and lower slopes with distinct morpho-tectonic character. Note the similarity of the submerged Antofagasta Ridge and Mejillones Peninsula, both formed as footwalls to large landward-dipping fault systems. (Ranero et al., in press, a)*

The collision zone of Juan Fernández and the change from thin to thick trench infill

South of the Punta Salinas Ridge, the Valparaiso Basin, a morphologically distinct lower continental slope, and the narrowest trench axis differentiate the area of the collision of the crest of the Juan Fernández Ridge (Fig. 2.2.5). The lower slope fronting the Valparaiso Basin rises above the segment of depressed eroded slope to the north. The structure in the seismic images is notably different from that to the north, and the frontal ~25 km contain thrust anticlines and the folded strata of an accretionary prism (Fig. 2.2.7). Yet, the structure and morphology seem to indicate that thrusting is waning (von Huene et al. 1997). The steep, frontal scarp along the base of slope (Fig. 2.2.5) has formed by mass wasting, and is imaged as seaward-slipping sediment packages (Fig. 2.2.7). Margin-parallel lineaments across the lower slope, that probably were accretionary ridges as in the south, are presently dissected by,margin-perpendicular lineaments. Some fault scarps indicate extensional faulting. The subducting sediment under the inactive prism is thicker than in the images from the north,

despite thinner trench sediment infill, which may indicate active basal erosion of the prism, an interpretation concurrent with the extending and collapsing margin front.

The trench south of the ridge crest is flooded by thick sediment and the accretionary prism is intact. This contrast indicates that tectonic erosion of the accretionary prism in this segment is probably a recent process associated with the progressive, southward migration of the ridge and that the change from accretion to subduction erosion along the trench occurs abruptly near the ridge crest.

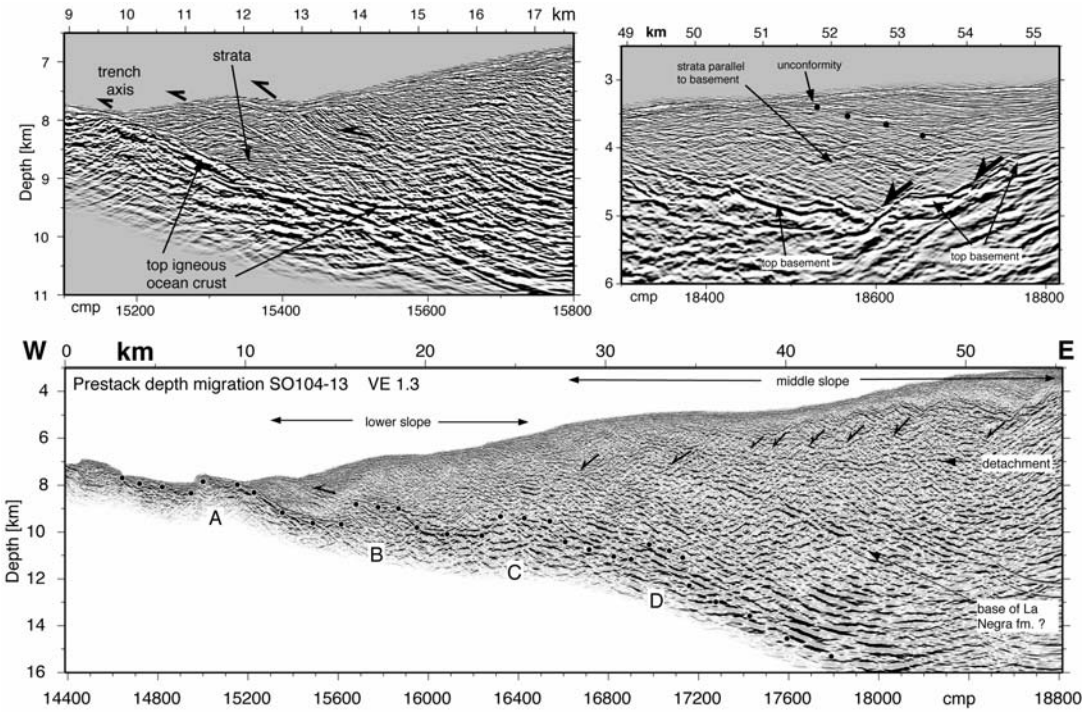

Figure 2.2.10: *Pre-stack depth migration of Sonne 104 line 13 offshore Antofagasta (see Fig. 2.2.9 for location). Vertical exaggeration is 1.3. Note landward-dipping faults cutting the middle slope and soling out at a subhorizontal detachment at ~7 km depth. Black-filled circles mark the top of the subducting plate and letters indicate subducting horsts. Left close-up shows the well-stratified debris filling an incoming graben and forming the frontal prism. Right close-up shows the top of basement and overlying sediment cut and extended by normal faults. cmp: common mid point gather. (Ranero et al., in press, a)*

The accretionary segment

The trench axis rapidly widens to ~40 km south of the mouth of the San Antonio canyon. Here, turbidites accumulate to thicknesses of up to 2.5 km (von Huene et al., 1997; Laursen et a., 2002), because the oceanic plate bends deeper into the trench axis than at the Juan Fernández Ridge (Figs. 2.2.5 and 8). The lateral variation in plate bending indicates that the oceanic plate covered by thick trench sediment is not affected by hot spot magmatism. The morphology of the continental slope in this segment contrasts markedly with the northern segment. Here the frontal ~40 km of the slope are characterized by margin-parallel, en échelon ridges of variable dimensions but increasing height upslope (von Huene et al., 1997).

Active accretion is inferred from the relief of the smooth trench area at the slope toe, which shows slope-toe parallel, low ridges, indicating active deformation of the trench turbidites (Figs. 2.2.8 and 9). These low ridges are also imaged in seismic records and correspond to active thrust anticlines (von Huene et al., 1997; Laursen et al 2002). Deep penetration multi-

channel seismic reflection data show accretionary structures in the frontal 20 to 30 km (von Huene et al 1997) and a relatively low velocity body extends ~40 km landwards of the trench (Flueh et al., 1998).

The accretionary ridges across the frontal 40 km of the margin are well displayed across the walls of the cross-cutting San Antonio canyon. Some trends appear to cross the canyon into the slope at the front of the Valparaiso Basin, where tectonic erosion is currently thinning that inactive part of the prism (Fig. 2.2.7). Upslope from the ridges, the slope is covered by a sediment blanket with a smooth seafloor topography, only disturbed by shallow canyons and shallow slide scars (Figs. 2.2.5 and 8).

A model of margin segmentation at central Chile
The distinct morphotectonic character and internal structure of the individual segments of the margin have formed responding to the changes in dominant tectonics caused by the southward migration of the collision zone of the Juan Férnandez Ridge. The ridge controls the distribution of trench turbidites and this distribution controls the prevailing tectonic process (accretion or subduction erosion) along each segment of the margin.

The accretionary segment represents margin structure unaffected by the passage of the ridge. The edge of the ridge is delineated by a sudden shallowing and narrowing of the trench axis and an abrupt decrease in the turbiditic infill. The edge of the obliquely converging ridge is underthrusting the slope facing the Valparaiso Basin, where an inactive accretionary prism is thinned by erosion and extension, and it is collapsing. The most dramatic deformation produced by the ridge is the Punta Salinas Ridge, marking where the ridge crest and seamounts tunnel under the margin and uplift the entire slope.

North of the Punta Salinas Ridge, the depressed slope segment contains a distinct three-fold structure. The thinning causing the comparatively depressed slope relief may have partially resulted from the past subduction of the ridge and seamounts that removed upper plate material during tunnelling, as observed elsewhere (Ballance et al. 1989; Ranero and von Huene, 2000). The less than 1000-m-thick turbidites in the trench are not sufficiently thick to restore accretion, and the small frontal sediment prism has an even width along the 200 km of surveyed segment. Seismic images show that most, or all, trench turbidites are currently being subducted.

The middle slope is pervasively faulted by dominantly seaward-dipping normal faults, causing upper plate extension associated to basal tectonic erosion. The upper slope exhibits a comparatively more stable morphology with canyons that end at the mid-slope terrace. The upper slope is cut by landward-dipping normal faults, also indicating progressive, albeit possibly slower, collapse of this part of the margin. In summary, the subduction of the hot spot ridge and seamounts causes pronounced deformation at the collision zone and the volume of trench turbidite infill fundamentally changes the tectonic style along the margin as the ridge migrates southwards.

2.2.3 The Sediment-Starved, Northern Chile Margin

The entire Chilean margin north of the collision zone of the Juan Fernández Ridge is dominated by tectonic erosion. The most extensively studied area is the margin offshore Antofagasta (Figs. 2.2.1 and 9) that exemplifies an end-member type where subduction erosion processes have been active for ~20 Ma since the ridge passed the region (Yañez et al., 2001).

The structure of the margin offshore Antofagasta resembles that observed in central Chile north of the collision area of the Juan Fernández Ridge, but the tectonic structure resulting from tectonic erosion appears somewhat more evolved. Multibeam bathymetry and seismic images support that tectonic erosion along the base of the upper plate is causing subsidence of the continental shelf that steepens the slope leading to landward-dipping extensional faulting (Figs 9 and 10). With a steepening continental slope, gravity-driven tectonics progressively breaks up the framework rock of the margin wedge coeval with hydrofracturation of the underside of the margin by upwardly migrating fluid, promoting tectonic erosion and crustal thinning (von Huene and Ranero 2003; Sallares and Ranero, 2005). Downslope, the progressive increase in weakening of the overriding plate, an increase in gravity tectonics, and the subducting plate eventually disaggregate the margin rock into fragments too small to be imaged with regular seismic reflection systems. The disaggregated, thin apex of the margin forms a frontal prism with the strength of accreting sedimentary prisms (von Huene and Ranero 2003).

2.2.4 Remarks

The more than 3500-km-long Chile convergent margin provides a unique opportunity to study along a single subduction system the factors governing tectonic processes at convergent plate boundaries. The supply of trench sediment, turbidite transport along the trench, and deformation produced by subduction of large positive relief in the oceanic plate are fundamental controls on the tectonic processes along convergent margins.

The along-trench migration of the collision zone of the Juan Fernández Ridge has two distinct effects. The ridge rapidly erodes the margin, locally removing most of the pre-existing accretionary structure. In addition, the shallow ridge topography restrains the transport of turbidites along the trench, causing a permanent change of the dominant tectonic process from sediment accretion to tectonic erosion.

South of the Juan Fernández Ridge, the trench contains more than 2 km of turbidites, and a broad accretionary wedge and a largely undisturbed morphology upslope indicate a more stable configuration. Sediment accretion dominates, but 1.0-1.5 km of trench turbidites underthrust the accretionary prism and are subducted (von Huene et al., 1997; Diaz, 1999). The area of the margin where frontal sediment accretion currently dominates extends southwards to near the Chile Triple Junction where trench infill and tectonics are modified by the subduction of the Chile Rise (Bangs and Cande, 1997). North of ~28˚S, the margin is an example of tectonics along a turbidite-starved trench. The margin shares a basic structural configuration with the depressed slope segment north of the crest of the Juan Fernández Ridge. High-pressure fluids expelled from the subduction channel hydrofracture the base of the overriding plate. The locus of seepage and tectonic role of fluids expelled from the subduction channel of the accretionary segments of the margin is an important topic for future research.

3. Participants

3.1 Scientists

Dr. Wilhelm Weinrebe	Chief Scientist	IFM-GEOMAR/ SFB 574
Dr. Cesar Ranero	Mapping - Bathymetry	ICREA
Dr. Jörg Petersen	Mapping - Magnetics	SFB 574
Dr. Christian Hensen	Pore Water Analytics	SFB 574
Rieka Harders	Pore Water Analytics	SFB 574
Vasileios Mavromatis	Pore Water Analytics	SFB 574
Dr. Jörg Bialas	DTS Sidescan / Streamer	IFM-GEOMAR
Dietmar Bürk	DTS Sidescan	SFB 574
Dr. Asrarur Talukder	DTS Streamer / PARASOUND	SFB 574
Wolfgang Queisser	Technician	IFM-GEOMAR
Dirk Schörner	Watchkeeper	SFB 574
Silke Schenck	Watchkeeper / Cruise Report	SFB 574
Mathias Weinrebe	Watchkeeper / Computers	IFM-GEOMAR
Lucia Villar Muñoz	Guest Scientist, Chile	UCV
Rodrigo Redenz Rodriguez	Guest Scientist, Chile	UCV
Paulina Lohse Muñoz	Guest Scientist, Chile	UCN
Andrea Bello Smith	Observer, Chile	UCV
Jörn Ewert	PARASOUND	ATLAS
Lothar Kaufeld	Meteorologist	DWD
Thorsten Truscheid	Meteorology Technician	DWD

Figure 3.1.1: *The scientist group of M67/1.*

3.2 Crew

Niels Jacobi	Master
Walter Baschek	Chief Mate
Uwe-Klaus Klimeck	1st Mate
Haye Diecks	2nd Mate
Anke Walther	Surgeon
Volker Hartig	Chief Engineer
Thomas Fischer	2nd Engineer
Uwe Schade	2nd Engineer
Rudolf Freitag	Electrician
Heinz Wentzel	Chief Electronic Engineer
Jörg Walter	Electronic Engineer
Paul Wintersteller	System Manager
Werner Sosnowski	Fitter
Karl-Heinz Lohmüller	Boatswain
Evgenios Drakopoulos	Able-Bodied Seaman
Kai Rabenhorst	Able-Bodied Seaman
Manfred Gudera	Able-Bodied Seaman
Bernd Neitzsch	Able-Bodied Seaman
Günter Ventzsch	Able-Bodied Seaman
Günter Stängl	Able-Bodied Seaman
Simmen Möller	Able-Bodied Seaman
Frank Sebastian	Motorman
Thomas Weber	Motorman
Hermann Rademacher	Motorman
Gerhard Lange	Motorman
Franz Grün	Cook
Willy Braatz	Cooksmate
Michael Both	1st Steward
Rainer Götze	Steward
Jan Hoppe	Steward
Peter Eller	Steward
Nan Sng Lee	Laundryman

3.3 Adresses of Participating Institutions

SFB 574 Sonderforschungsbereich 574 der Christian-Albrechts-Universität zu Kiel
IFM-GEOMAR
Wischhofstraße 1-3
24148 Kiel, GERMANY

IFM-GEOMAR Leibniz-Institut für Meereswissenschaften der
Christian-Albrechts-Universität zu Kiel
Wischhofstraße 1-3
24148 Kiel, GERMANY

ICREA Instituto de Ciencias del Mar
CMIMA, CSIC
Paseo Marítimo de la Barceloneta 37-49
080003 Barcelona, SPAIN

UCV Pontificia Universidad Católica de Valparaíso
Av. Altamirano 1480
Valparaíso, CHILE

UCN Universidad Católica del Norte
Av. Angamos # 0610
Antofagasta, CHILE

DWD Deutscher Wetterdienst
Geschäftsfeld Seeschifffahrt
Bernhard-Nocht-Str. 76
20359 Hamburg, GERMANY

ATLAS ATLAS Hydrographic GmbH
Kurfürstenallee 130
28211 Bremen, GERMANY

4. Meteorology

Kaufeld, L.

4.1 Weather Conditions during the First Part of the Cruise, 20 February- 3 March 2006

During this period, the weather was characterized by the ridge of the southern Pacific subtropical high. Corresponding to the season, single cold fronts from the southerly west wind zone penetrated down to 30° S. With the approach of those cold fronts, e. g. on February 25 and 26, the usually southerly winds turned to westerly, partly to NNE directions.

During the night from March 1 to 2, wind directions changed irregularly, despite of increasing wind speed. These variations were produced by a very low inversion caused by cooling of the air above relatively cold water.

After the cold fronts had passed, the air pressure rose and the subtropical anticyclonic ridge extended into the direction of the Chilean coast. In several of these cases, flat troughs which were situated along the coast intensified which led to an increase of wind speed to up to 7 Bft with squalls of up to 9 Bft. These wind conditions caused sea heights of up to 3 m. At the same time the heave reached significant wave heights of 2 ½ m, which caused relatively rough sea surface conditions.

During this part of the cruise, the sky was partly clear and partly covered with stratocumulus clouds. During the passage of a cold front, it rained for a few hours on February 26. Contrary to the high temperatures on land, the water temperatures and as a result also the air temperatures only reached values of 14 to 18 °C.

4.2 Weather Conditions during the Transit to Balboa, 4 – 12 March 2006

The journey from the research area near Concepcion to Balboa led through various climatic zones, from the southern subtropical belt and the trade wind region through the Intertropical Convergence Zone (ITCZ), which appeared weak and diffused when we passed it, to tropical Panama. In March, the dry season is still continuing there within the northerly trade winds.

During this part of our cruise, the water and air temperatures continually rose with two exceptions: The first one occurred on 9 and 10 March when we approached the northern Peruvian coast and ran into coastal upwelling water. The second exception was found on 12 March at latitudes from 4 to 5° N. Here, the water temperatures reached a record low of less than 20 °C, so that shallow fog formed because the moist equatorical air was cooled to below its dew point of 22.5 °C.

From 4 March on, we travelled with the south to southeast trade winds, which blew with “normal” 4 to 5 Bft. Sometimes, for example from March 4 to 7, the sky was covered with low stratocumulus clouds and sometimes the sky was clear.

The ITCZ, as stated before, was relatively weak and we only observed medium high and high clouds without rain. The winds inside this zone were weak, and until March 12 they blew mainly from southerly directions. Then we passed the surface convergence and the wind turned to northerly directions. When we reached Balboa on 13 March, the sky was bright and air temperatures reached 32 °C.

5. Cruise Narrative

Weinrebe, W.

When cruise M67/1 started on 20 January, we were in a first-time situation concerning many aspects: It was to be the first cruise of R/V METEOR under the flag of F. Laeisz GmbH, the first cruise to start from a Chilean port and the first cruise after a long stay in a shipyard, during which METEOR had undergone major restructuring and received new systems. The work the ship had undergone was so extensive that the time allocated for the shipyard had not been sufficient for testing. Thus, the group of 17 scientists that arrived on 20 February 2006 was pleased to find a ship with a newly painted hull, new laboratory interiors and new echosounder systems, yet they had to cope with a three-day postponement of the scientific programme as the echosounders were still to be tested and approved.

Figure 5.1: *December 31, 2005 flag of RF GmbH is dipped*

Figure 5.2: *January 1, 2006 flag of F. Laeisz GmbH is set*

METEOR left the pier of the Talcahuano ASMAR shipyard on 21 February for a three-day test cruise. First of all, the new bow thruster and the dynamic positioning system were adjusted, the rest of the time was then dedicated to testing and calibration of the new KONGSBERG EM710 and EM120 multibeam echosounders. The EM710 shallow-water system was calibrated and tested in an area north of the Rio Biobio Canyon at water depths of 130 – 230 m. Afterwards, the EM120 deep water system was tested in the mouth of the canyon at a water depth of about 5000 m. The tests were observed with great interest, because due to the shape of the hull and an unlucky positioning of the transducers METEOR's former HYDROSWEEP system had been prone to being disturbed by to air bubbles even under moderate sea conditions. Thus, the keel had been opened and widened to contain the transducers, mounted in a blister, in the middle of the hull. The first tests, which took place under relatively good weather conditions, scarcely showed any disturbance by bubbles, so that the restructuring can be deemed successful, especially as no negative effect was registered on the ship's speed.

After the tests had been completed, METEOR reached the roadstead of Talcahuano bay on 24 February at 10:00. Five technicians and engineers who had been involved in the testing left the vessel. After the ship had been cleared by the Chilean administrative authorities, the transit to the working area started at 11:30.

The scientific programme started with bathymetric and magnetic mapping on 24 February at 3:15 pm. Two long profiles each about 120 nm and two shorter ones each about 40 nm in length along the transition from the upper to the middle slope were recorded until Sunday morning 26 February at 09:30 am. The profiles mainly cover the backstop of the accretionary wedge, which is marked by a number of steep thrust faults.

The highlight of the work so far was a sampling programme comprising 4 deployments of the gravity corer on Sunday, 26 February. Unfortunately, a site we had previously selected for sampling, where Danish and Chilean colleagues had run a seismic profile revealing structures similar to mud volcanoes, was not accessible as fishermen were working with longlines and ground nets in this area. Thus, we had to find some adjacent alternative sites from which we were able to retrieve three cores, each a few meters in length, which mainly consisted of consolidated mud. One of the cores let off a smell of sulfide.

The coring programme was followed by a bathymetric survey with EM120, EM710 and PARASOUND mapping of an area showing water depths of 800 m to 1100 m (see figure). Chilean colleagues had found gas hydrates in a gravity core from this area. We had planned to complete our studies in this area by a DTS survey and gravity coring, which were scheduled to start on Tuesday 28 February at noon after two more bathymetric profiles along the middle slope almost up to 34°S had been recorded. With a strong south-western wind of up to 7 Bft and a 3-m heave, mapping along these profiles went well as long as our course was set before the wind, yet against the wind the ship's speed had to be reduced to 7 kn in order to get useful data. Before the deep-towed DTS system comprised of the sidescan sonar and the deep-towed seismic streamer could be deployed, the „POSIDONIA" USBL system for submarine positioning of the DTS had to be calibrated. The portable IFM-GEOMAR system was calibrated as well as the new ship-owned POSIDONIA, which had been installed during METEOR's stay at the shipyard. After some unexpected problems, which are usual for new systems, had been overcome, the calibration was finished by Tuesday, 22:00. Unfortunately, a last test before deployment showed a DTS communication error. The rest of the night was used for locating and fixing the error while recording four further short bathymetric profiles. The DTS error appeared to be fixed and the system was safely deployed on Wednesday February 28 in the morning. However, the communication to the DTS still turned out unstable. Therefore we decided to break off at a depth of 300 m and recover the instrument. Subsequent tries to fix the error were unsuccessful, so that we did not schedule a new DTS deployment.

A prominent aim of this leg was to find indications of fluid venting along the continental margin and prepare a geochemical characterization. We found that the area we had mapped before was very suitable for this purpose. On Wednesday evening, 6 gravity cores were taken from 5 different sites. The sites were chosen in areas of marked topographic and tectonic structures on the basis of the new, high-resolution bathymetric data and PARASOUND recordings. The most interesting geochemical results can be expected from two cores taken from a small elevation that forms a prolongation of the N-S striking fault line. The upper 50 cm of these cores showed very high H_2S concentrations, which clearly indicate an active ascent of fluids rich in methane. A further, mound-like elevation yielded a sample of authigenic carbonates and cemented shells which also indicate fluid venting. Unfortunately, we did not get a sample of sediments and fluids from this structure.

After the sampling programme had been finished on Thursday March 2 at 01:00 am, we recorded a long bathymetric profile along the deep sea trench to map the deformation front. The profile was directed towards the north, already signalling the near end of our scientific programme. Two short parallel profiles on the ocean plate were recorded until on Friday, 14:30 we reached the point from which we had to start our long transit in order to reach the port of destination of M67/1, Balboa, Panama, in time.

The research permission for work in Chilean Waters allowed us to record bathymetry up to 33°S. The survey was continued during the transit until we reached that parallel on Friday in the evening, however, during the transit the ship's speed was increased to 11.5 knots. Surprisingly, the data quality both of the EM120 and the PARASOUND system were good, yet, due to the high speed the along-track beam spacing was increased and a total coverage of the seafloor was not achieved.

In order to gain as much time as possible for the investigations in the survey area, the shortest possible route had been chosen for the 11-day transit to Panama. During the transit no considerable scientific data acquisition was done, apart from occasional operation of the multibeam and PARASOUND systems in international waters for several tests. The transit time was used for failure analysis and repair of the DTS, for analyzing and archiving the samples of the gravity cores and for processing of the multibeam bathymetry data. The equator was passed on Saturday March 11 early in the morning. Due to favourable weather conditions the anchorage at Balboa was reached in time on Monday March 13 at noon.

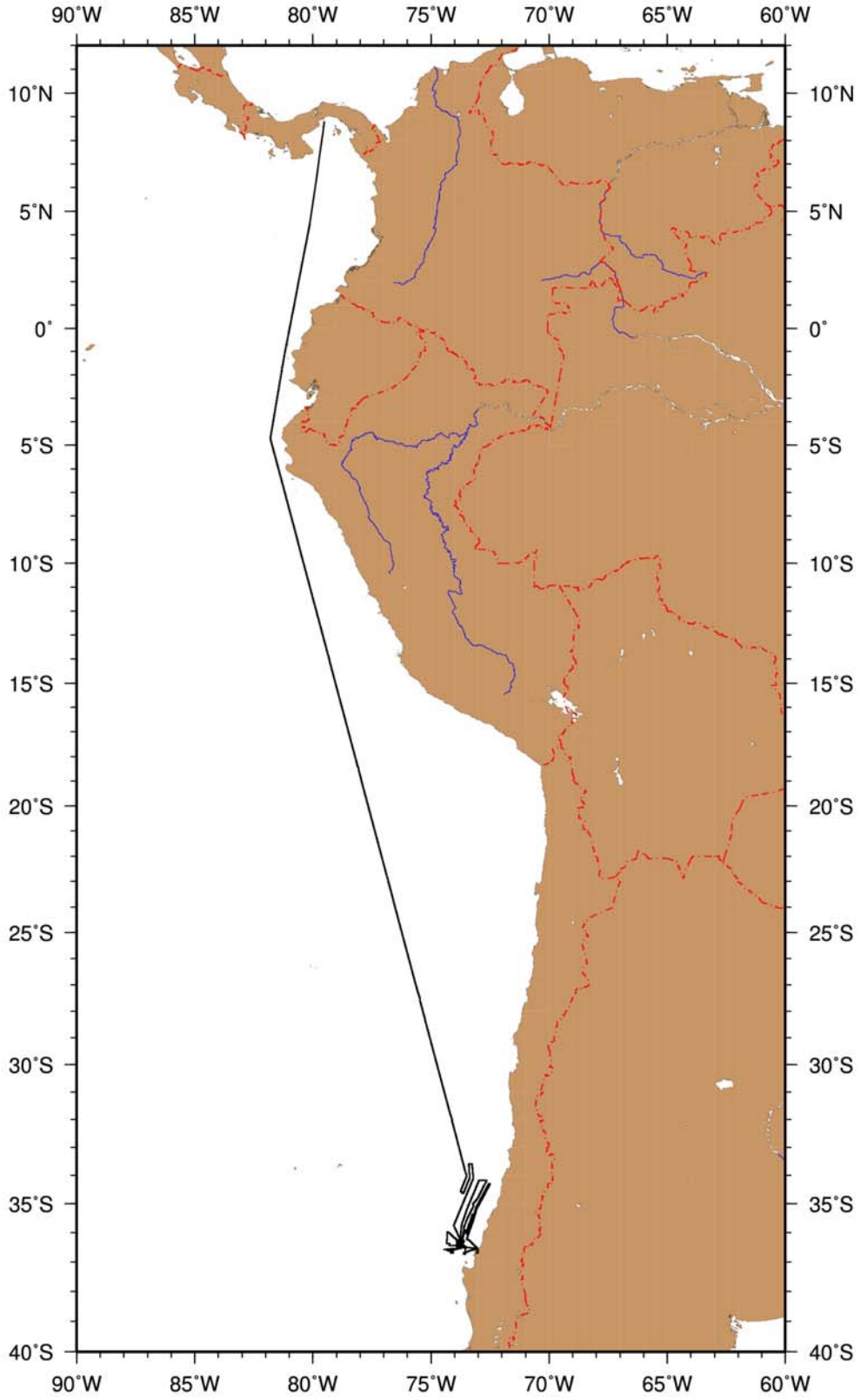

Figure 5.3: *Total track of the cruise METEOR M67/1 from Talcahuano (Chile) to Balboa (Panama)*

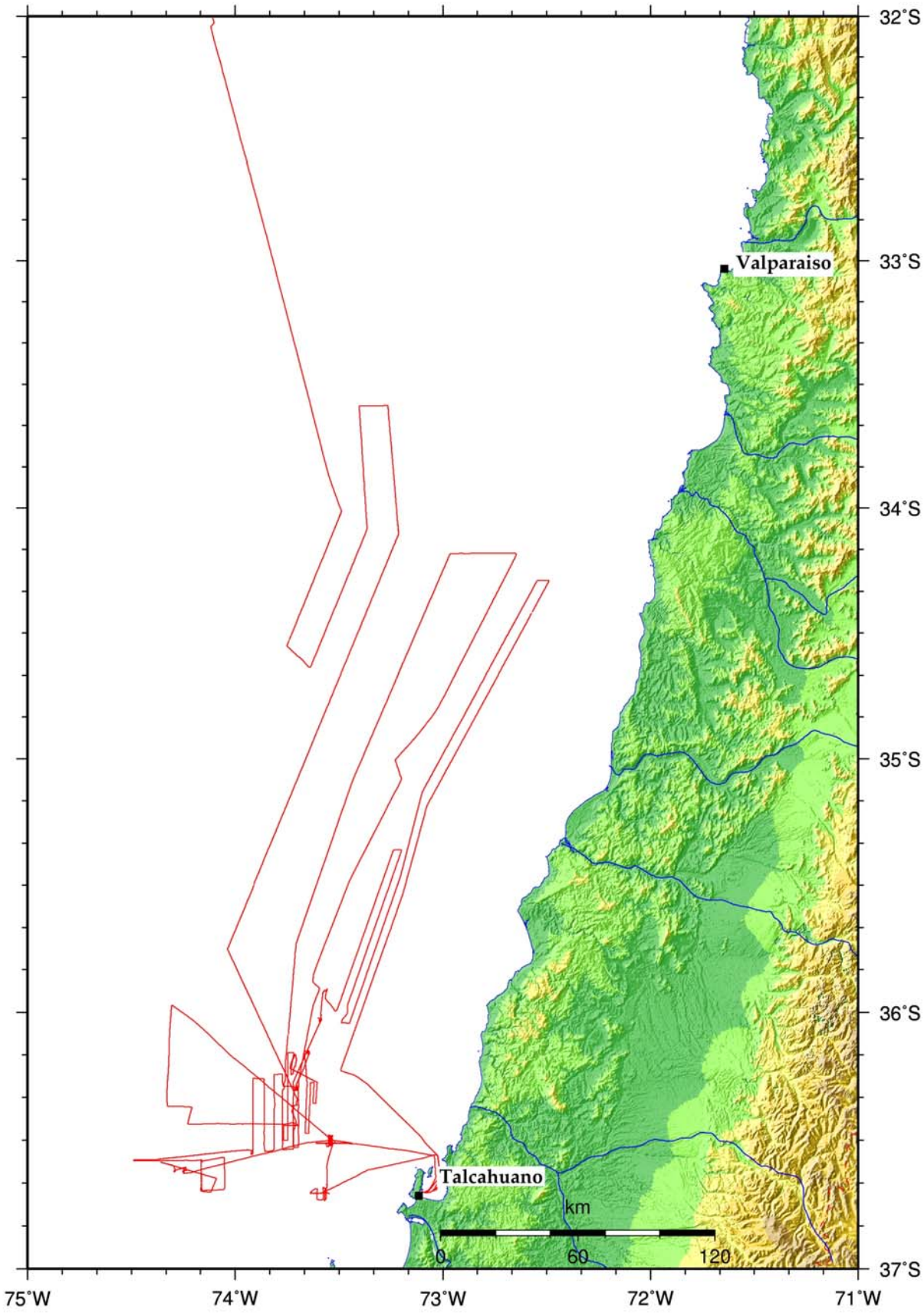

Figure 5.4: *Cruise track of METEOR M67/1 in the main working area*

6. Equipment

6.1 Computer Facilities

Weinrebe, W.

To process the bathymetry and magnetic data onboard and to be able to produce different maps of the collected data, a set of three PCs was set up in laboratories 4 and 5. The systems were operated by LINUX as operating system. The specifications of the systems are as follows:

name	type	specifications
coromandel	fat - minitower	Hardware: CPU: AMD Sempron 2800+ 2 GHz takt rate 1 GB main memory 2x 250 GB disk space Operating system: SuSe LINUX 10.0
tauranga	Dell Optiplex GX520	Hardware: CPU: Intel Pentium IV 2 GHz takt rate 2 GB main memory 1x 150 GB disk space Operating system: SuSe LINUX 10.0
wuerm1	Prisma - tower	Hardware: CPU: AMD Athlon 900 MHz takt rate 256 MB main memory 1x 100 GB disk space Operating system: SuSe LINUX 9.0

The data disk "/data1" of coromandel (250 GB capacity) was exported and mounted at the other stations and was used as central storage and working space. Portable external disks connected to the systems with USB2.0 or IEE1394 were used to mirror the data partition of coromandel. This setup provided an easy way of achieving redundancy. In addition, the portable disks were used to transfer the data to IFM-GEOMAR after the cruise. In addition, several laptops of different type were used and connected to the network.

For plotting purposes and for the generation of maps the GMT release 4.1 software (Wessel and Smith, 1998) had been installed on all three systems. To process the multibeam data from the KONGSBERG EM120 echosounder, the MB System release 5.0.8 software (Caress and Chayes, 1996) had been installed. The KONGSBERG-SIS data acquisition software for the EM120 on R/V METEOR operates under Windows XP on PC architecture whereas the EM120 system on R/V SONNE operates under SUN architecture on SUN Solaris. Both systems have different orders of storing the data. MB-System release 5.0.8 is the first version of the MBSystem which is able to process multibeam data from both data acquisition systems.

6.2 DTS-1 Deep Tow Sidescan Sonar and Seismic Streamer

Bialas, J., Bürk, D., Petersen, J.

The deep-towed sidescan and multichannel seismic streamer system (Fig. 6.2.1) was developed to investigate acoustic properties of the seafloor and seismic images below the seafloor with high resolution. The system was developed and funded as part of the "Gas-hydrate" framework within the "Geotechnologien-Programm" run by the German Ministry of Science (BMBF) and the German Science Foundation (DFG).

Figure 6.2.1: *Photography of the DeepTow digital seismic array and sidescan sonar*

The vertical and lateral resolution of marine subsurface structures in reflection seismic images strongly depends on the marine seismic source and streamer system used for signal generation and data acquisition. One limiting factor is the size of the Fresnel zone, which can be decreased in-line by Migration techniques. The cross-line resolution can only be improved by lowering the streamer and - in the ideal case - the source towards to the sea floor. Such a hybrid configuration (deep-towed streamer and surface source; Fig. 6.2.2) has been available at IFM-GEOMAR since 2002.

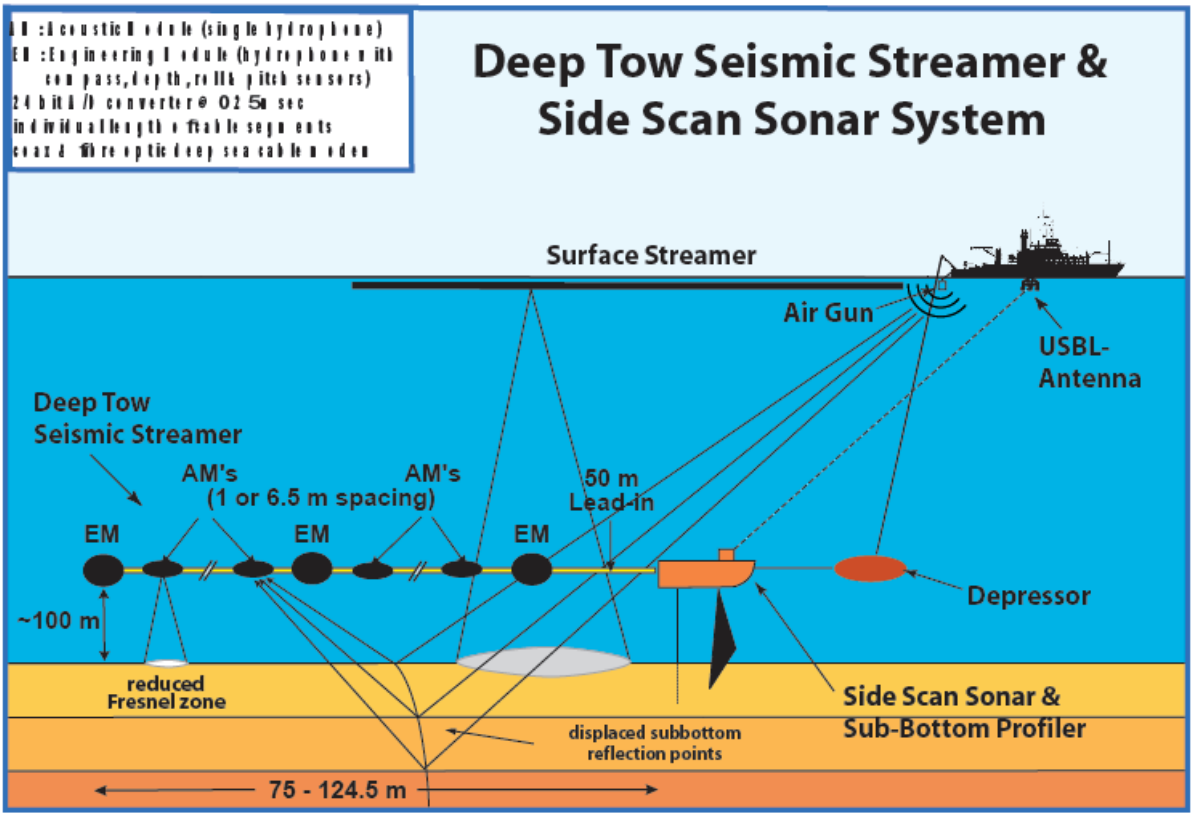

Figure 6.2.2: *Drawing of the towing geometry of the DeepTow digital seismic array and sidescan sonar*

Whereas reflection seismic studies provide an image of subsurface structures, sidescan sonar surveys are intended to map the acoustic properties of the seafloor. The general principle of sidescan sonar mapping is that an acoustic beam is scattered at targets on the seafloor, and the amount of scattering that is directed back to the instrument is recorded. This amount of back-scattering is related in decreasing order to the regional slope, the microtopography of the sea-floor and the physical properties of the material on the seafloor. The resolution of these back-scatter images and the penetration depth of the acoustic beam, and thus the depth interval over which the backscatter image is averaged, depends on the frequency used by the sidescan sonar instrument. The IFM-GEOMAR DTS-1 system comprises a high-resolution dual-frequency deep-towed sidescan sonar instrument (DTS-1) and a sub-bottom profiler (Fig. 6.2.2).

DTS-1 uses a dual-frequency, chirp sidescan sonar (EdgeTech Full-Spectrum) working with centre frequencies of 75 and 410 kHz. The pulse emitted by the 410-kHz sidescan sonar has a bandwidth of 40 kHz and a duration of 2.4 ms (resulting in a range resolution of 1.8 cm), while the 75 kHz sidescan sonar offers a choice between two pulses with bandwidths of 7.5 or 2 kHz and pulse lengths of 14 or 50 ms, respectively. They provide a maximum across-track resolution of 10 cm. As the system is towed at speeds of of 2.5 to 3.0 kn and has a range of 750 m, maximum along-track resolution is on the order of 0.75 m. In addition to the sidescan sonar sensors, the DTS-1 contains a 2 - 16 kHz, chirp sub-bottom profiler providing a choice of three different pulses, each of them with a pulse length of 20 ms. A 2 - 10 kHz pulse, a 2 - 12 kHz pulse and a 2 - 15 kHz pulse render a nominal vertical resolution between 6 and 10 cm. The sidescan sonar and the sub-bottom profiler can be run with different trigger modes, namely internal, external, coupled and gated triggers. The coupled and gated trigger modes also allow to specify trigger delays. The sonar electronics provide four serial ports (RS232)

for additional sensors (Fig. 6.2.3). One of these ports is used for a Honeywell attitude sensor providing information on heading, roll and pitch. A second one is used to read depth information from an external pressure sensor. Finally, there is the possibility of recording data directly in the underwater unit through a mass-storage option with a total storage capacity of 60 GByte.

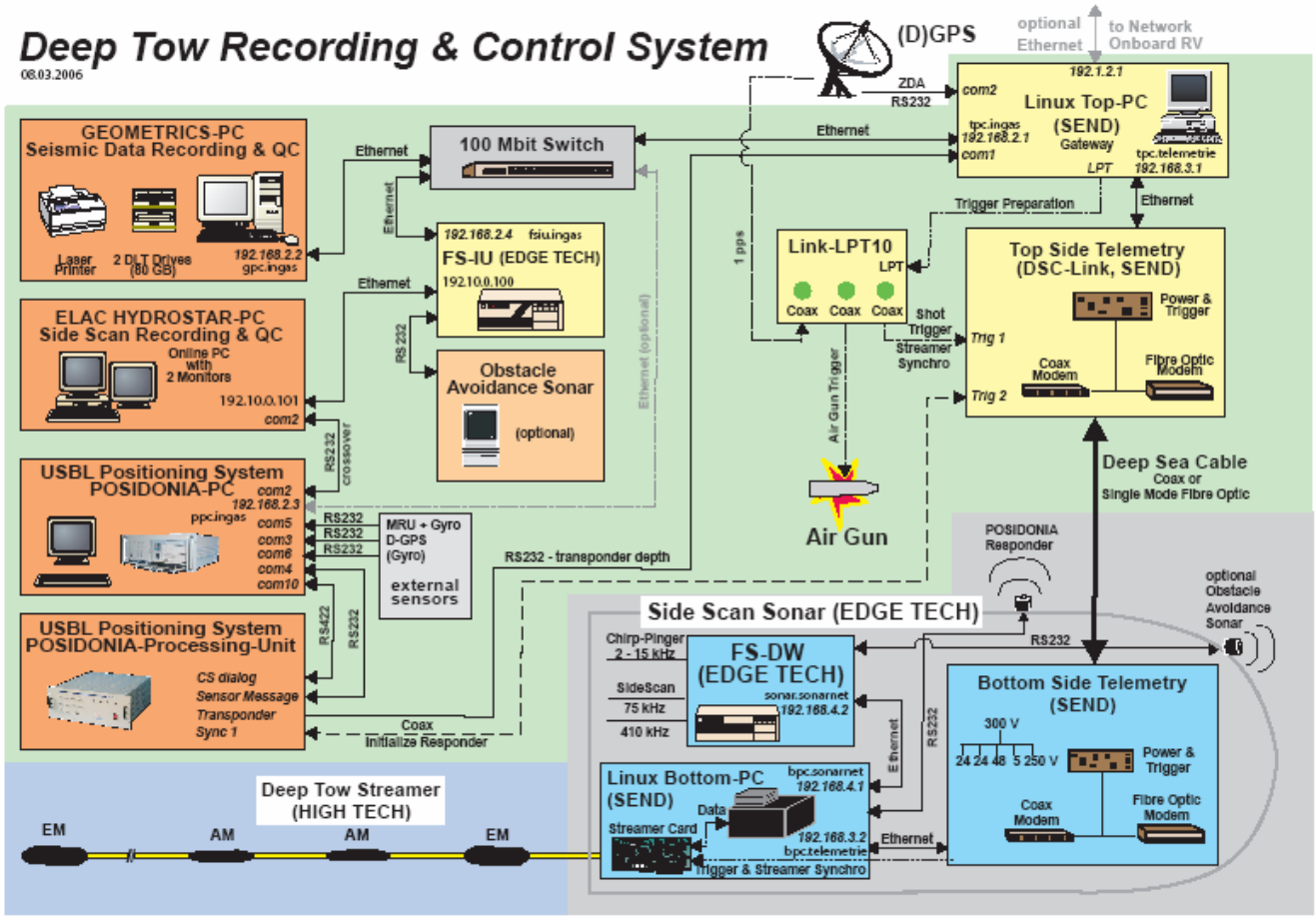

Figure 6.2.3: *Drawing of the single modules of the system and the network connections*

The streamer is a modular digital seismic array (HTI, High Tech Inc..) which can be operated at water depths of up to 6000 m (Fig. 6.2.2). It consists of 26 single hydrophone channels towed behind the sidescan sonar fish. Two different types of modules - acoustic and engineering - exist. Each acoustic module (AM) houses a single hydrophone and a low- and high-cut filter, pre-amplifier and 24-bit AD converter in a pressure vessel. Special engineering modules (EM) additionally include a compass, a pressure sensor and a motion sensor (Crossbow) which provide information on the depth of the module below the sea surface, on its geographical position (magnetic heading) and on its roll and pitch during the survey. Modules are interchangeable and can be connected arbitrarily by cables of 1 or 6.5 m length. A sample interval of 2.5 ms and pre-amplifier gains between 0 - 36 dB respectively as well as two different high-pass filters with a low-cut frequency of 4 Hz allow the use of high-frequency seismic sources to guarantee both a very high vertical and lateral resolution. Geographic and depth position values for each node will be calculated in a post processing procedure which makes use of the absolute tow fish position information provided by the ultra-short-baseline (USBL) navigation system POSIDONIA (iXSea) described in chapter 5.5.

The sonar electronics (Edge Tech), the underwater part of the telemetry system (SEND DSC-Link) and the Linux-based Bottom PC (SEND) of the seismic streamer data acquisition system are stored in two titanium pressure housings in the tow fish (Fig. 5.2.3). In addition, a releaser capable of working with the USBL positioning system POSIDONIA (iXSea) with a separate transducer, and an emergency flash and sender (Novatech) are included in the tow-fish.

The towfish is connected to the deep sea cable by a 40-m-long umbilical cable via a two-ton depressor (Fig. 6.2.1 and 6.2.2). The umbilical cable is tied to a buoyant rope that takes the actual towing forces. An additional rope is taped to the buoyant rope and serves to pull in the instrument during recovery.

The deep tow recording and control system consists of a top and a bottom side part (Fig. 6.2.3). The top side part includes a Linux-based Top PC (SEND), a DSC Link (SEND) as top side part of the telemetry system, the Full Spectrum Interface Unit (FS-IU) of the sidescan sonar system (Edge Tech) and two PCs running the HydroStar Online (ELAC) and the Geometrics StrataVisor NX (GEOMETRICS) software for deep tow sidescan sonar and multi-channel seismic online data recording and quality control. Another Win2000 PC runs the USBL positioning system POSIDONIA (see chapter 6.5) for online recording and display of the measured positions of the sidescan sonar tow fish.

At the bottom side a Linux-based PC (BPC) with a storage capacity of 120 GB and the underwater part of the telemetry system (SEND) are installed in a pressure-proof housing mounted in the sidescan sonar fish (Fig. 6.2.3). The BPC handles the data transfer between underwater and onboard systems while the telemetry provides all necessary power supplies for the bottom electronics. Additionally, the Full Spectrum Deep Water (FS-DW) part of the sidescan sonar system (Edge Tech) is installed in a second pressure vessel mounted in the sidescan sonar fish, too.

The deep-towed seismic streamer and side scan sonar system can be controlled completely from the top side by the Linux-based Top PC (TPC) and the dedicated HydroStar PC (Fig. 6.2.3). Seismic and sidescan sonar data are stored both underwater on the Linux-based Bottom PC and the FS-DW as well as onboard by the PCs running the HydroStar Online (on hard disk) and the Geometrics StrataVisor NX software (on two DLT 8000). Commands which control the seismic recording parameters like sample interval, record length, delay, filter or pre-amplifier gain, and which initialize the data transfer between underwater and onboard systems, are sent from the top to the bottom side, whereas seismic and sidescan sonar data are transferred from the underwater to the top side via telemetry through a coaxial or fibre optic deep sea cable.

All seismic bottom and top side components as well as air gun shooting are synchronized by D-GPS time-based trigger signals generated by the Linux Top-PC via the LPT10 link. The Linux Top-PC also acts as a router for the Ethernet connection through the deep sea telemetry.

6.3 Magnetometer

Petersen, J.

During cruise M67-1 magnetic data were acquired using a GeoMetrics G801/3 Marine Proton Precession Magnetometer. The system consists of a control unit and a gasoline-filled sensor attached to a 200-m-long marine cable. To measure the earth magnetic total field, the control unit first generates an electric current in the sensor coil resulting in a strong magnetic field. The magnetic spins of the protons in the gasoline align parallel to this magnetic field. In the following, the magnetic field is removed by switching the electric current off, causing the magnetic spins to realign with the earth magnetic field. During this realignment they are preceding around the earth magnetic field vector with the precession frequency being directly proportional to the intensity of the geomagnetic field. The precession frequency is measured as an AC electric current generated by magnetic induction in the coil, which is then amplified and transformed into total magnetic field values measured in nT (1 nT = 10^{-9} Tesla).

The sensor is towed approximately 180 m behind the ship to minimize magnetic disturbances due to the magnetization of the ship hull. Thus, a resolution of the magnetic measurements of about 5 nT is achieved.

The measured total magnetic field values were displayed on a console and written as digital output coded in BCD values. The system was set to deliver one data value every 3 seconds, which was stored in an ASCII table together with the UTC time.

On board of R/V METEOR, the magnetometer winch was positioned on the starboard side at the stern. During deployment the cable was guided through a block centered in the A-frame.

6.4 Gravity Corer and Analytical Facilities

Hensen, C., Harders, R., Mavromatis, V.

Surface sediments were taken using a gravity corer (GC). As soon as cores arrived on deck, they were cut into 1-m-long segments and sampled at both ends for subsequent hydrocarbon gas analyses. To prevent a warming of the sediments after retrieval all cores were immediately placed in a cooling room and maintained at a temperature of about 5°C. The core segments were then split into archive and work halves. Work halves were immediately sampled for further geochemical analysis. Sediment characteristics of the archive halves were described using the Munsell Color Chart and lithology classification. Photographs of 1-m-long sediment segments and close-up photographies of particular features were taken with a Sigma SD10 Camera. For sediment properties such as water content and density, metal cylinders of 2 cm x 4 cm were used to take a sediment sample from the middle of each segment. The samples were weighed prior and after drying (at 60 °C for 3 days) to measure the average water content.

Sample intervals between 10-50 cm were taken for pressure filtration. At sampling locations where a presence of methane was expected, syringe samples were taken on deck from every cut segment surface. Occasionally, higher resolution sampling for methane analysis was carried out in the cooling laboratory. Syringe samples of ~5 ml sediment were injected into 24-ml septum vials containing 9 ml of a concentrated NaCl-solution. Pore water was

separated from the sediments using PE squeezers. The squeezers were operated with argon at a pressure gradually increasing to up to 5 bar. Depending on the porosity and compressibility of the sediments, up to 30 ml of pore water were received from each sample. The pore water was retrieved through 0.2 µm cellulose acetate membrane filters.

Dissolved phosphate, silica, ammonia, and sulphide were determined in the pore water samples using standard photometric procedures (i.e. Grasshoff, 1997). Subsamples for nutrient analysis were taken and purged with N_2 gas for 90 minutes to remove dissolved sulphide prior to analysis. Total alkalinity (TA) was determined by titration with 0.02 N HCl. Most of the samples were also analyzed for dissolved chloride using argentometric titration in order to control the IC results. Acidified subsamples (35µl suprapure HCl + 3 ml sample) were prepared for ICP analyses of major ions (K, Li, B, Mg, Ca, Sr, Mn, Br, and I) and trace elements. Methane, sulfate, DIC, $\delta^{18}O$ and $\delta^{13}C$ of CO_2 will be determined on selected subsamples in the shore-based laboratories.

6.5 POSIDONIA USBL System

Bialas, J., Bürk, D., Petersen, J.

Underwater navigation of the sidescan sonar tow fish and determination of its depth and position are enabled by the POSIDONIA ultra-short base line (USBL) system (iXSea). POSIDONIA mainly consists of a deployable acoustic array (antenna) installed in the moon-pool (Fig. 6.5.1) and a transponder with a remote transducer mounted on the side scan sonar fish (Fig. 6.2.3). Either the responder function is triggered via cable link through a coaxial or fibre-optic deep sea cable transmitted via the telemetry system or transponder mode is used, triggering by acoustic signal through the acoustic array.

Figure 6.5.1: *Photography taken during mounting the mobile antenna in the moon pool*

The USBL positioning principle of the POSIDONIA system is based on a bi-directional exchange of submarine acoustic signals between one or several acoustic transponders and the acoustic array, which consists of one transmission transducer and two pairs of hydrophones Together with the D-GPS, gyro compass and motion sensor (MRU) information provided by the ship, the POSIDONIA system allows determination of the depth and position of the side-scan sonar fish. An absolute accuracy of 0.5 - 1% of the water depth is obtained if the side-scan sonar fish's position is within a cone of 60° or 120° opening angle. Within a cone of 140° or 170° opening angle the accuracy is 2 - 5%.

The POSIDONIA positioning system can be run in two different tracking modes, namely free mode tracking and towed fish mode tracking. In free mode all four hydrophones are used to calculate the position of the transponder. In towed fish mode only the hydrophones aligned with the towed vehicle are used together with depth information provided by a depth sensor of the transponder mounted on the towfish.

As the POSIDONIA antenna is not fixed to the hull of the ship, the antenna has to be calibrated prior to operation. Before calibration the offset of the deployed acoustic array relative to the position of the D-GPS receiver has to be introduced into the processing system. For the calibration measurement an acoustic transponder has to be moored on the seafloor at water depths ranging from 1000 - 2000 metres. The ship will then sail a figure of eight above the mooring point in order to interrogate the transponder at any angle and from either side of the vessel (Fig. 6.5.2). After the ship has sailed this calibration curve the POSIDONIA software calculates correction factors of roll, pitch and yaw for correct positioning of the transponder. Filters are set in order to eliminate bad navigation points from the final data file. The under-water navigation can thus be smoothed, a feature particularly interesting for towed instruments.

Based on the geographical positions of the sidescan sonar tow fish (POSIDONIA transponder position) determined by the POSIDONIA system, the (magnetic) heading values measured by the engineering nodes (EM's) of the streamer and and the D-GPS data provided by the ship's antenna, the geographical positions of each streamer node as well as the seismic source can be determined at each shot trigger time by temporal and spatial interpolation of the D-GPS, POSIDONIA and engineering data sets.

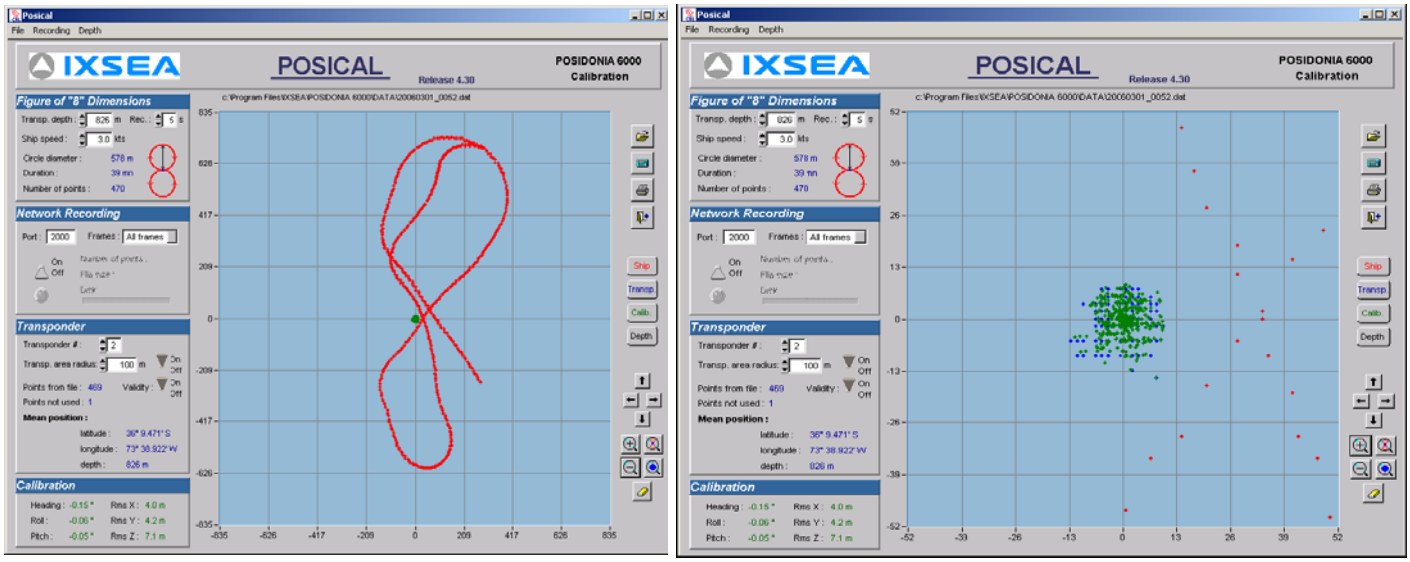

Figure 6.5.2: *Screen shot of the calibration procedure*
Left: Red points indicate the ship's positions during the calibration measurement
Right: Blow-up of the transponder location, blue points indicate positions before calibration, green points indicate positions after calibration. This screen shot was taken after the second calibration run, hence the positions after calibration do not differ much from those before

Prior to the calibration a water sound velocity profile from a previous calibration procedure for the SIMRAD Multibeam Bathymetry system was copied into the POSIDONIA data base. Due to system restrictions on board of METEOR it had not been possible prior to this cruise to extract heading information from the ship's Gyro. Therefore there were no transmission cables to provide the heading information. As a compromise, heading was provided by the D-GPS system for POSIDONIA. When it was tried to calculate the deviation angles for pitch, heave and roll it turned out that the slight delay in heading calculation inside the GPS unit was too large for the calibration procedure. As feeding this information into the ship's motion reference unit was only scheduled for a later time, the Chief Electronic Engineer of R/V METEOR installed additional cables to provide immediate heading information from the Gyro to the motion sensor. Afterwards, the calibration runs for the IFM-GEOMAR mobile system and the hull-mounted METEOR system were repeated and deviation values were successfully calculated.

6.6 KONGSBERG Multibeam Bathymetry Systems

Weinrebe, W.

One of the major upgrades during R/V METEOR's stay at the ASMAR shipyard in Talcahuano was the replacement of the old ATLAS HYDROSWEEP DS multibeam echosounder by new multibeam systems from KONGSBERG MARITIME (formerly SIMRAD). To allow for efficient and economic bathymetric mapping in shallow and in deep water, two systems, a shallow-water EM710 as well as a deep-water EM120 system had been installed. The complete system diagram of both systems as installed on R/V METEOR is shown in Fig. 6.6.1. In addition, the construction of the hull below waterline which holds the transducers was completely modified to achieve a more stable performance of the systems and to reduce the influence of air bubbles on sound transmission, which had been a great problem with the former installation of the HYDROSWEEP transducers that prevented the successful

operation of the system even in moderate weather. Fig. 6.6.2 – fig. 6.6.4 are photographs of the construction of the hull below waterline holding the transducers of the EM120 and of the EM710.

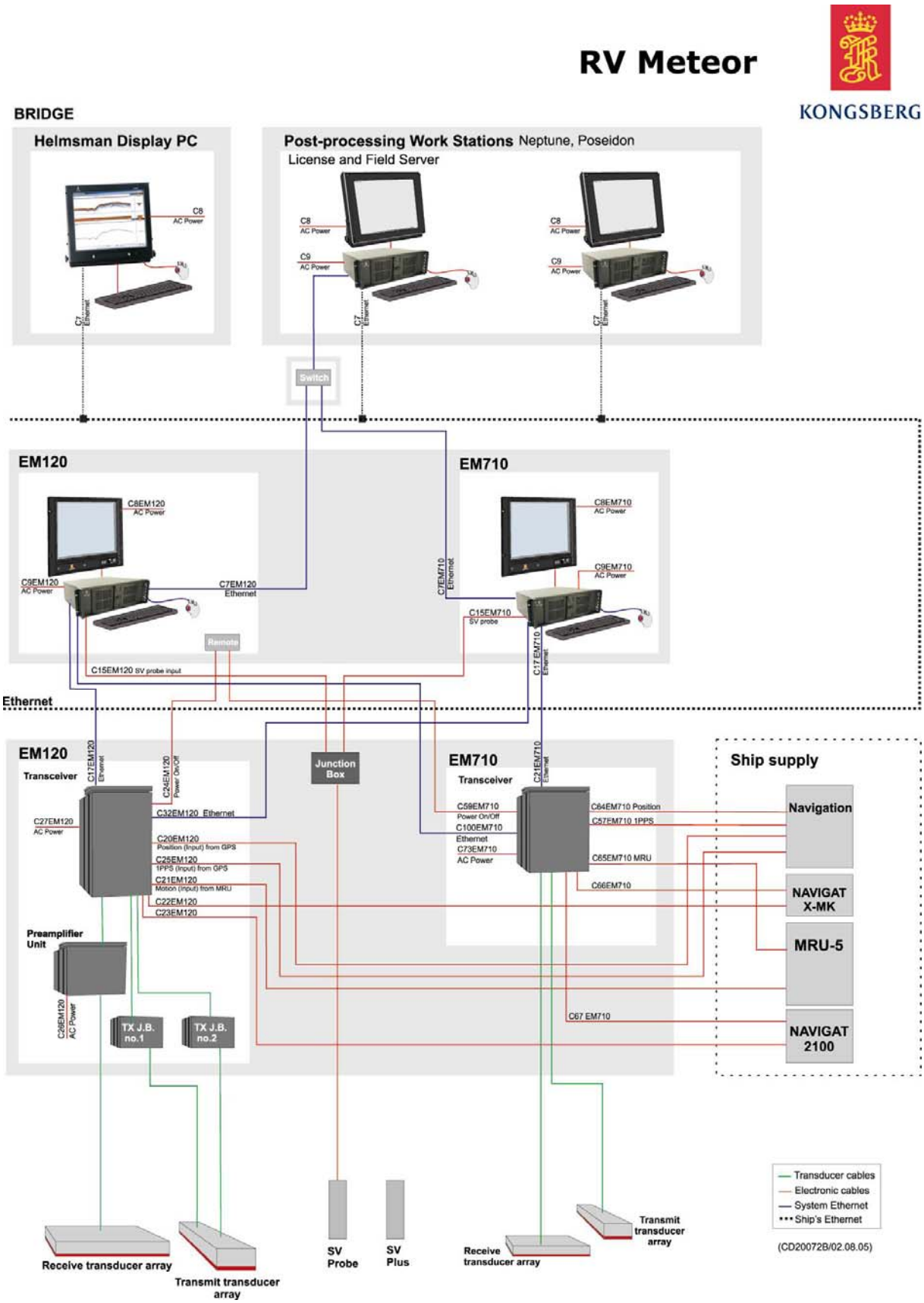

Figure 6.6.1: *System diagram of both Multibeam echosounders on R/V METEOR.*

The EM710 installed is a new 1-by-1-degree broadband multibeam echosounder operating in the 70-kHz to 100-kHz band. It uses CW (continuous wave) pulses in shallow modes and FM (chirp) pulses in deep modes. The maximum water depth for this system is up to 1500 m to 2000 m, however, the most efficient depth range for the EM710 is less than 500 m. In this depth it has a better resolution and a slightly wider swath than the EM120. For greater depths, the EM120 is the system of choice. Several features of the EM710 had not been tested before the cruise and several problems had still to be settled by KONGSBERG. For example, a synchronized operation of both multibeam systems is not yet possible which led to interference with the EM120. As the main area of investigation of cruise M67/1 had water depths of more than 500 m the EM710 was operated only in test mode. Data from the EM710 were not processed and used in this report.

Figure 6.6.2: *METEOR's hull below waterline, construction holding the transmitting (front) and receiving transducer of the EM120*

Figure 6.6.3: *transmitting transducer of the EM120*

Figure 6.6.4: *transmitting and receiving transducer of the EM710*

6.6.1 EM120 System Description

The EM120 system is a deep-water multibeam echosounder providing accurate bathymetric mapping up to full ocean depth. A system overview is presented in Fig. 6.6.1. Basic components of the system are two linear transducer arrays in a Mills cross configuration with separate units for transmitting and receiving. The nominal sonar frequency is 12 kHz with an angular coverage sector of up to 150° and 191 beams per ping. The emission beam is 150° wide across track, and 1° along track direction. The reception is obtained from 191 beams, with widths of 2° across track and 20° along track (Fig. 6.6.5). Thus the actual footprint of a single beam has a dimension of 1° by 2°. The achievable swath width on a flat bottom will normally be up to six times the water depth dependent on the character of the seafloor (Fig. 6.6.6). The angular coverage sector and beam pointing angles may be set to varying automatically with depth according to achievable coverage. This maximizes the number of usable beams. The beam spacing is normally equidistant with equiangle available.

For depth measurements, 191 isolated depth values are obtained perpendicular to the track for each ping. Using the 2-way-travel-time and the beam angle known for each beam, and taking into account the ray bending due to refraction in the water column by sound speed variations, depth is calculated for each beam. A combination of amplitude (for the central beams) and phase (slant beams) is used to provide a measurement accuracy practically independent of the beam pointing angle.

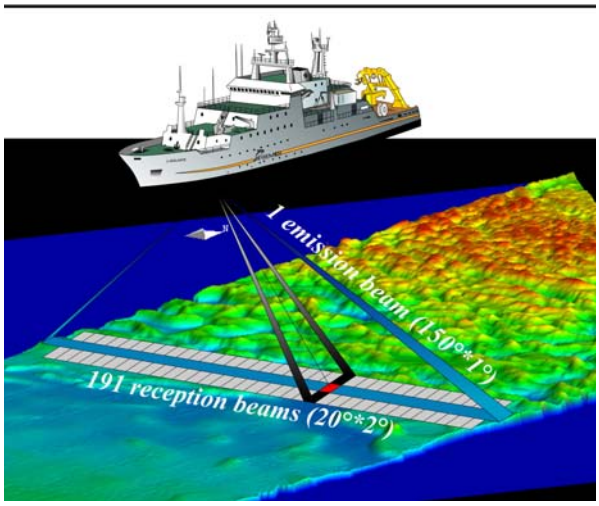

Figure 6.6.5: *Basic principle of multibeam echosounding with EM120*

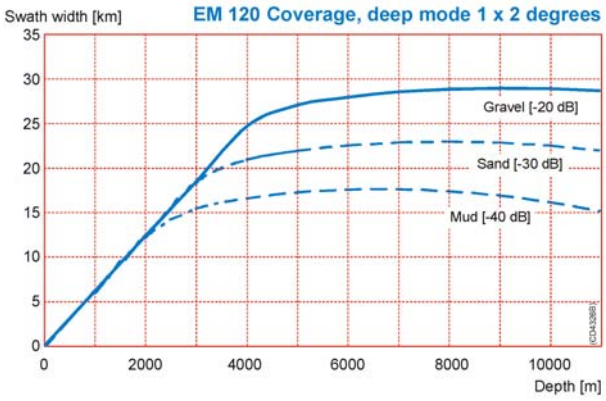

Figure 6.6.6: *Coverage diagram for the EM120*

6.6.2 EM120 Multibeam Data Processing

Processing of multibeam data generally requires two sequences of processing steps: a profile–oriented sequence followed by area-based processing. The profile-oriented processing of the EM120 data comprises the check of navigation data, interpolating missing navigation values, the calculation of water depth and positions of the footprints of the beams by ray tracing through the water-column taking into account the sound velocity profile, and removing artefacts and erroneous data points. Area-based processing comprises the calculation of a digital terrain model (DTM) and the visualisation of the data in various different presentations. For these purposes the NEPTUNE software package from KONGSBERG is available onboard R/V METEOR. However, mainly for easier integration of other data from different systems in various data formats, the “open source software” packages MB-System (Caress and Chayes, 1996) and GMT (Wessel and Smith, 1995) were used for the processing of the multibeam data during M67/1 cruise.

During operation, the data collected by the KONGSBERG EM120 multibeam system is continuously stored on the disks of the operator workstation in a vendor-specific raw-data format. The data is organized in SURVEYS. A survey is initiated by the operator on the operator console. Generally, a new survey was initiated when work was started in a new area . The raw data was copied to the disks of the IFM-GEOMAR workstation coromandel through a Samba-network connection under Windows XP.

In the MB-System software the KONGSBERG vendor-specific raw data format is defined as format 56. Further processing of the data requires the conversion of the data to the MB-System format 57. In addition, some ancillary files have to be created, containing meta information for each file. These files speed up the further processing steps. In MB-System the management of the data is maintained by so-called datalist-files, which contain names, paths, format-ID and a weighting factor for each file. Datalist files can be set up recursively, i.e. entries in a datalist refer to another datalist, which points to the actual data files. This structure helps to keep track of all data files easily, as up to several thousand files can be collected for a normal-sized project. For the M67/1 cruise, the number of raw data files just of the main

investigation area sums up to more than 1100. The conversion of format, the creation of ancillary files and the setup or updating of the respective datalist files is accomplished by the script

```
prepare_work.sh <cruise> <survey_name>.
```

Two steps follow in the processing sequence which have to be carried out interactively. The cleaning of the raw data by flagging outliers and artefacts os done with the programme

```
mbedit –F57 -I<filename>
```

for each of the raw data files. This is a quite time-consuming step, requiring careful inspection of all pings and beams in each raw data file. Subsequently, the navigation has to be checked interactively with the programme

```
mbnavedit –F57 -I<filename>
```

for each raw data file. The interactive editor programmes do not change the data files, they only store the edit instructions to a file. Following the interactive editing, the data files are actually updated by a call to the programme

```
mbprocess –F-1 -I<datalist file>
```

Any intended further data processing step, e.g. application of a different water sound velocity profile or additional roll- or pitch- bias correction, is accomplished by parameter files. The programme mbprocess checks the existence of an adjunct parameter file for each data file and takes the instructions contained therein into account during processing. After successful completion of mbprocess the profile-oriented data processing is finished.

An area in the context of “area based multibeam data processing” is a rectangular survey area defined by its geographical coordinates (minimum and maximum latitude, minimum and maximum longitude). All processed multibeam data that fall within this box will be integrated in the calculation of a digital terrain model (DTM) for this survey area. For each survey area a directory with its name is created. Key parameters for a survey area (name, boundaries, scale) are stored in the file .hsdefaults in that directory. The access to the processed data files is accomplished by a datalist file, as already introduced above. For the calculation of the DTM of the area the script

```
process.cmd
```

is executed. The DTM is represented by a regular grid. Basic parameters for the DTM calculation are the name of the datalist-file and the grid size in latitude and longitude as well as the number of grid cells without data, which will be filled by interpolation.

The basic script for the presentation of the DTM is

```
fig_bathy.cmd
```

which follows the successful calculation of the DTM. Different presentation modes (isocontours, colour coded, colour coded with illumination and combinations) are available (c.f. comments in the scripts, appendix 6, for a complete description).

6.7 ATLAS PARASOUND DS-3

Talukder, A.

During cruise M67/1, along with the multibeam bathymetric survey, PARASOUND sub-bottom profilings were carried out using the ATLAS PARASOUND for simultaneous scanning of the ocean bottom to sub-bottom. The total PARASOUND operation time was approximately 200 hours.

ATLAS PARASOUND is ATLAS Hydrographic's next generation hull-mounted parametric sub-bottom profiler. It offers rapid high-resolution sub-bottom and water column analyses at a maximum operational speed of15 knots. The system utilizes the parametric effect to generate a very low-frequency secondary signal by emitting two primary signals of higher frequencies. The parametric secondary signal incorporates the high spatial resolution of the primary source signals for maximum measurement accuracy with the low frequency for maximum penetration and range. In deep sea conditions, it can penetrate to depths of up to 200 m and more and samples data with a frequency of up to 50 kHz. Through digital pulse modulation, optimum signal-to-noise ratios can be achieved. Chirp and Barker code modulations are available as standard.

In single-beam sub-bottom profiling mode, ATLAS PARASOUND uses transmission beam steering to calculated bottom slopes, so that the beam hits the bottom almost orthogonally. This way, echo amplitudes are increased substantially.

As can be seen in Figure 6.7.1, the major component groups are the transducer array, the analog electronic unit (AEU), the digital electronic Unit (DEU), the control and survey management software package ATLAS Hydrographic Processing Suite and the advanced scientific visualisation and processing package ATLAS Parastore-3. Two versions of ATLAS PARASOUND are available: ATLAS PARASOUND P70 and P35.

6.7.1. Transducer Design

The flat hydroacoustic transducer array of ATLAS PARASOUND is subdivided into modules. Two different types of modules are available:

- The transducer array of version P70 consists of four indentical transducer modules, each having dimensions of approximately 0.3 m x 1.0 m. This version contains 384 acoustic elements combined to form 128 stave channels.
- The transducer array of version P35 consists of two indentical transducer modules each having dimensions of approximately 0.6 m x 1.0 m. This version offers a total of 192 acoustic elements combined to form 96 stave channels.

6.7.2 Electronics

Depending on the configuration of the transducer, the AEU consits of up to four transission capacitor modules and eight transceiver blocks. Four A/D conversion boards handle the 24-bit quantization. The DEU houses the echosounder's control module and the reception signal processing module as well as the power supply.

6.7. 3 Software Configuration

The ATLAS hydrographic processing suite is ATLAS Hydrographic's universal survey management and echosounder control software. ATLAS Parastore-3 is a highly sophisticated visualisation, acquisition and processing package, specialized for ATLAS PARASOUND. With its multi-window graphical use interface, the software allows differentiated investigations on sub-bottom and water column details. Both software packages communicate with ATLAS PARASOUND via the local area network and can also be run several times in parallel accessing the same sensor. In this way redundant data recording for independent applications or additional remote operator stations can be made available very easily upon request.

During our survey, a transducer of version P70 was used with a sampling rate of 4 kHz. The maximum penetration achieved was ca. 50 m.

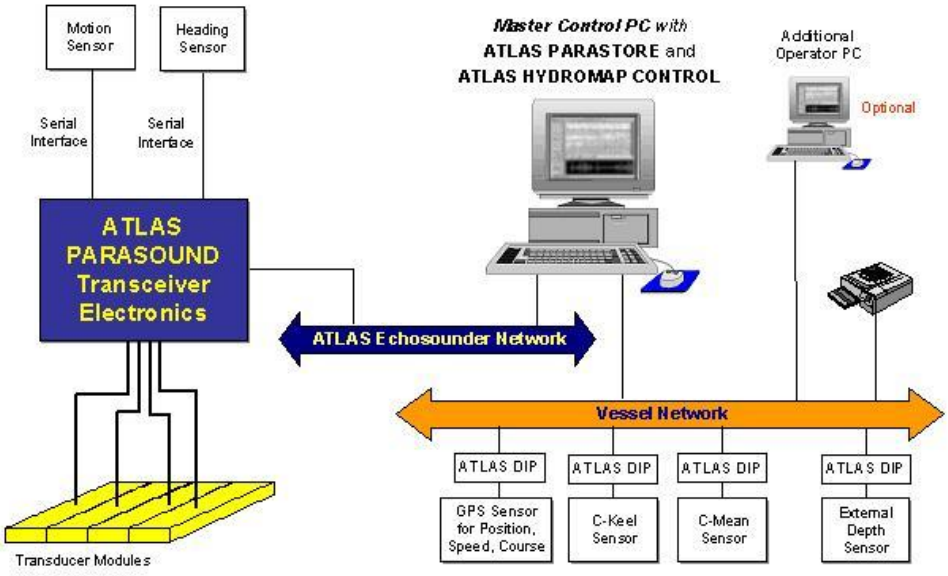

Figure 6.7.1: *ATLAS PARASOUND hull mounted echosounder layout*

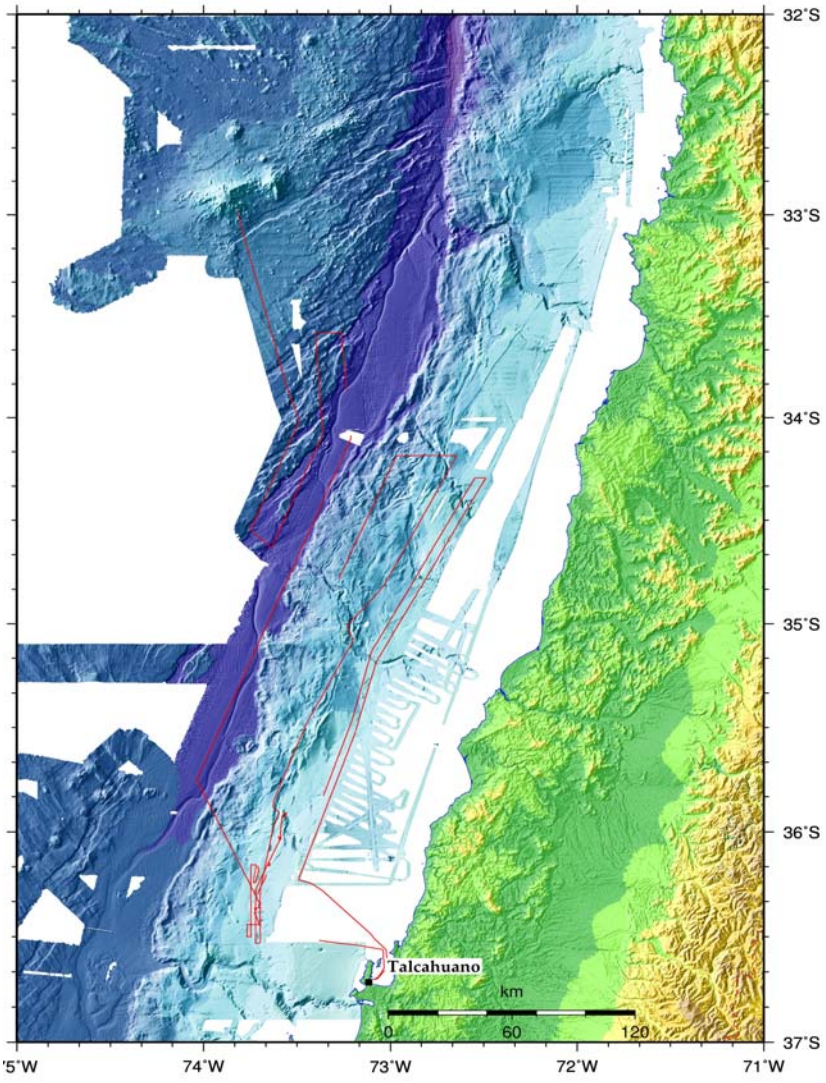

Figure 6.7.2:
PARASOUND profile track

7. Work Performed and First Results

7.1 Multibeam Bathymetric Mapping

Ranero, C. R. and Weinrebe, W.

Mapping goals were to cover the area where two distinct transitions in structure occur. A major change in oceanic plate structure and in margin tectonic structure occurs where the Juan Fernández Ridge collides with the continent. This major discontinuity had been studied with the data collected between 32°S-34°S during Sonne 101 (e.g. von Huene et al., 1997), but those data did not cover the entire extension of the discontinuity. Neither was the evolution of the structure south of the collision zone known.

In spite of the limited time available for mapping, the new data provides a fairly complete view of the lower continental slope, some parts of the middle slope, as well as much of the trench axis (Figs. 7.1.1a, 7.1.1b, and 7.1.1c).

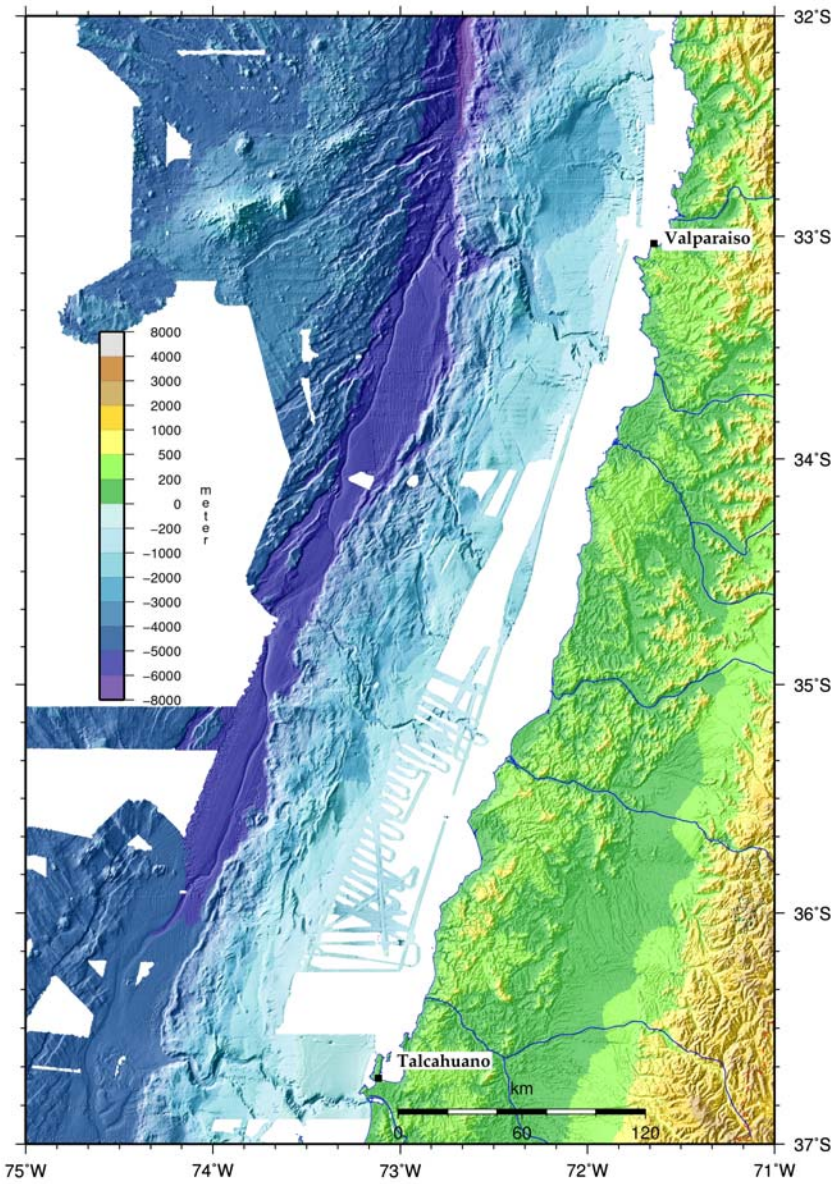

Figure 7.1.1a: *Colour- coded, shaded relief map of the topography and bathymetry comprising the study area*

The existing gaps in coverage on the oceanic plate and the upper continental slope were little mapped due to time constraints. New lines were strategically located to take advantage of data collected on transit lines of previous cruises (SONNE 161 and 181). However, using data from those transit tracks is problematic because they may degrade the quality of the final grid, as they were collected with low quality standards (e.g. high ship speeds, no sound velocity profile available) and in cases even without watchkeeping for quality control (e.g. SONNE 181).

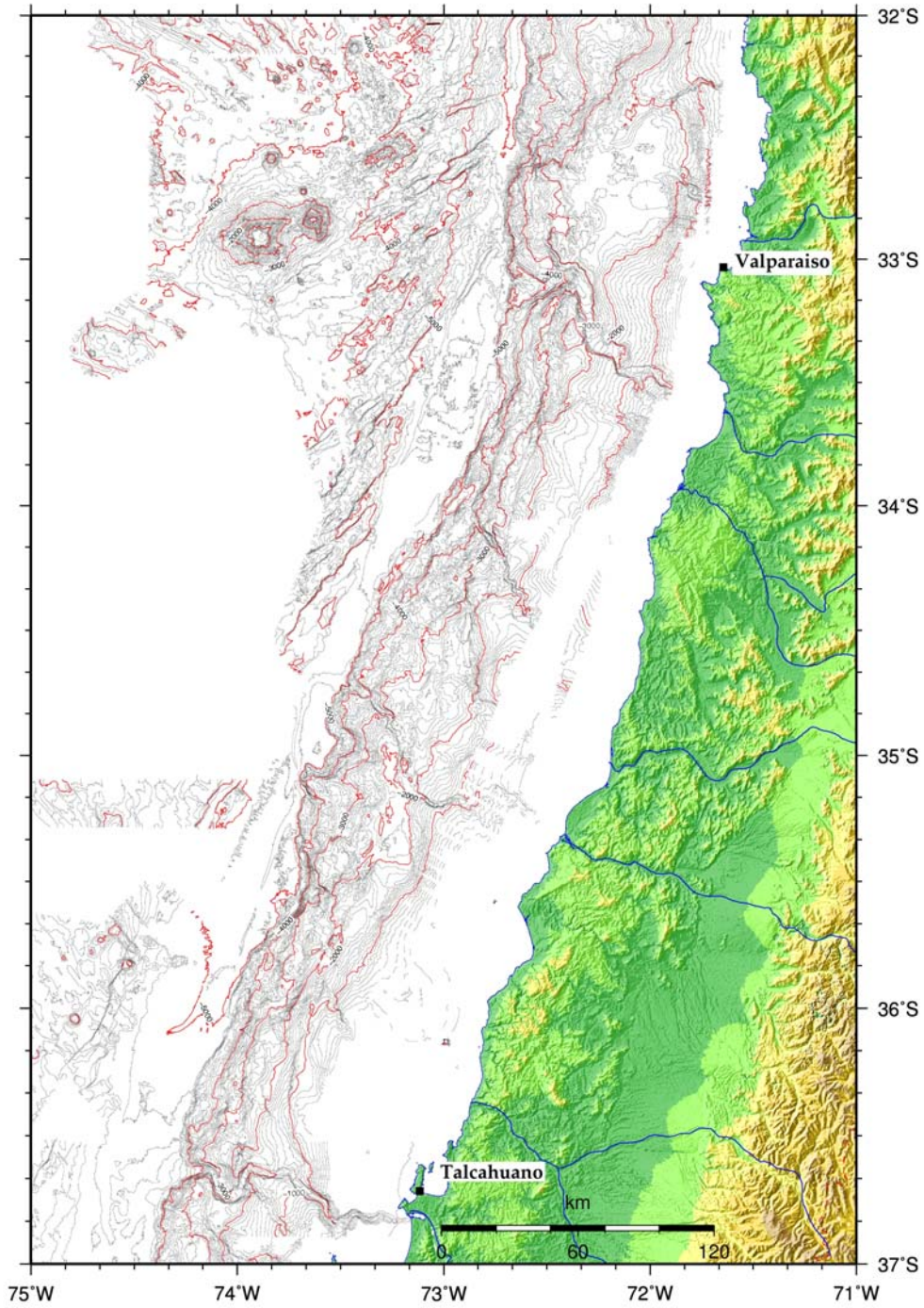

Figure 7.1.1.b: *Contour map of the bathymetry comprising the study area, and coloured coded, shaded relief map of the topography*

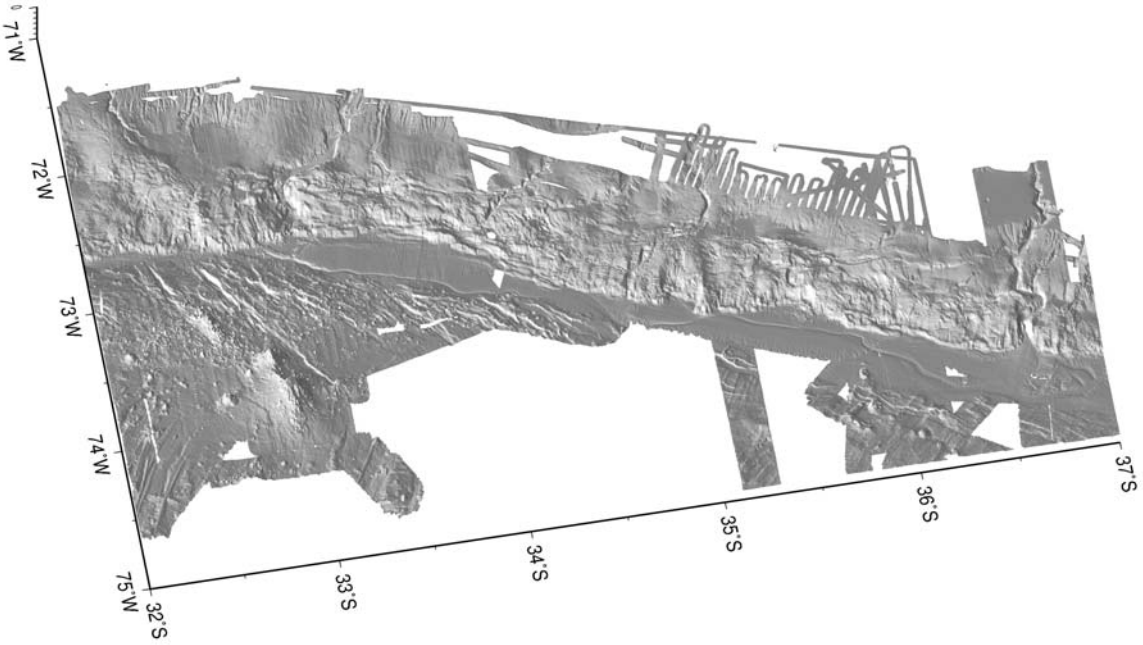

Figure 7.1.1c: *Shaded relief perspective view of the bathymetry, comprising the study area, south of the collision zone of the Juan Fernández Ridge*

7.1.1. Structural Overview

The new data partially fills the coverage gap between the CONDOR cruise SONNE 101 data from 32°S-34°S and the SPOC cruise SONNE 161 south of ~35.5°S (Figs. 7.1.1a, 7.1.1b, and 7.1.1c). The data from CONDOR shows the transition from a sediment-starved trench and a continental margin dominated by subduction erosion, both located from the collision zone of Juan Fernández Ridge to the north, to a segment where a shallower and broader trench axis is flooded with turbidites south of ~33°S (see chapter 2.2 for a more detailed description of this area). The data from SPOC shows a series of ridges at the trench, similar to the accretionary ridges of the CONDOR area, albeit smaller in scale. The new METEOR 67-1 data shows an irregular slope toe facing the flooded trench, however, a well-developed system of accretionary ridges is lacking (Figs. 7.1.1a, 7.1.1b, and 7.1.1c).

The smooth morphology of the trench gradually increases in depth from south to north, and is disrupted by a fairly continuous meandering channel that distributes turbidites along the trench. The channel stops close to the collision zone of the Juan Fernández Ridge where turbiditic infill also decreases abruptly.

Irrespective of the detailed structure of each segment of the continental margin, the continental slope systematically displays three different regions. The lower slope typically displays a rugged terrain that gives way upslope to a series of smooth terraces probably representing mid-slope basins. Across a moderate change in slope dip, sometimes associated to a steeper segment carved by small canyons and rills. the middle slope grades into the upper slope, which, where mapped, displays a smooth morphology and gentle dips (Fig. 7.1.1c). The threefold morphology of the slope from a rugged slope toe to a smooth upper slope appears to

indicate that each of them corresponds to a different degree of tectonic activity and that in general stability increases upslope.

The continental slope is cut by several prominent canyons that meander traversing across other morphological fabric of the slope. In some cases, they produce deep-sea turbiditic fans at the trench opposite the mouth of the canyon (e.g. Bio-Bio canyon at ~36°45'S). Where mapped, canyons extend to close to the shore at locations where the mouths of large rivers bring weathering products from the Andes (Figs. 7.1.1a, 7.1.1b, and 7.1.1c).

The new data also provides partial coverage of the area of the trench where bending-related deformation of the oceanic plate takes place prior to subduction. In particular, the new data cover some of the region between 33°S to 34°S where bend-faulting parallel to the Juan Fernández Ridge (Ranero et al., 2005) seems to be less important and most faulting occurs at trench-parallel structures.

7.1.2 The Transition from Erosion to Accretion

The transition from a margin dominated by tectonic erosion to a margin dominated by accretion corresponds to the change in turbidite infill at the trench, which in turn is controlled by the topography of the subducting plate and has been discussed in detail in chapter 2.2. The new data show that the change in trench infill corresponds to the change in bending-related faulting style on the ocean plate from hotspot ridge-parallel faulting to trench-parallel faulting, supporting that trench infill is controlled in detail by the amount of bending of the subducting plate (Fig. 7.1.2). Surprisingly, across the newly mapped area (up to ~34.5°S), the oceanic plate displays numerous small volcanic cones probably similar to those around the crest of the Juan Fernández Ridge (Figs. 7.1.1a and 7.1.2) and thus probably also created by the hotspot activity, but the plate was actually little modified by volcanism in this area.

The area of currently active accretion is located south of 33°10', and is well displayed by a series of low ridges that are parallel to the slope toe forming gentle structures in the otherwise smooth trench floor morphology. The ridges correspond to the roof of anticlines that are rooted by thrust faults cutting the trench infill and frontally accreting sediment into a growing accretionary prism (Figs. 7.1.1a and 7.1.2).

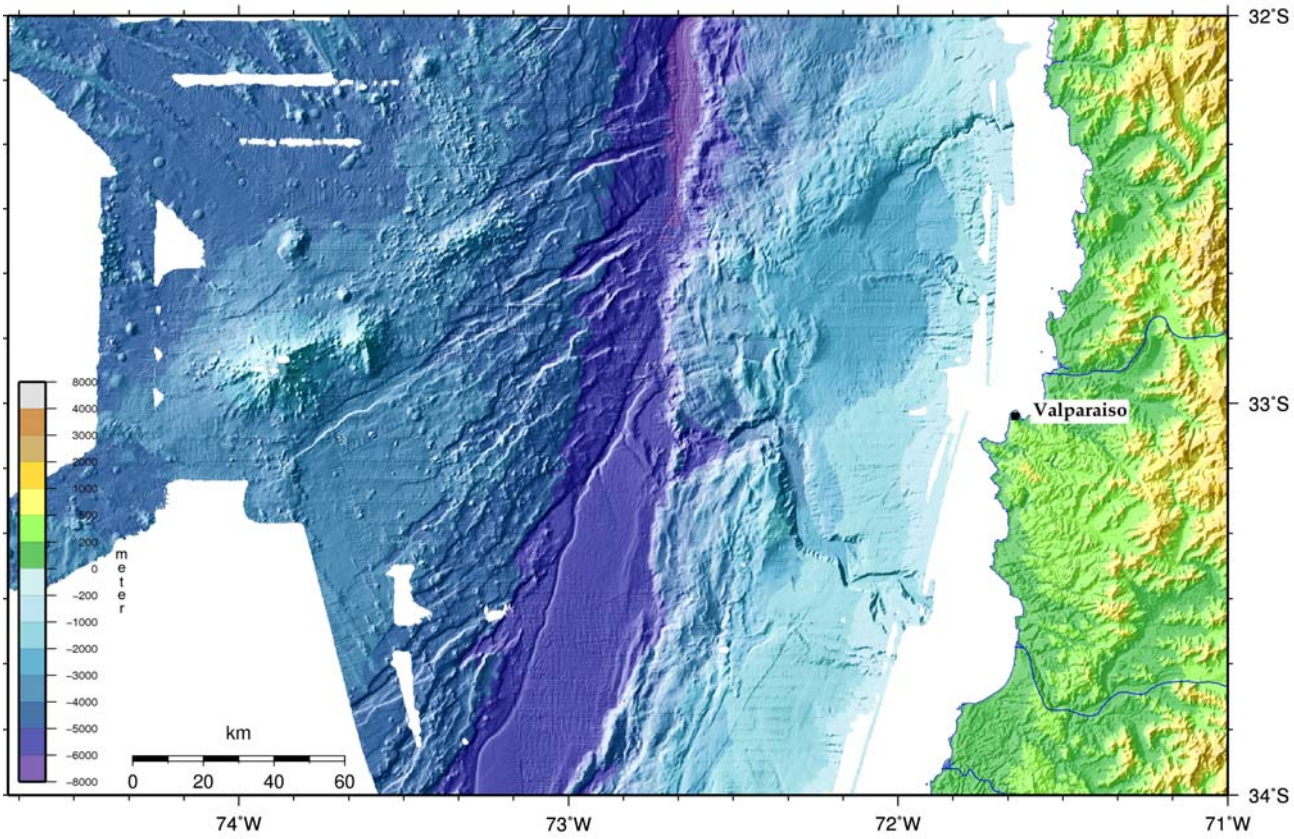

Figure 7.1.2: *Colour-coded, shaded relief map of the topography and bathymetry of the area of transition from the narrow, sediment-starved trench to the turbidite-flooded trench*

7.1.3 The Trench Flooded Segment

Active accretion of trench turbidites, clearly indicated by the morphology of the ridges, occurs from ~33°10’ to ~34°20’. Southwards of ~34°20’ the ridges parallel to and seawards of the slope toe suddenly die out (Figs. 7.1.3a and 7.1.3b). The ridges do not only occur at the trench seawards of the slope toe, but older ridges run en-echelon along much of the lower slope. Similar to the ridges seawards of the slope toe, the lower slope terrain structure changes south of ~34°20’S and no old en-echelon ridges are observed in the morphology. This abrupt change in lower slope morphology does not correspond to any apparent change in trench sediment infill, thus this noticeable lack of accretionary ridges is surprising (Figs. 7.1.3a and 7.1.3b). South of ~35°10’S two en-echelon ridges define the slope toe, suggesting limited recent accretion (Figs. 7.1.4 and 7.1.5), but there is no clear evidence of deformation of the smooth surface of the trench indicative of incipient thrusting (Fig. 7.1.5).

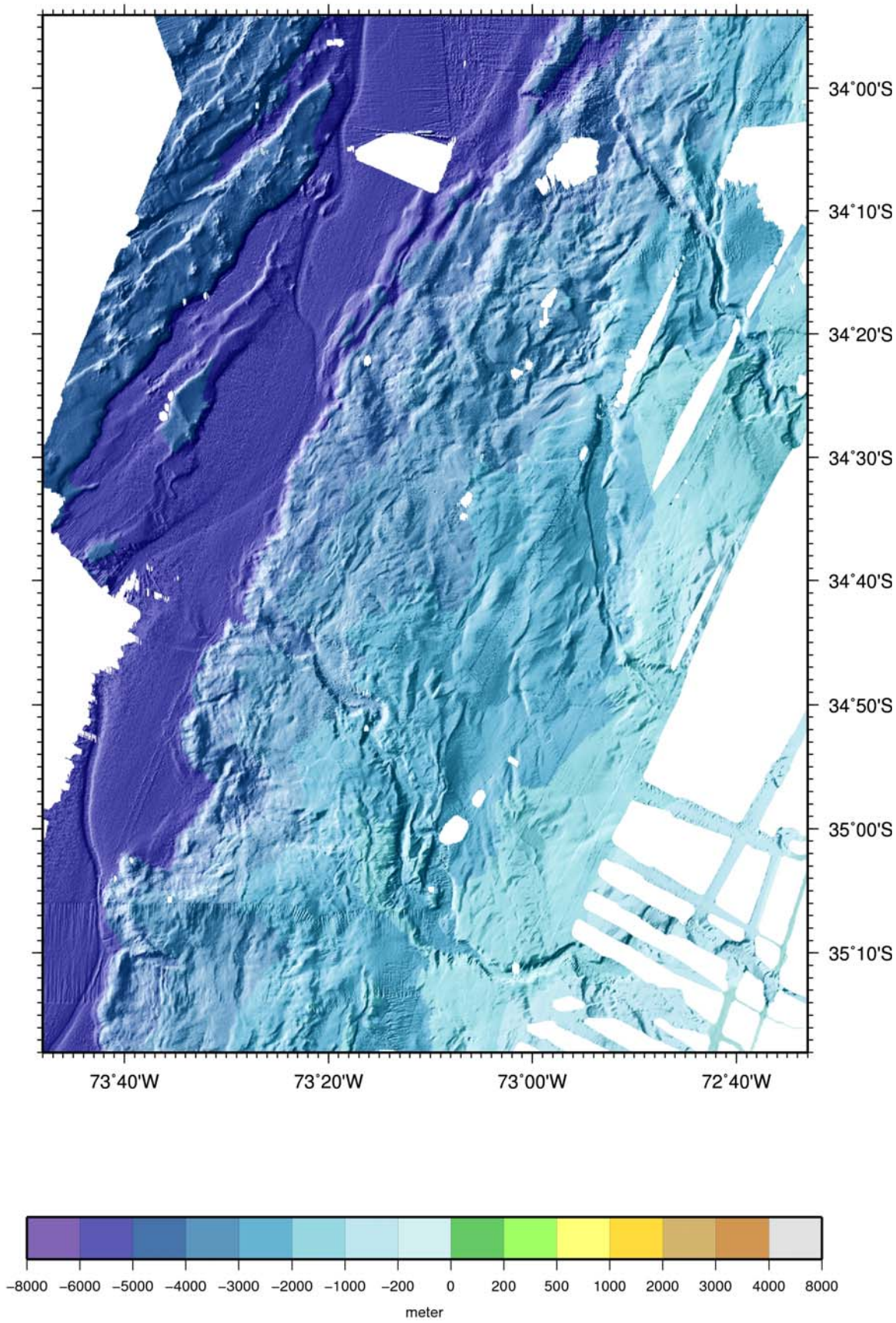

Figure 7.1.3a: *Colour-coded, shaded relief map of the bathymetry of the northern sector of the study area showing the transition from a lower slope with numerous 'en-echelon' accretionary ridges to the sector lacking clear accretionary ridges*

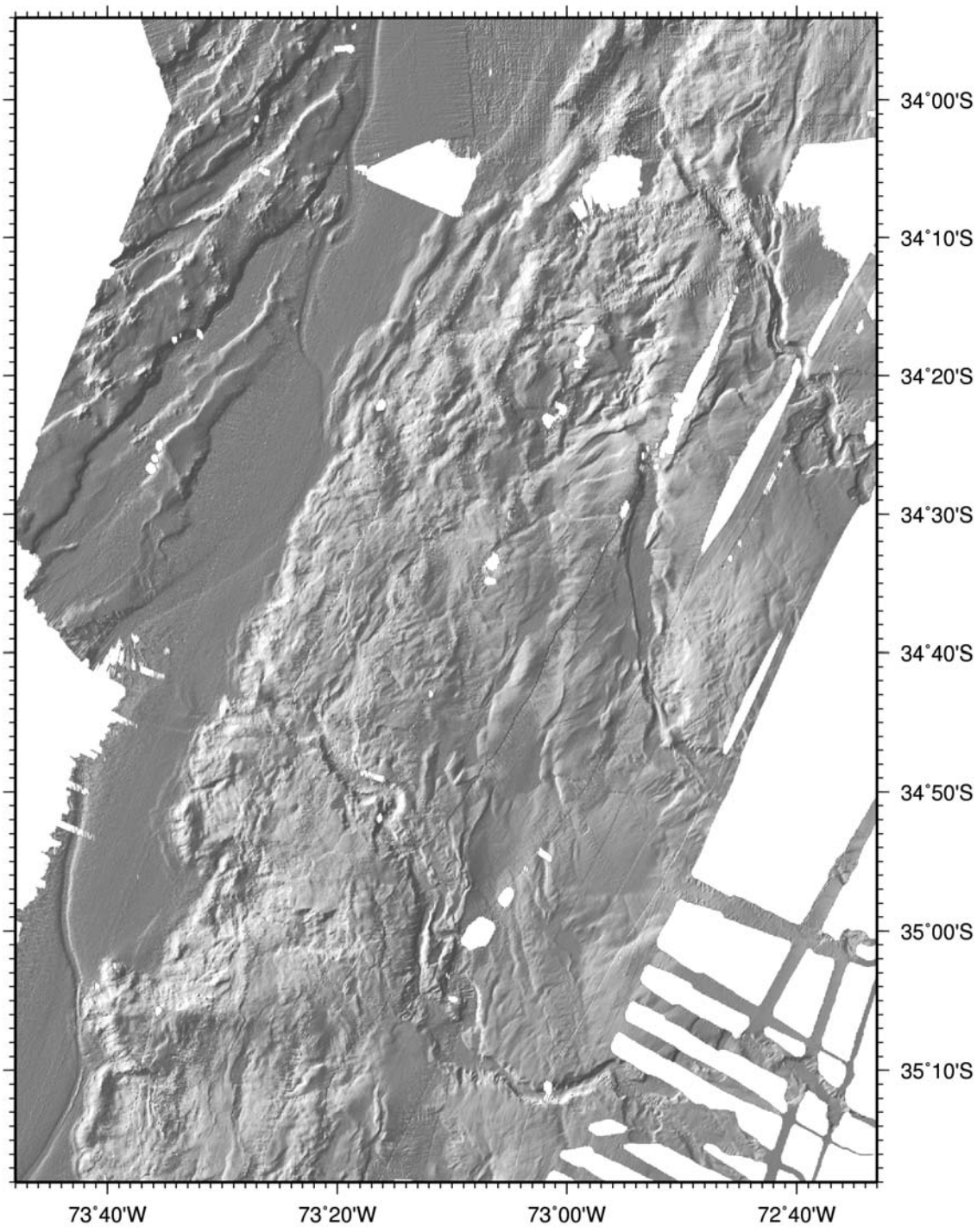

Figure 7.1.3b: *Shaded-relief bathymetry map of the northern sector of the study area (see Fig 7.1.3a caption)*

In between the two areas with clear accretionary ridges, from ~34°20'S to ~35°10'S, the lower slope generally displays a low relief topography lacking morphological features that can be laterally traced for more than a few km (Figs. 7.1.3 and 7.1.4). A very subtle low relief in the trench floor -highlighted by the illumination from the west in the figures- parallels the irregular slope toe. This subtle topographic feature is located 3-4 km seawards from the base of the slope, and extends along much of this section of the margin. It might represent incipient thrusting of the trench turbidite that is starting to deform the trench floor and that will be involved in frontal accretion.

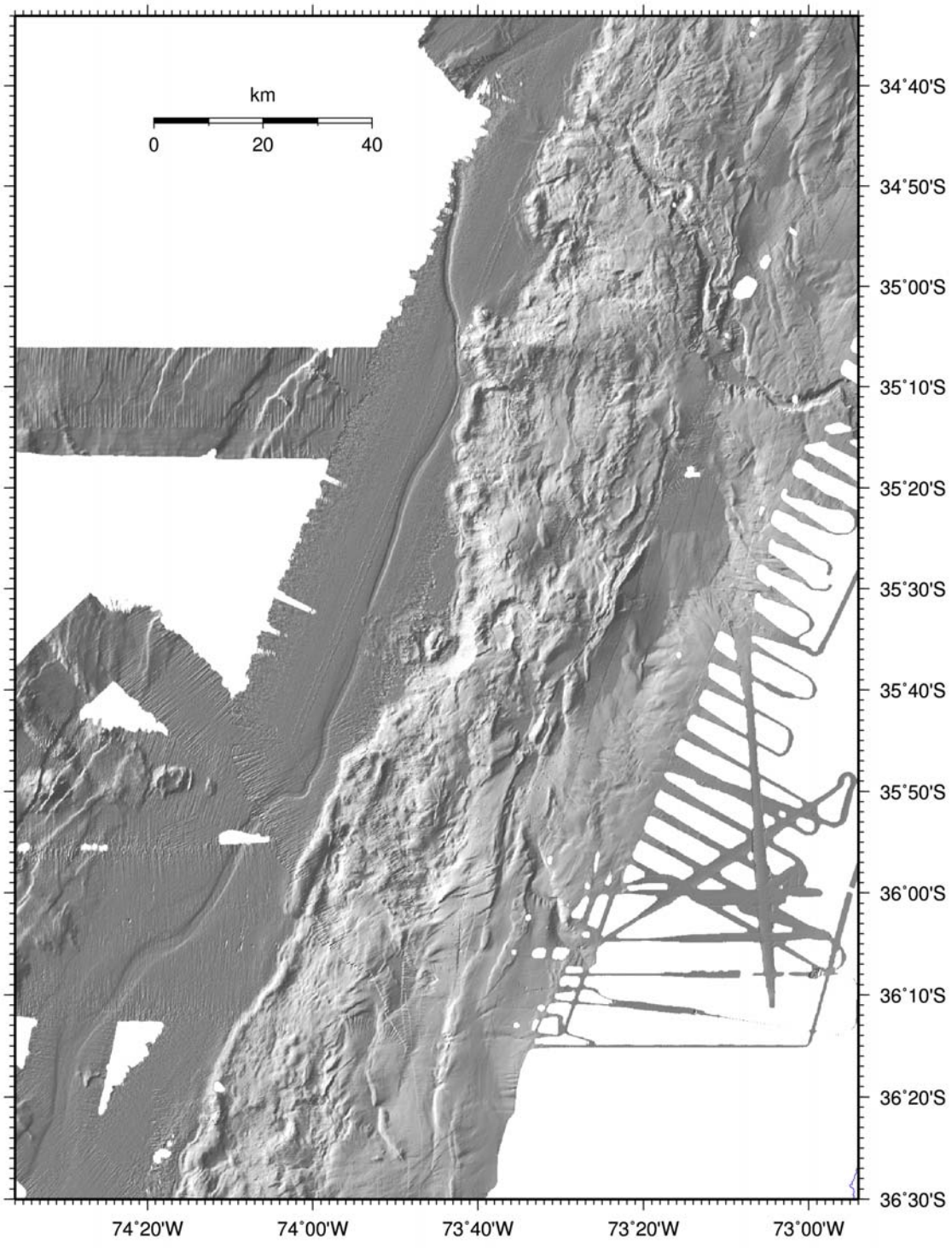

Figure 7.1.4: *Shaded-relief bathymetry map of the central sector of the study area. Note the two large embayments in the lower slope, and the large avalanche of material reaching the channel on the trench floor at ~35°35'S. Note the prominent mid-slope, margin-parallel lineament of ridges and troughs running along much of the sector*

In this sector, the slope toe also displays two large embayments centered at ~34°55'S and ~35°35'S reminiscent of the structures produced by the collision of underthrusting seamounts with overriding plates elsewhere (Figs. 7.1.4). However, no large seamounts are observed in the oceanic plate opposite the embayments area that could indicate the presence of a volcanic chain (Fig 7.1.1a). In spite of this, the embayment at ~35°35'S contains associated structures

that may also support recent underthrusting of a large subducting feature on the oceanic plate. Seawards of the embayment, a ~4-km-long block and a possible avalanche sediment deposit extending to and partially covering the channel at the trench floor may indicate that a large topographic feature has recently subducted in the area causing a large slide of lower slope material (Figs. 7.1.4). The northern embayment at ~34°55'S does not have obvious slide deposits, but the southernmost branch of the embayment seems to extend into the trench floor to partially cover, or deviate, the turbidite channel (Fig. 7.1.4 at ~35°04'S).

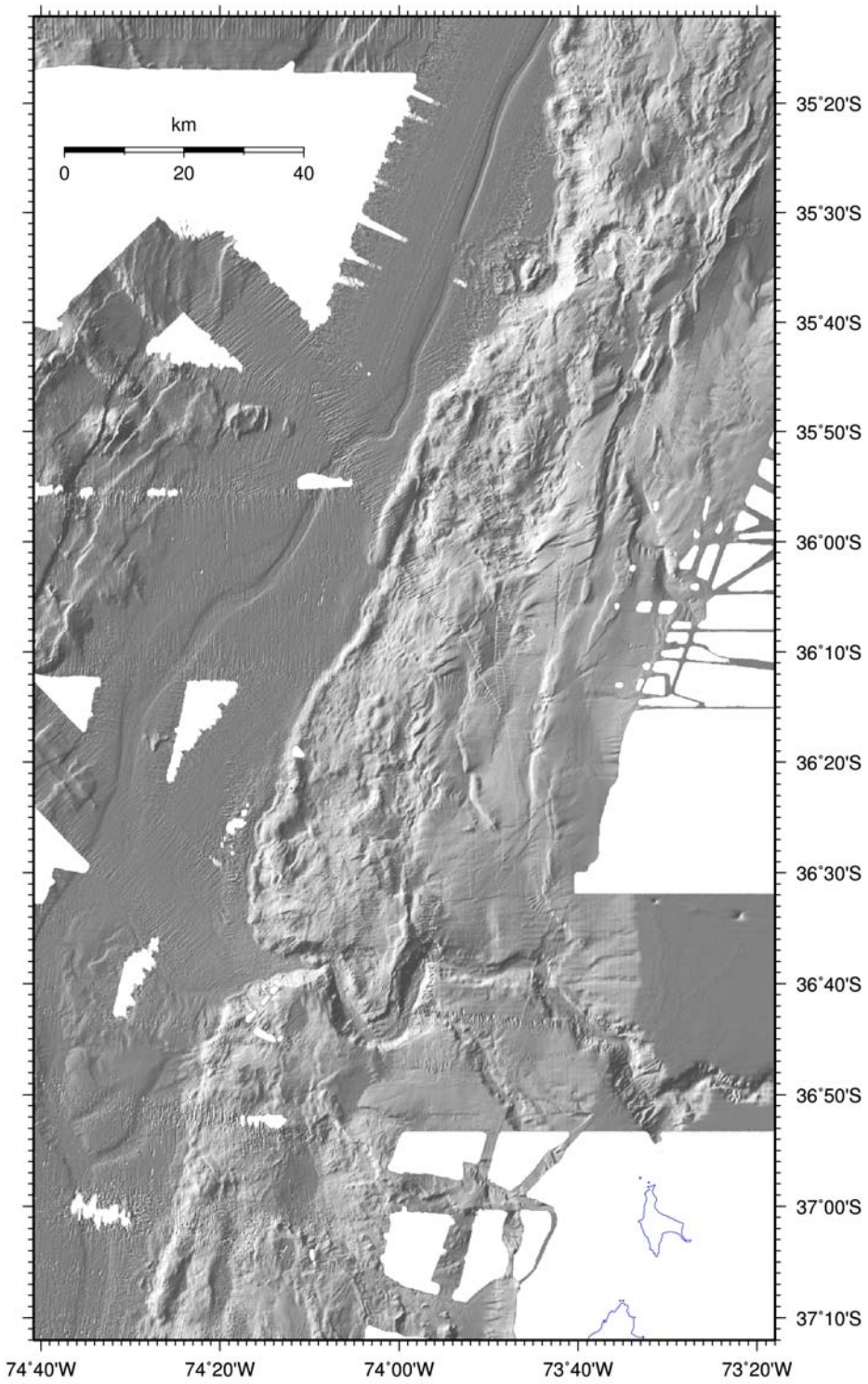

Figure 7.1.5: *Shaded-relief bathymetry map of the southern sector of the study area showing the mid-slope, margin-parallel lineament of ridges and troughs running along much of the sector*

A second characteristic of the area with little evidence of active sediment accretion is that the entire sector is slightly oblique to the convergence vector (Fig. 7.1.1) and thus strain might potentially be partitioned into a normal and margin-parallel components. However, the obliquity is very small and the margin-parallel strain should also be minor.

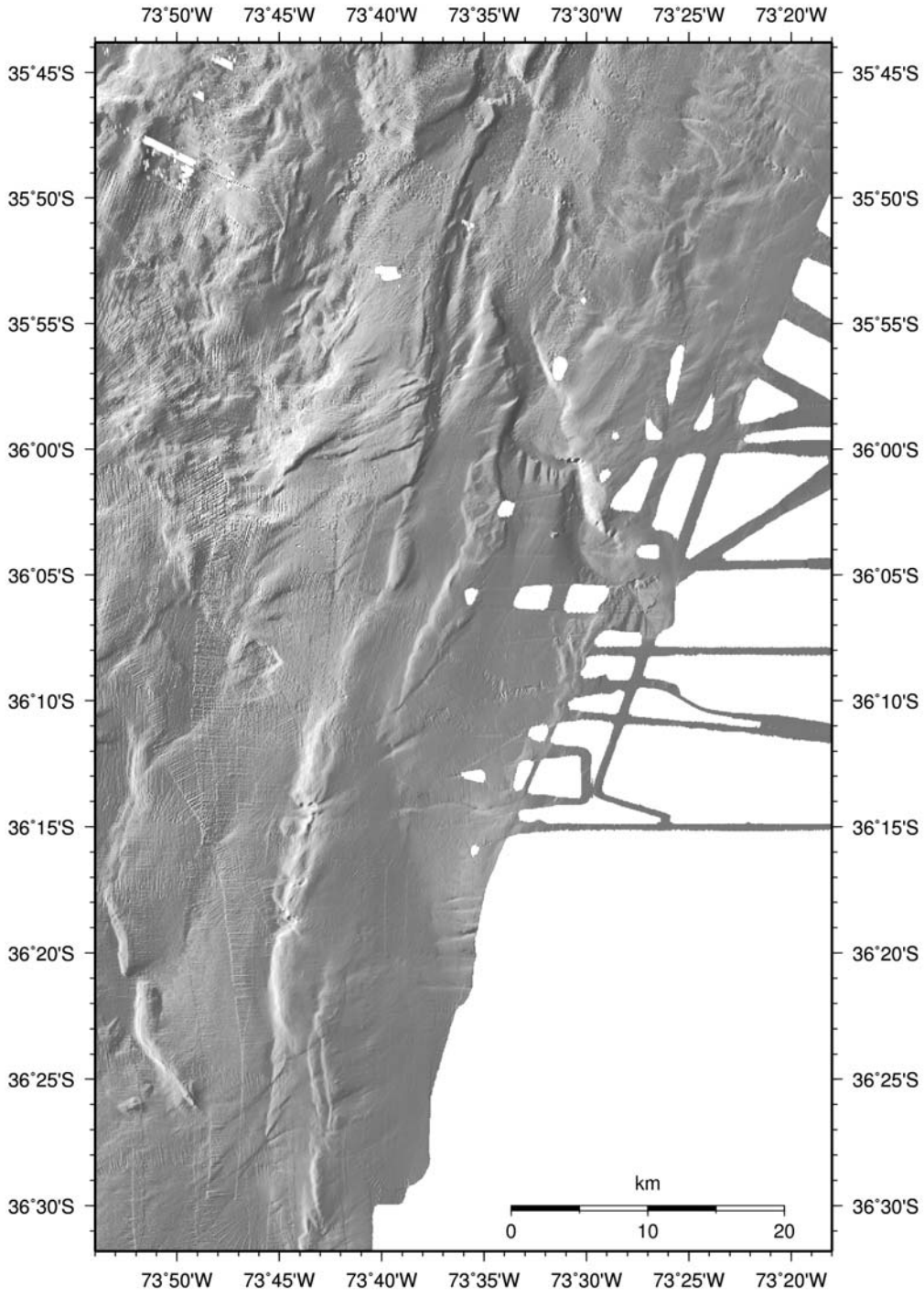

Figure 7.1.6.a: *Shaded-relief bathymetry map of a close-up of the middle slope in the southern sector of the study area showing the mid-slope, margin-parallel lineament of ridges and troughs cut by margin-oblique (roughly NE to ENE trending) shorter features. The margin-parallel lineament of ridges and troughs may indicate transtension and transpression structures in a strike-slip environment. The margin-oblique conjugate shorter features may accommodate some of the margin-parallel deformation*

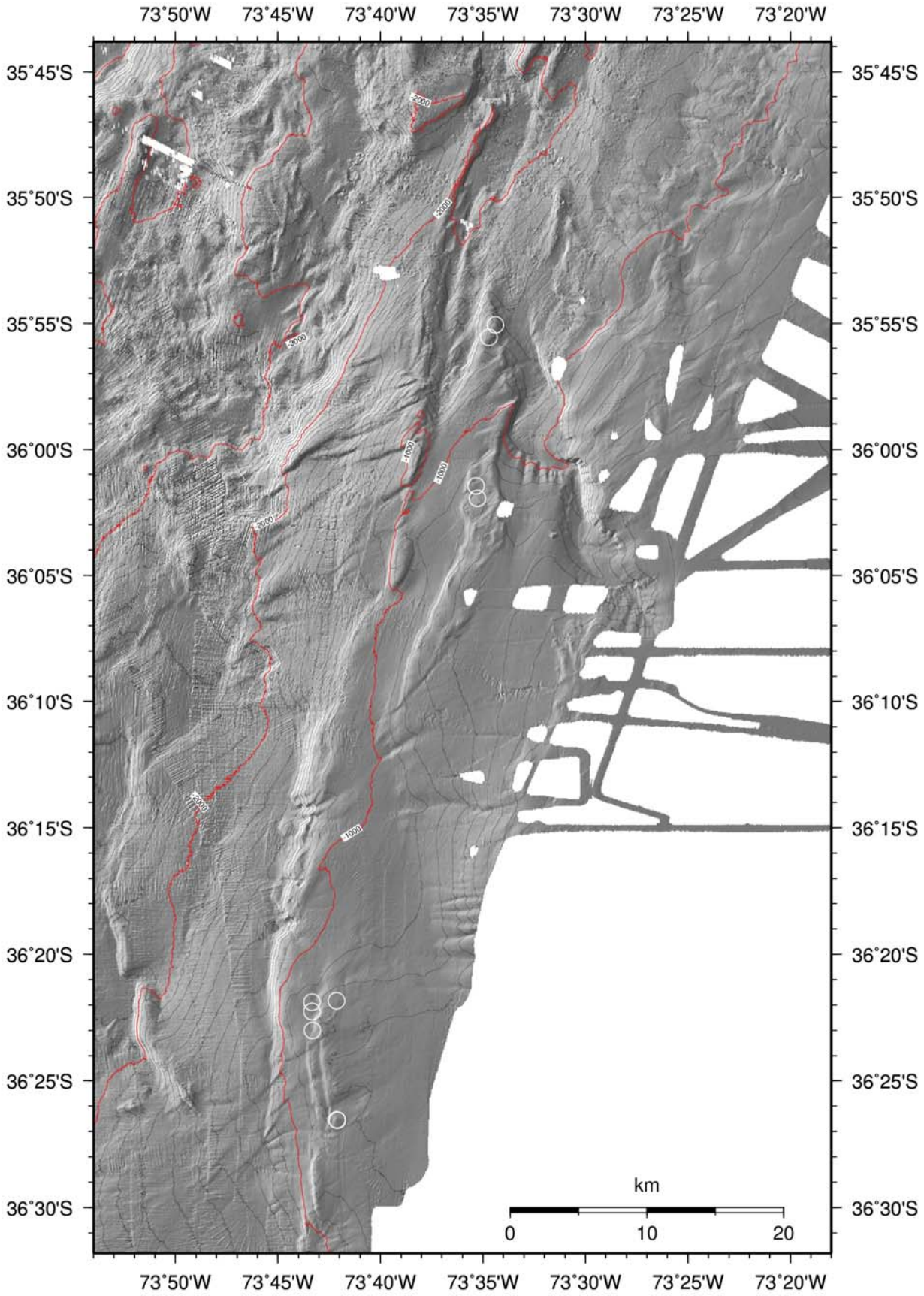

Figure 7.1.6b: *Shaded-relief bathymetry map of a close-up of the middle slope in the southern sector of the study area (same as Fig 7.1.6a) showing the location of the gravity cores collected on features related to the mid-slope deformation*

Interestingly, the transition from a rugged terrain to a smooth morphology upslope occurs, along much of this sector, across a roughly margin-parallel lineament of alternating narrow highs and troughs (Figs. 7.1.4, 7.1.5). These structures meander along the middle slope and indicate local uplift and subsidence along the same lineament, suggesting strike-slip deformation causing local transpression and transtension along the same fault structure. Their sharp relief, and the upslope morphological transition, from a rugged to a smooth terrain, across them also suggest that they are probably currently active. A closer view of the terrain along these tectonic features clearly shows the transition from a ridge to a trough along the same structure (Figure 7.1.6a). In addition, the dominant margin-parallel main lineament of highs and troughs is cut by a second set of margin-oblique (roughly NE trending) shorter features that produce clear scarps in the seafloor and dissect the main lineament in shorter segments, both indicating that they are active tectonic features (Figure 7.1.6a). These structures may be accommodating some of the margin-parallel strain. Around these two conjugate sets of active tectonic features a number of small mound-like structures was sampled by gravity cores (see chapter 7.4), fundamentally at mound-like structures spotting some of the margin-parallel ridges (Figure 7.1.6b).

7.2 Deployment of the DTS-1 System

Bialas, J., Bürk, D., Petersen, J.

Within two days after R/V METEOR had left the port of Talcahuano the equipment of the DeepTow system was set up in the laboratory. First dry tests with a 50-m-long deck cable confirmed a stable availability of all sensors. Due to planned gravity corer operations METEOR's coaxial deep sea cable could not be provided at that time as the layout of the cable guide path onboard METEOR does not allow mounting the working wire of winch W11 to the crane on the starboard side and the wire of winch W12 to the A-frame in the aft at the same time. To switch between the cables, the one that is used first has to be drawn back to the winch completely before the other one can be pulled out. Moreover, the cable termination has to be cut off each time such an exchange is done. Therefore, the data transmission through the deep sea cable and the towing umbilical could only be tested right before the deployment. When this was done in the evening of 28 February it turned out that the newly installed umbilical led to unusually high power currents that were interpreted as a short cut within the cable. An immediate test with the deck cable confirmed that no damage had been done to the system, hence the cable was replaced by an umbilical designed for use on board of R/V SONNE. As on SONNE pin usage is opposite to that on METEOR, an adapter had to be attached. In order to get some time for the exchange, the deployment was postponed to the morning of 1 March. At this time, the synchronization of the digital streamer did not provide stable results any more. Due to the dense time schedule it was nevertheless decided to deploy the system hoping that the streamer could be synchronized later so that there would at least be the chance to record sidescan data. The deployment procedure went smoothly and the system was switched on while being lowered to depth continuously. After a few pings the data connection to the sidescan underwater unit was lost although the connection between top and bottom gateways was still available. As reestablished data connections failed again after a short time, it was decided to stop the deployment and to recover the entire system. At first, a malfunction of the telemetry system was assumed. It was therefore substituted with the spare telemetry immediately after recovery. Surprisingly this did not fix the problem, moreover, it

was no longer possible to establish any connection between top and bottom unit of the sidescan although the gateways were still connected. Further tests pointed towards malfunctions of an Ethernet card inside the Top PC and another card inside the bottom sidescan unit. As time was too limited, the operation of the DeepTow could no longer be postponed and was cancelled. Further analysis of the systems confirmed a malfunction of the Ethernet card in the Top-PC and a wrong pin connection of the Ethernet wiring inside the second bottom telemetry unit.

7.3 Magnetic Survey

Petersen, J.

Between 24 February and 3 March 2006 a total of 11 magnetic profiles were acquired along with the bathymetric profiles. The numbering of the profiles was chosen according to the associated bathymetric profiles (see Appendix 2).

Most of the time the system operated well, but unfortunately, the data quality deteriorated significantly during the second deployment. Along the associated magnetic profiles 5,6,7 and 8 nearly constant values of about 27000 nT were measured, possibly due to a malfunction of the system. Thus, these profiles were excluded from further analysis.

For the remaining profiles, the magnetic values were linked to geographic positions taken from the ship's navigation system. The magnetic and navigation data were resampled to intervals of 10 s. Because the software to calculate the international geomagnetic reference field (IGRF) was not available on the cruise, a reduction to magnetic anomalies with respect to the reference field could not be performed. Instead an average value of 25300 nT was assumed and subtracted from the measured magnetic values. After median filtering the resulting magnetic anomalies were plotted along the bathymetry tracks and are shown together with the bathymetry in Fig. 7.2.1.

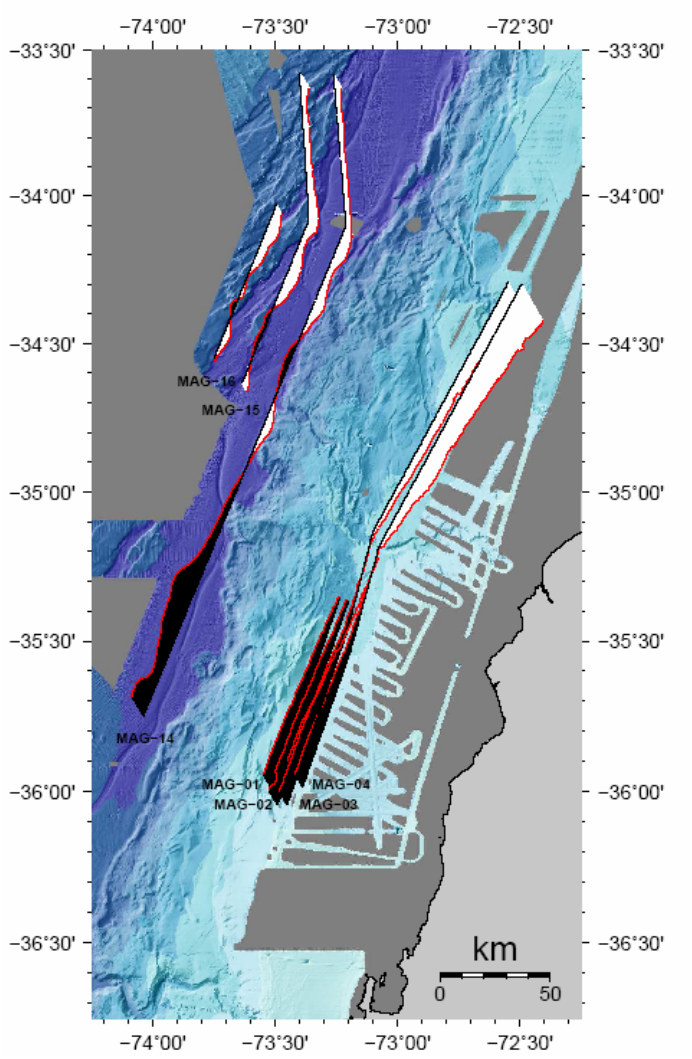

Figure 7.2.1:
Magnetic data acquired during M67/1

In the slope area the magnetic profiles 1, 2, 3 and 4 consistently show a positive anomaly in the south decreasing by about 540 nT to the northern end of profiles 1 and 2. These anomalies might be strongly influenced by the subducting plate since profile 14, which is located on the oceanic plate, trends to generally larger positive values towards the south.

Undulations of the anomalies of line 14 south of 34°:50'S imply that with better reduction values from the IGRF even here a magnetic stripe pattern has been recorded. To the north the undulations along profiles 14, 15 and 16 line up systematically. The change from positive to negative anomalies shows a NW-SE trend, which is parallel to the orientation of the spreading centre where the magnetisation was imprinted.

7.4 PARASOUND Data

The PARASOUND survey was carried out from the continental shelf to the trench at water depths from ca. 100m to 5500m (Fig. 6.7.2). The sub-bottom profiles are mainly margin-parallel. On the continental shelf, in some places the ocean bottom is characterized by small wave-like topography, most probably suggesting submarine dunes. An erosional surface produces an angular unconformity between an upper thin horizontal layer (5 to 10 m) and dipping reflectors beneath (Fig. 7.4.1). Laterally, this erosive surface reaches to the current sea floor (Fig. 7.4.2).

In the survey area, continental slope is characterized by deeply incised canyons. Some of them are imaged on the sub-bottom profiles (Fig. 7.4.3).

On the upper to mid slope, some mound-like positive topographic structures are imaged. In some places these structures are associated with the current seafloor connecting faults (Fig. 7.4.4). Some of these positive topographic structures were sampled by gravity coring (Figs. 7.4.5, 7.4.6, 7.4.7 and 7.4.8). Some fault traces were observed on the seafloor. In some places, these faults have produced a vertical offset of 50 m on the seafloor (Fig. 7.4.9).

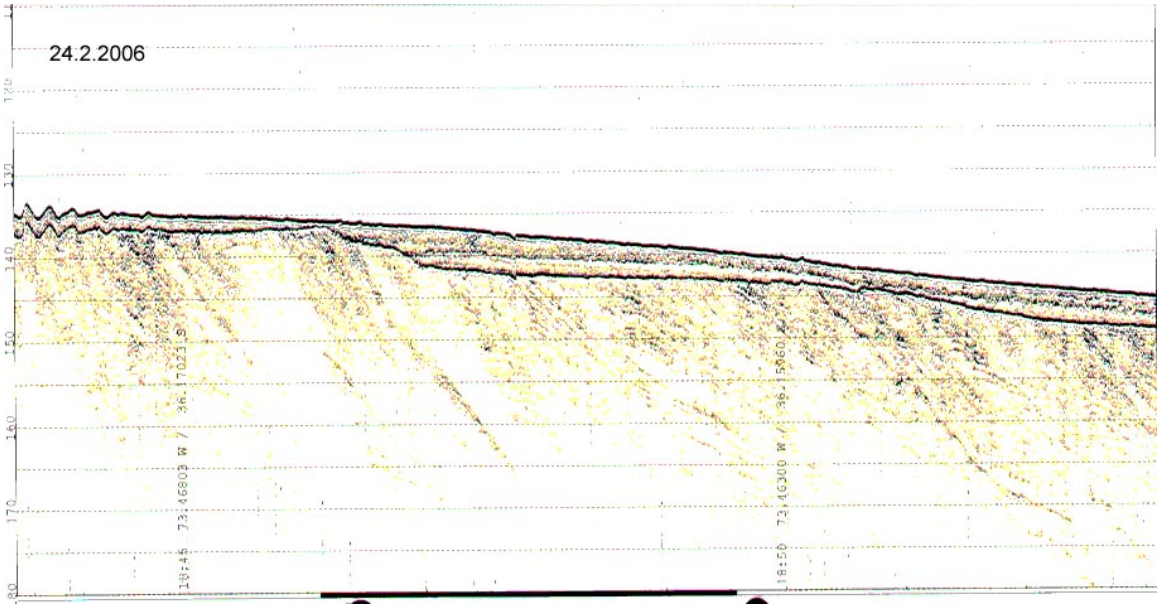

Figure 7.4.1: *Erosional surface producing angular anconformity*

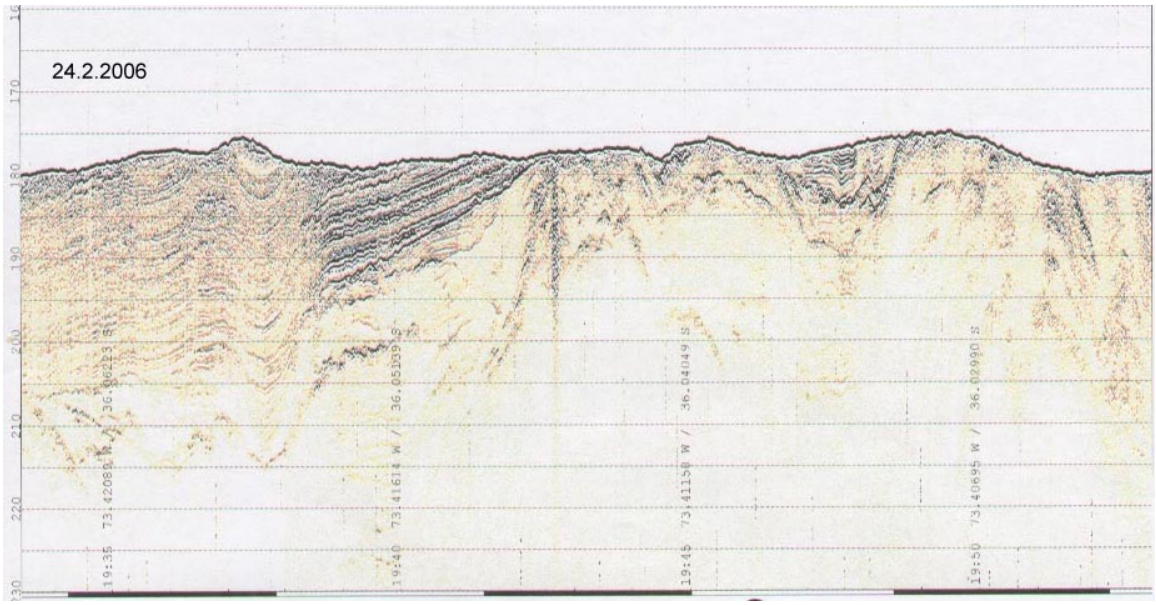

Figure 7.4.2: *Erosional surface reaches current seafloor*

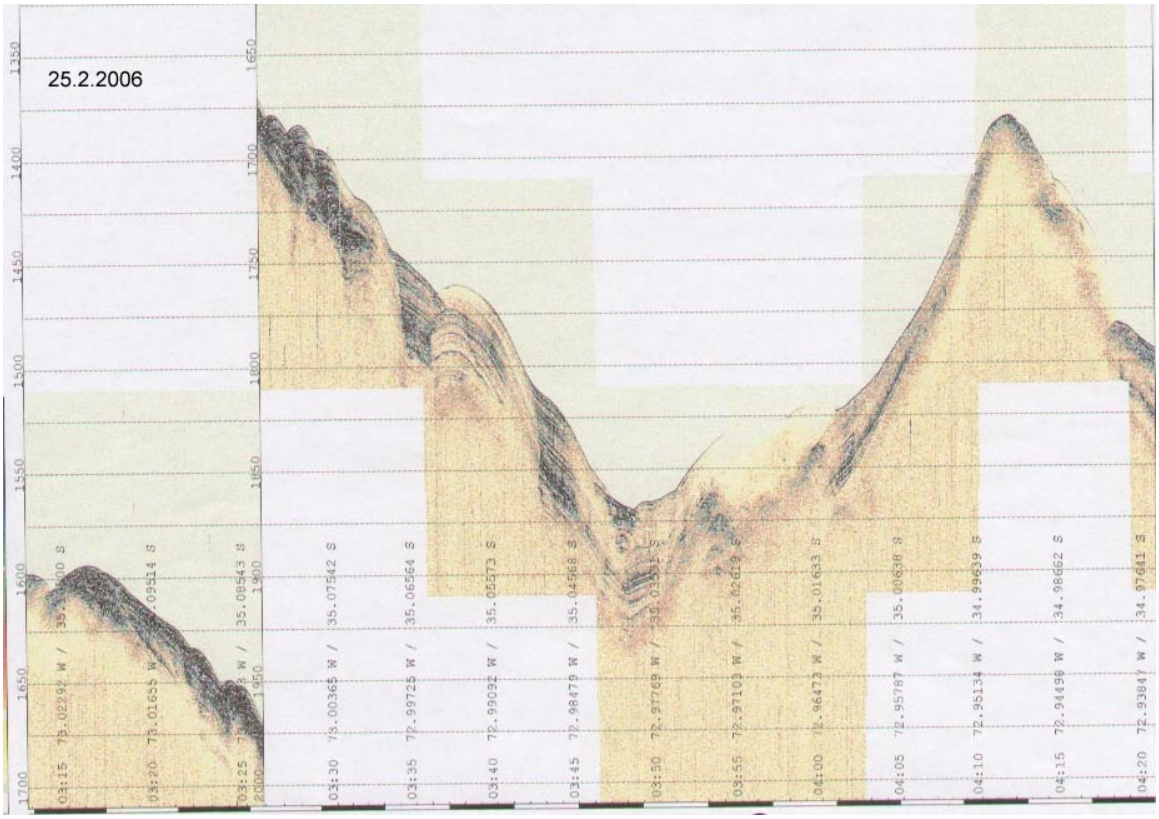

Figure 7.4.3: *Deep canyon in the continental slope*

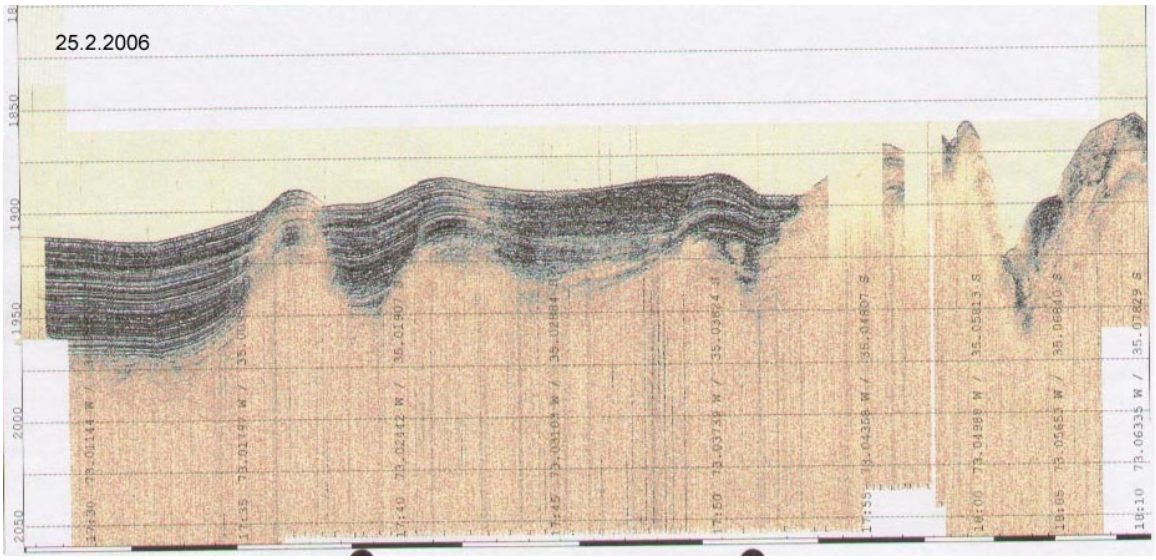

Figure 7.4.4: *Mound-like structures associated with faults*

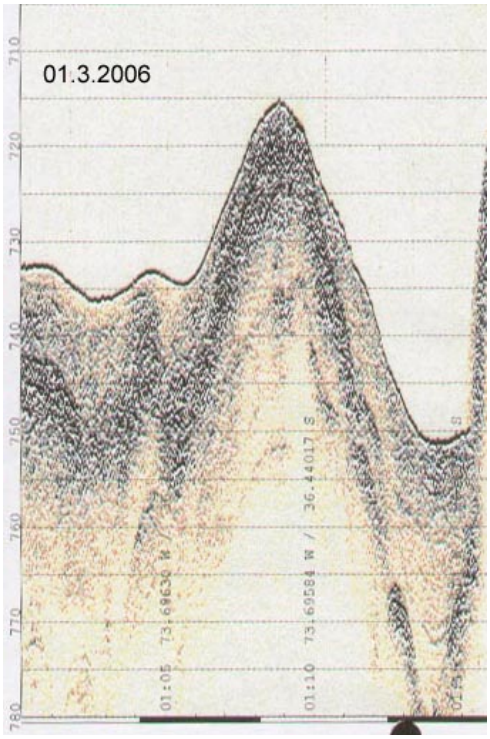

Figure 7.4.5: *Mound-like positive topographic feature sampled by gravity coring*

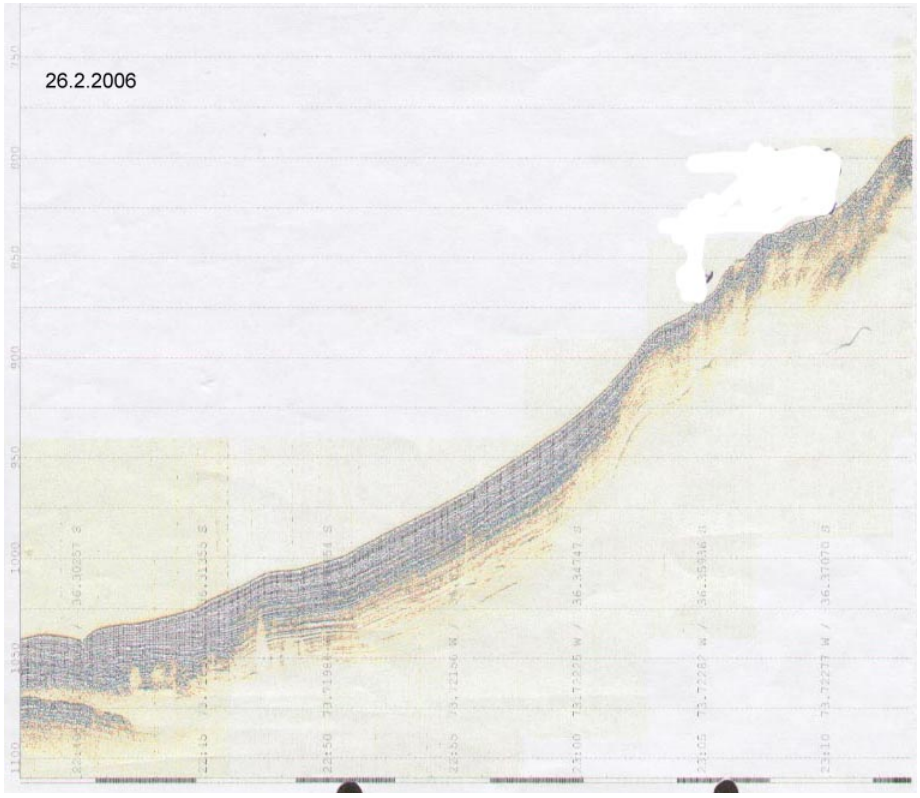

Figure 7.4.6: *Small positive topographic feature sampled by gravity coring*

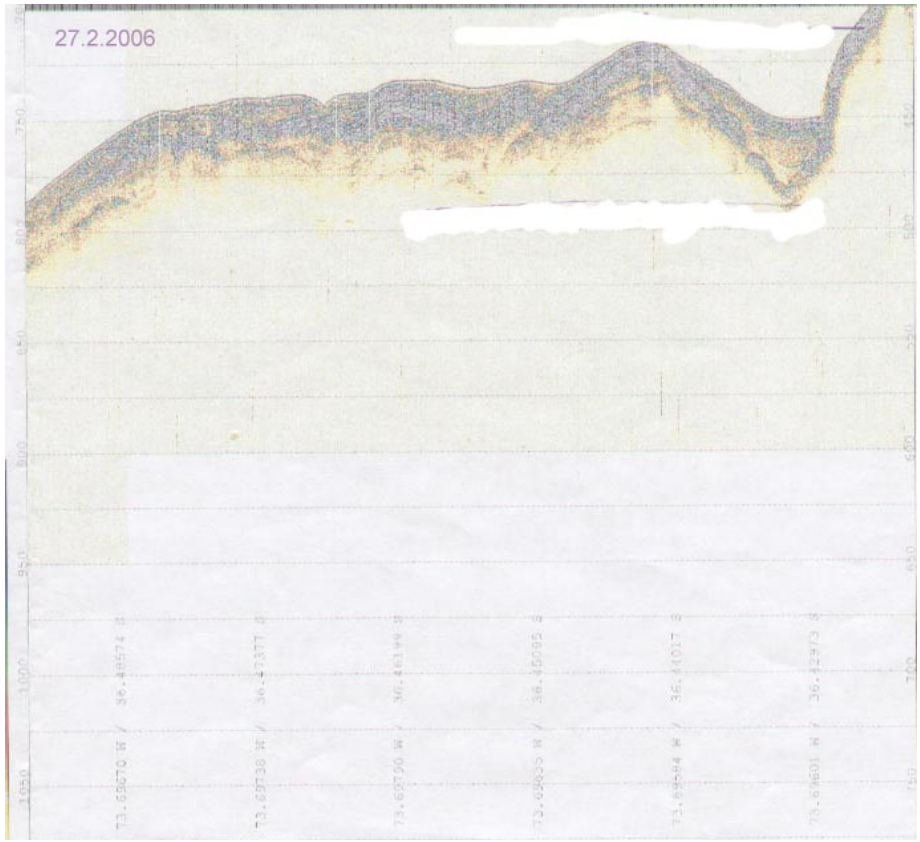

Figure 7.4.7: *Small positive topographic feature sampled by gravity coring*

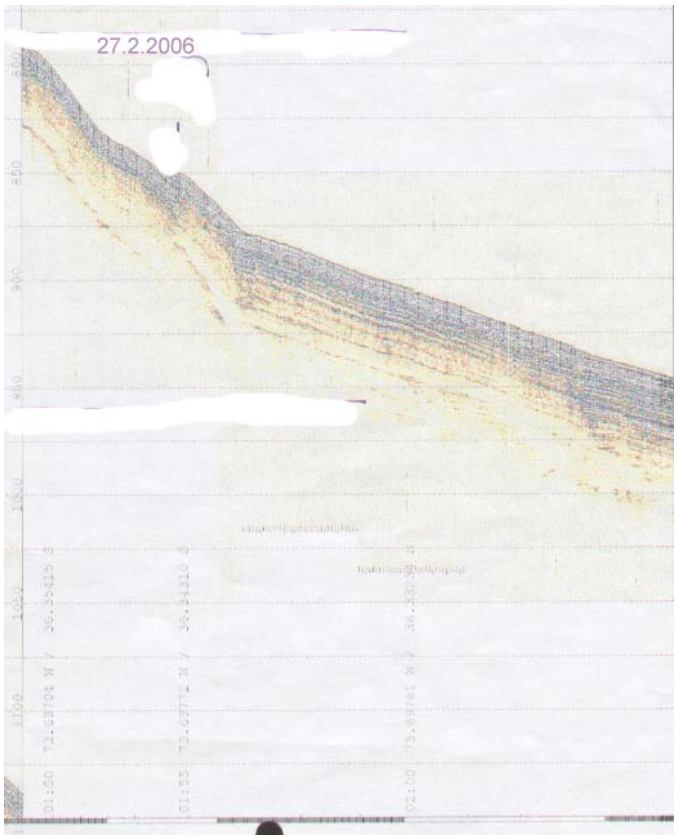

Figure 7.4.8: *Small positive topographic feature sampled by gravity coring*

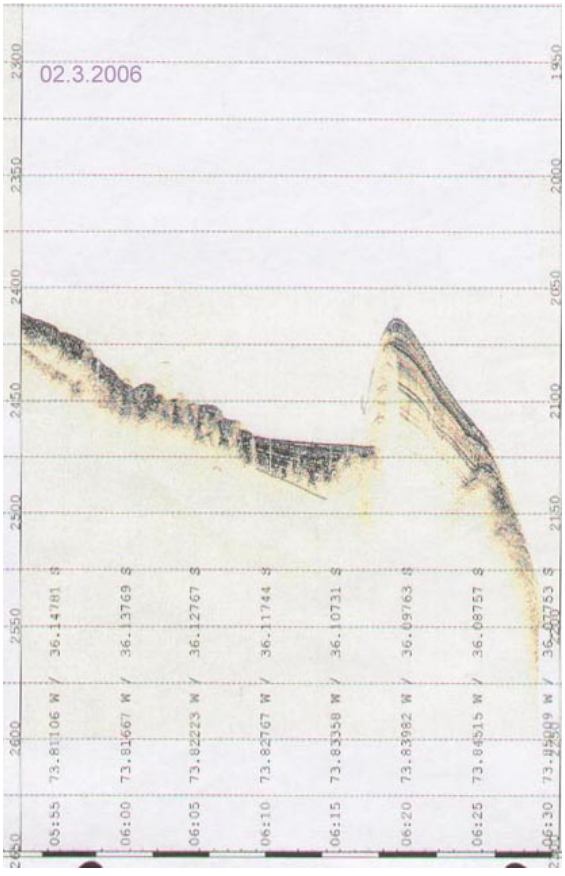

Figure 7.4.9: *Fault traces producing in places ca. 50 m offset on the seafloor*

7.5 Gravity Coring and Pore Water Geochemistry

Harders R, Hensen C, Mavromatis V

The major focus of the sediment-sampling program on M67/1 was to obtain preliminary information on potential sites of active fluid venting and the composition of the respective pore waters. In total, 8 cores could be recovered out of 11 GC deployments, and 7 were processed and investigated for pore water composition. The results of core description and pore water processing are presented below for each station. All stations are summarized in Table 7.5.1. GC deployments 5 to 8 were performed on top of prominent seafloor elevations aligned along a submarine canyon in the central part of the working area (see Fig. 7.1.1). GC deployments 15 to 20 were performed at a number of sites showing conspicuous structures in seafloor bathymetry and hydroacoustic records in the southern working area. The results of the water content measurements are provided in Table 7.5.2.

Table 7.5.1: List of gravity core stations

Station N°	**Latitude (S)**	**Longitude (W)**	**Water Depth**	Recovery
5	S 35°55,07	73°34,40	1170 m	core catcher, consolidated mud
6	S 35°55,37	73°34,66	1172 m	85 cm, consolidated mud
7	S 36°01,45	73°35,30	780 m	146 cm, consolidated mud
8	S 36°01,94	73°35,28	746 m	core catcher, consolidated mud
15-1	S 36°26,55	73°42,14	706 m	core catcher, cemented shells
15-2	S 36°26,57	73°42,10	707 m	36 cm, mud + carbonates
16	S 36°23, 74	73°43,31	787 m	370 cm, soft sediment
17	S 36°21,90	73°43,34	848 m	88 cm, soft sediment, H_2S smell
18	S 36°22,25	73°43,35	832 m	201, soft sediment, H_2S smell
19	S 36°21,84	73°42,14	748 m	260, soft sediment
20	S 36°20, 54	73°41,87	858 m	500, soft sediment

Table 7.5.2: Water content of selected sediment samples

Core No.:	weight of plate [g]	wet weight and plate [g]	dry weight and plate [g]	wet weight [g]	dry weight [g]	water content [g]	water content [%]
M67-1/7/0-46 cm at 20 cm	1.2802	16.2602	10.5349	14.9800	9.2547	5.7253	38.2199
M67-1/7/46-146 cm at 100 cm	1.2703	15.9415	9.7509	14.6712	8.4806	6.1905	42.1953
M67-1/15-2/0-36 cm at 15 cm	1.2795	18.1459	11.8754	16.8664	10.5959	6.2706	37.1778
M67-1/16/0-70 cm at 35 cm	1.2771	16.4663	10.0415	15.1892	8.7644	6.4248	42.2984
M67-1/16/70-170 cm at 100 cm ?	1.7300	16.6300	10.1239	14.9000	8.3939	6.5061	43.6654
M67-1/16/170-270 cm at 200 cm	1.2779	17.0820	10.6885	15.8041	9.4106	6.3935	40.4546
M67-1/16/270-370 cm at 300 cm	1.2856	16.9244	10.3420	15.6388	9.0564	6.5824	42.0902
M67-1/17/0-87 cm at 40 cm	1.2815	17.3943	11.5524	16.1128	10.2709	5.8419	36.2565
M67-1/18/0-101 cm at 50 cm	1.2500	17.1623	11.0006	15.9123	9.7506	6.1617	38.7226
M67-1/18/101-201 cm at 150 cm ?	1.2500	16.7705	10.5336	15.5205	9.2836	6.2369	40.1846
M67-1/19/0-60 cm at 30 cm	1.2908	17.4263	11.3261	16.1355	10.0353	6.1001	37.8056
M67-1/19/60-160 cm at 100 cm	1.2850	16.6524	10.4696	15.3674	9.1846	6.1828	40.2334
M67-1/19/160-260 cm at 200 cm	1.2796	17.2420	11.0594	15.9624	9.7798	6.1826	38.7325
M67-1/20/0-100 cm at 50 cm	1.2810	18.3976	12.3376	17.1166	11.0566	6.0600	35.4041
M67/1/20/100-200 cm at 150 cm	1.2710	17.1283	10.8744	15.8573	9.6034	6.2539	39.4388
M67-1/20/200-300 cm at 250 cm	1.2836	17.0553	10.5064	15.7717	9.2228	6.5489	41.5233
M67-1/20/300-400 cm at 350 cm	1.2930	18.3281	12.5441	17.0351	11.2511	5.7841	33.9538
M67-1/20/400-500 cm at 450 cm	1.2915	17.1119	10.7609	15.8204	9.4694	6.3511	40.1447

7.5.1 Central working area - Canon Ridge

The sediments on top of the canon ridge area turned out to be extremely consolidated and hence difficult to sample by means of a gravity corer. Only at station 6 and 7 sediments could be retrieved.

-Station 5-
At the first deployment in the canon ridge area, only 30 cm of sediment were recovered in the core catcher. The material consisted of dense greyish clay with some carbonaceous clay clasts.

-Station 6-
This core was taken from the same ridge-like station 5 with a yield of 77 cm of very dense clayey sediment overlain by a few centimetres of fresh muddy sediments (Fig. 7.5.1). The sediments appear to be overcompacted compared to their present position in the sediment strata and may have been uplifted along the ridge.

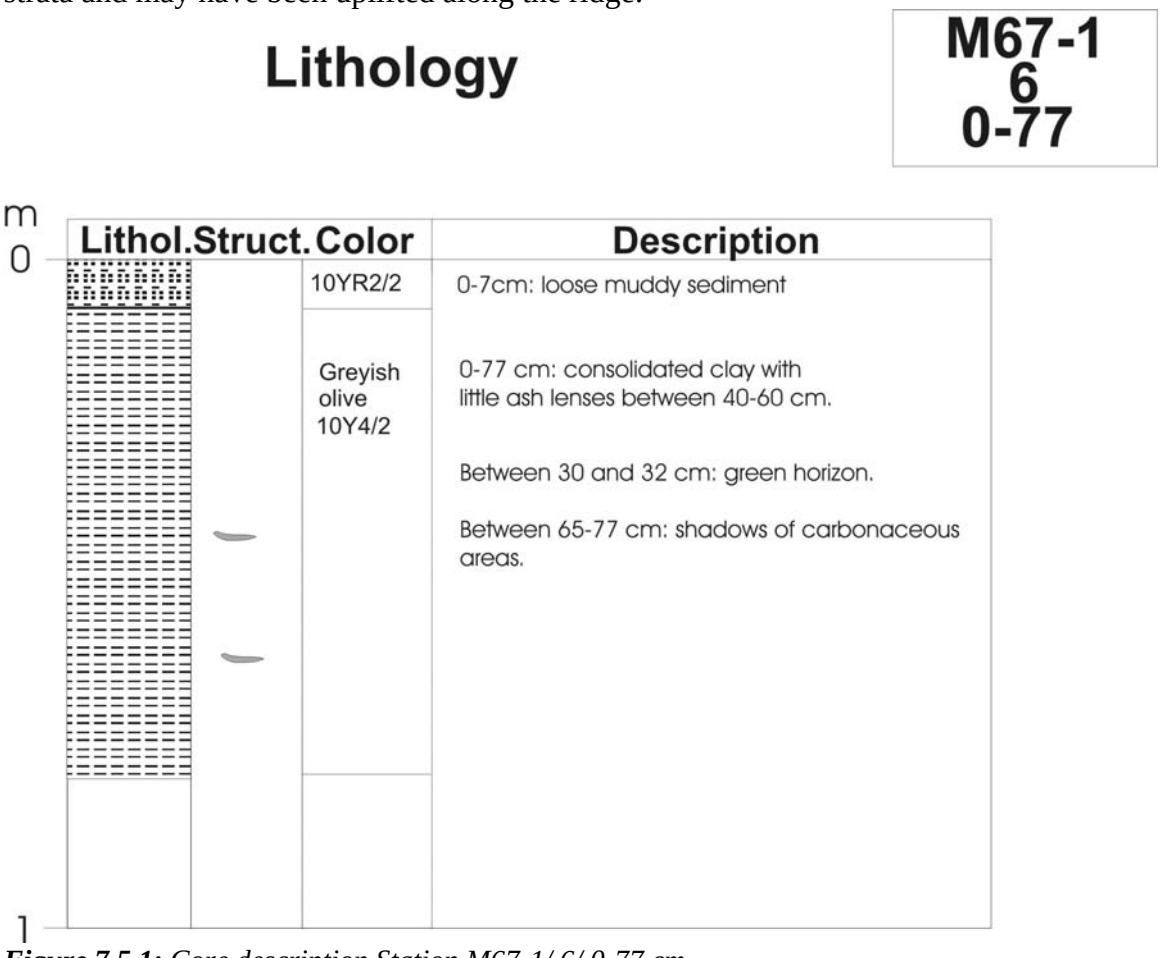

Figure 7.5.1: *Core description Station M67-1/ 6/ 0-77 cm*

-Station 7-
The core was taken near a mound structure and recovered 146 cm of the same type of consolidated clay as described above (Fig. 5.5.2). The core from station 7 could also be processed for pore water squeezing. After retrieval, a slight smell of H_2S was noticed at the bottom of the core.

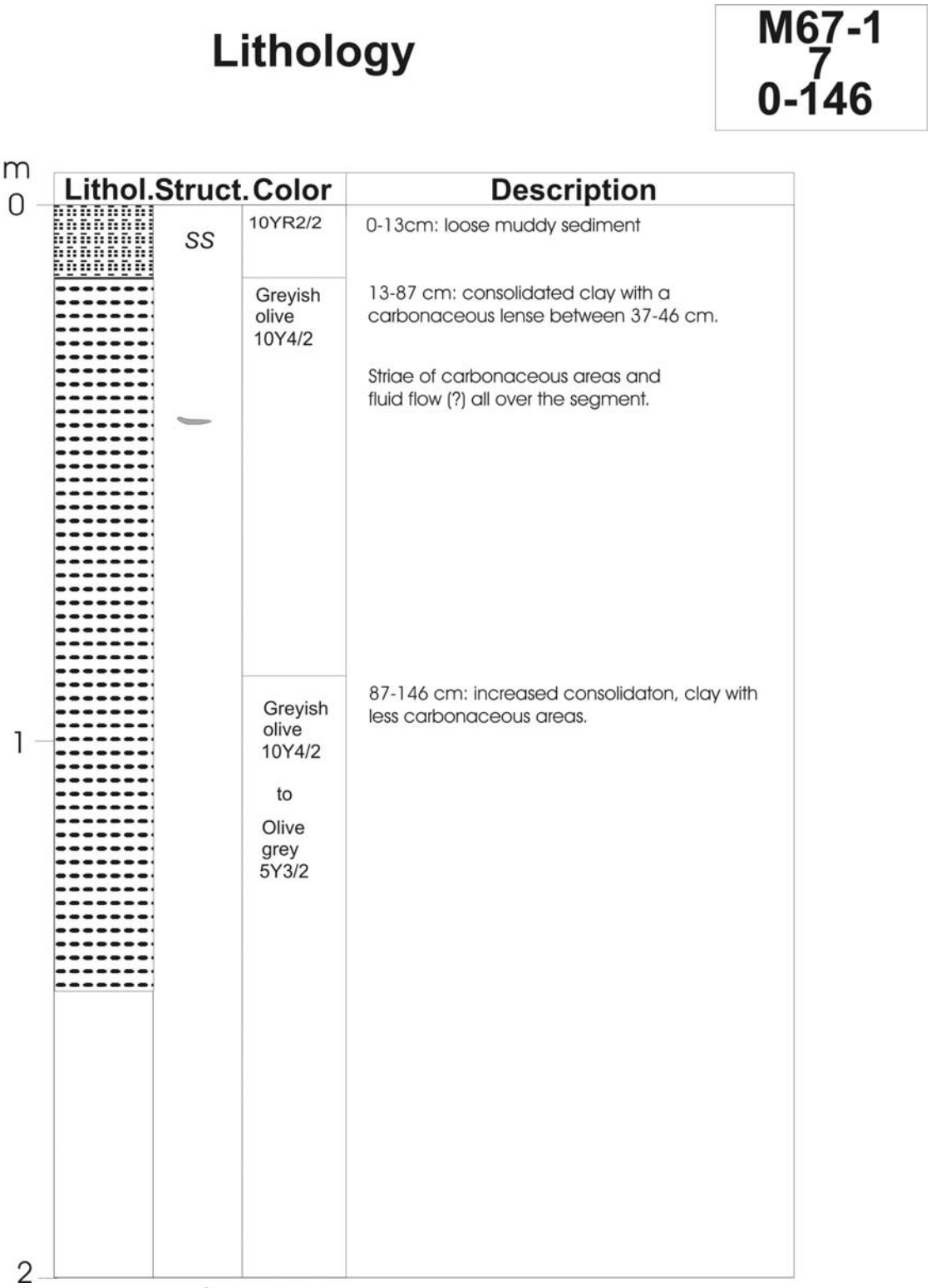

Figure 7.5.2: *Core description Station M67-1/ 7/ 0-146 cm*

Extracted pore waters did not contain H_2S any more, suggesting that the concentrations must have been very low. Overall, the pore water analyses are indicative of normal subsurface diagenetic processes. The moderate increase in alkalinity (C), ammonia (N), and phosphate (P) reflects the degradation of organic material, whereas elevated silica concentrations can be referred to the dissolution of opaline skeletons (Fig. 7.5.3). Chlorinity values remain constant over the whole depth of the core. Overall, there are no indications for active fluid flow or venting of methane-rich fluids at this site.

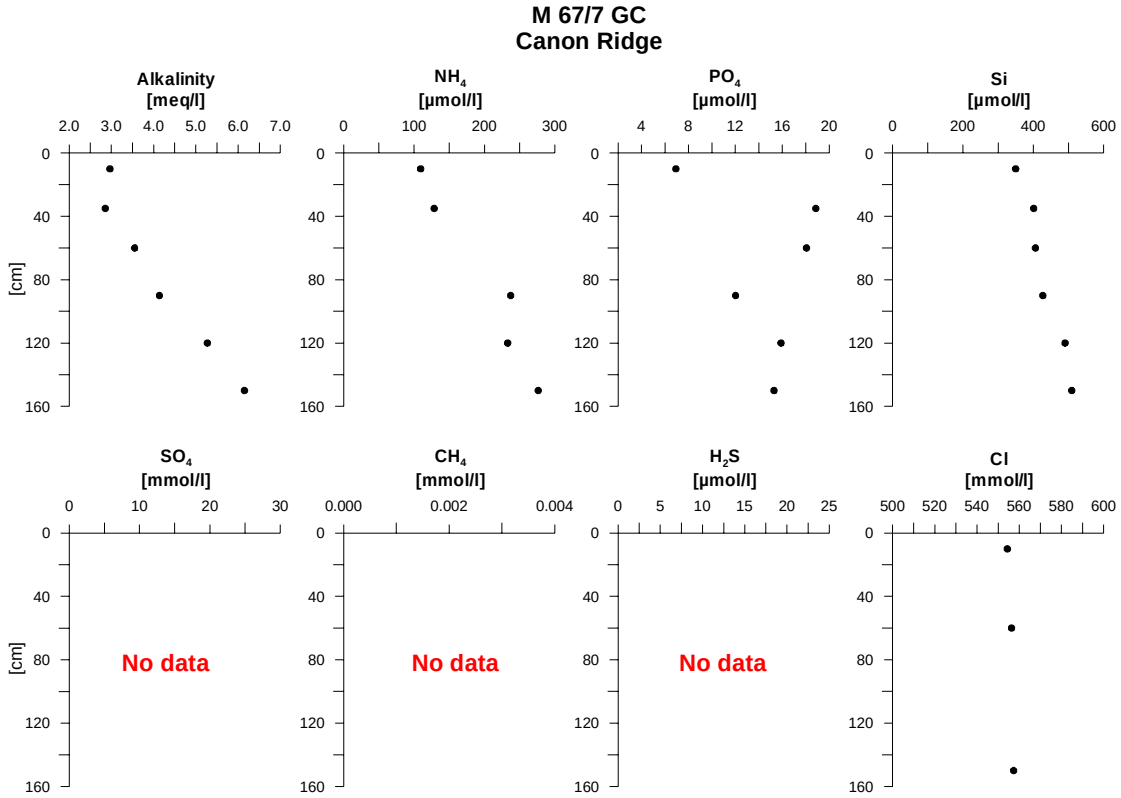

Figure 7.5.3: *Pore water geochemistry at station 7, Canon Ridge*

-Station 8-

There was almost no sediment yield at this site. Only approximately 15 cm of dense clay with several clay clasts of different grain sizes were recovered in the core catcher**.**

7.5.2 Southern Working Area

-Stations 15-1 and 15-2-

At station 15 two attempts were made to sample sediments from the top of a large mound-like structure (some hundreds of metres in diameter; Fig. 7.1.1). Unfortunately, the recovery was very low in both cases. Core 15-1 only revealed some cemented clams and pieces of irregularly formed carbonates. At site 15-2 we obtained about 36 cm of dense carbonaceous clay which slightly smelled of H_2S (Fig. 7.5.4). Brown and silty surface sediment reached down to 9 cm without indications for bioturbation. A green layer at 5 cm bsf, interrupted by a clayey clast, separated the surface sediment into two parts. From 9 cmbsf to the bottom the sediments consist of dense clay.

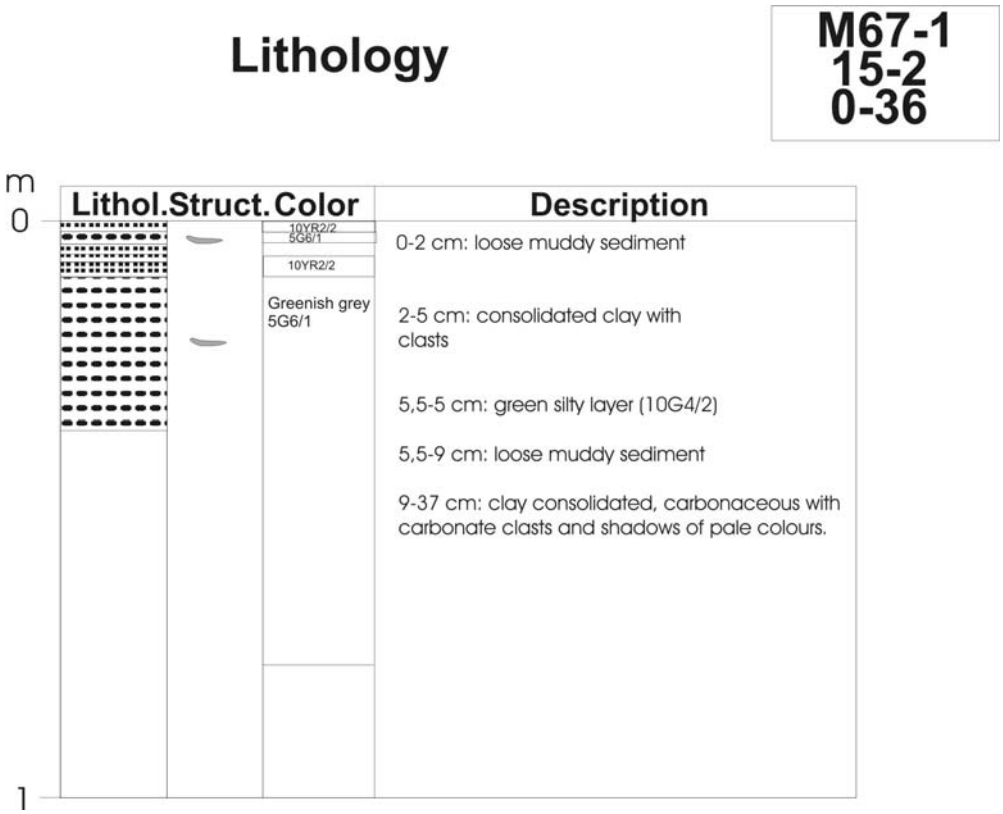

Figure 7.5.4: *Core description Station M67-1/ 15-2/ 0-36 cm*

Pore water data from this site are not indicative of active fluid venting (Figure 7.5.5). The chlorinity is normal and alkalinity and nutrients are only slightly elevated above sea water levels. However, cemented shells and –most likely – authigenic carbonates are clear indications for venting of methane-enriched fluids at this site.

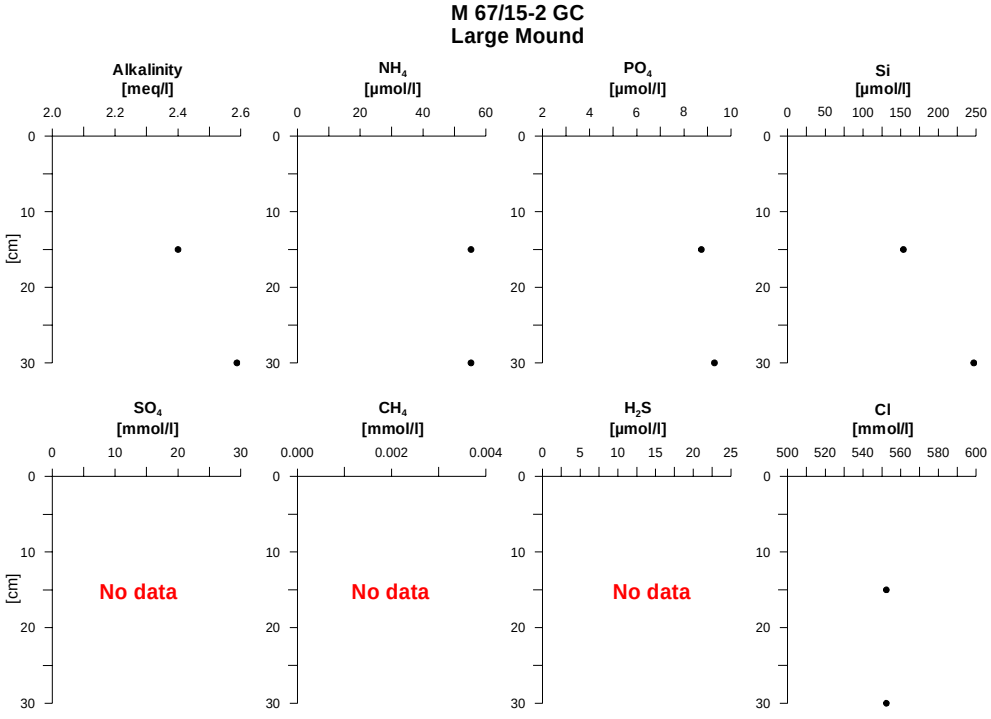

Figure 7.5.5: *Pore water geochemistry at station 15/2, Large Mound*

-Station 16-

Station 16 was taken at the intersection of a very prominent N-S-trending and another SW-NE-trending fault (Fig. 7.1.1). The core recovered 370 cm of clay with increasing consolidation towards the bottom and strong bioturbation near the top (Figure 7.5.6). Brownish-silty surface sediment was transported downward to about 55 cmbsf along channels and burrows indicating intense bioturbation. The clayey sediments are less consolidated compared to the mound ridge area. Small black silt particles – assumed to be pyrite – within the clayey sediment are distributed homogeneously throughout the whole core.

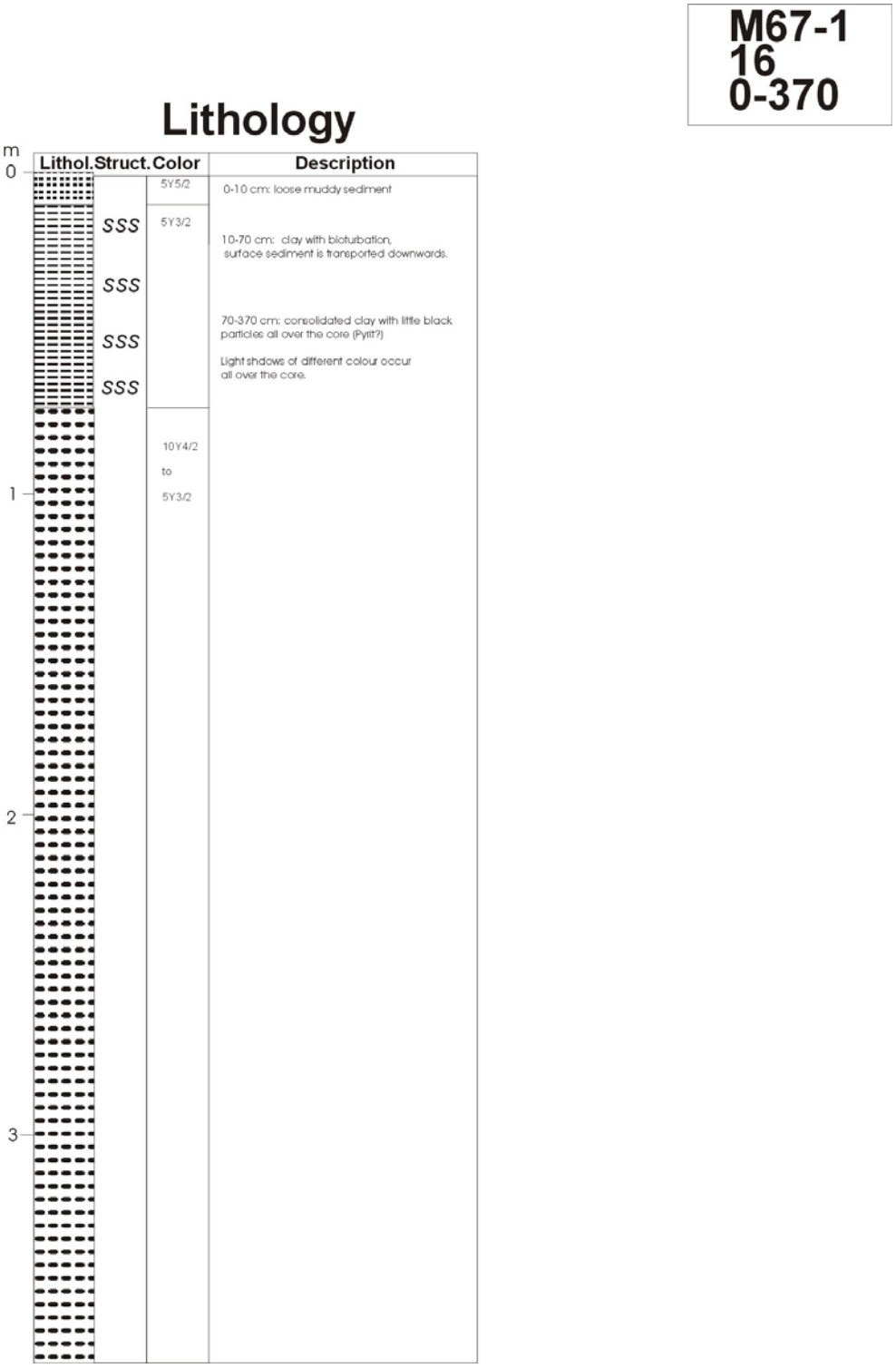

Figure7.5.6: *Core description Station M67-1/ 16/ 0-370 cm*

The pore water profiles of this nearly 4-m-long core indicate enhanced diagenetic processes at this site as can be deduced from clearly higher levels of alkalinity, ammonia, and phosphate compared to sites 7 and 15-2 (Figure 7.5.7). Again, no signs of fluid venting could be observed and chlorinity displays normal sea water values.

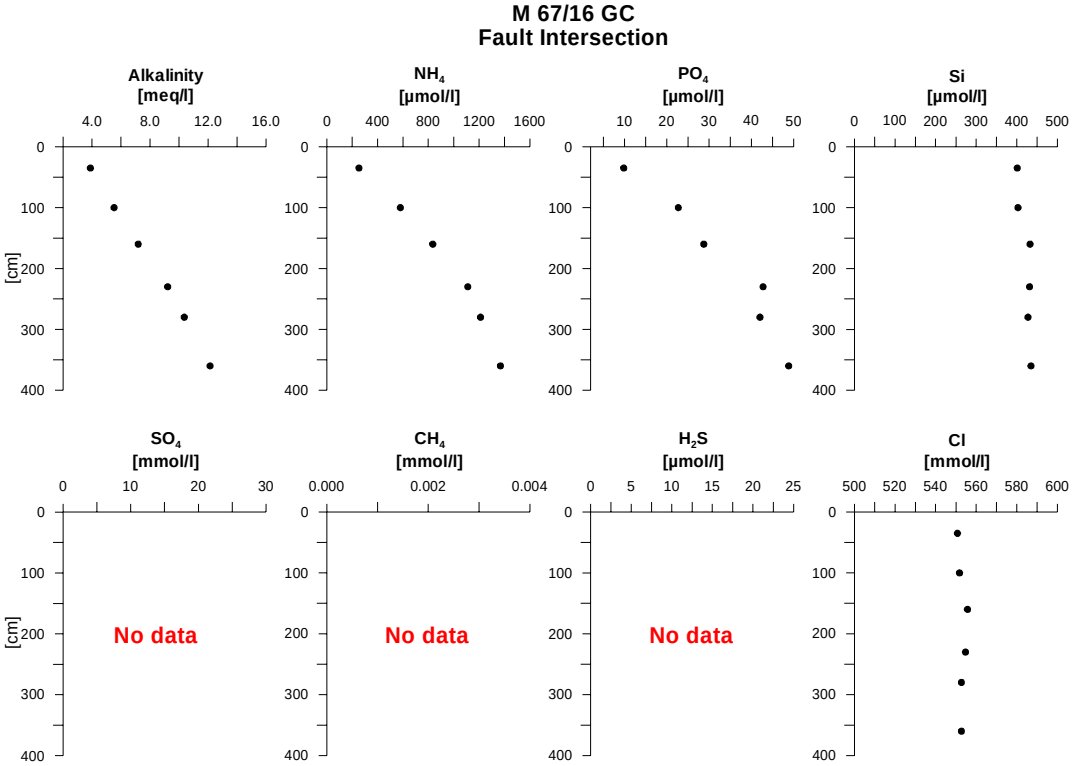

Figure 7.5.7: *Pore water geochemistry at station 16, Fault Intersection*

-Station 17 and 18-

Stations 17 and 18 were selected because gas hydrate had been found at this location before. On the bathymetric map the sites appear to be located on a small sea floor elevation (mound). The PARASOUND record displays a clear destruction of the shallow subsurface layers in this area. Core 17 recovered 88 cm of silty clay and smelled strongly of H_2S (Fig. 7.5.8). Some bioturbation was visible near the top, reaching down to 20 cmbsf. Remarkably, a yellow-orange biofilm or fat-liquoring substance was exposed within a 10-cm-long crack (possibly a fluid channel) in the sediment (archive half) between 70 to 80 cmbsf.

Core 18 was taken in the vicinity of station 17 where gas hydrate had been found on a former cruise. The core recovered 201 cm of silty clay and gave off a strong smell of H_2S (Fig. 7.5.9). There were strong indications for bioturbation near the top of the core. Especially burrows filled with brown and silty surface sediment are a dominant feature within the consolidated clay down to 50 cmbsf. As in core 17, there were areas covered by biofilms appearing as transparent, fatty and shiny coatings, well pronounced between depths of 80 and 90 cm. Similar to core 16, small, homogeneously distributed black particles could be observed within the clay in cores 17 and 18, which were regarded as precipitations of pyrite.

Both cores are clearly indicative for active venting of methane-rich fluids. Although neither methane nor sulphate were measured during the cruise it is obvious from the alkalinity profiles and the H_2S profiles that the zone of anaerobic oxidation of methane (AOM) is

reached within the uppermost 40 cm (station 17, Fig. 7.5.10) and at about 100 cm (station 18, Fig. 7.5.11). The shallow depth of the zone of AOM and the extremely high concentrations of H_2S are typical for sites of fluid venting or gas ebullition. However, these are accompanied by very low to moderate levels of ammonia and phosphate. In addition, no chlorinity anomalies could be observed. Compared to extensive data sets obtained on METEOR cruises M 54 and 66 and SONNE cruise 173 offshore Central America we can probably rule out a deep origin of the fluids as those generally display negative chloride anomalies and higher nutrient levels. In analogy to the results of M 66, we assume that methane is not transported to the surface with ascending fluids but rather as free gas. Another explanation can be offered by the existence of shallow hydrological systems, mixing sea water into the surface sediments so that the chemical signature of any deep fluids may be overprinted by the bottom water signature.

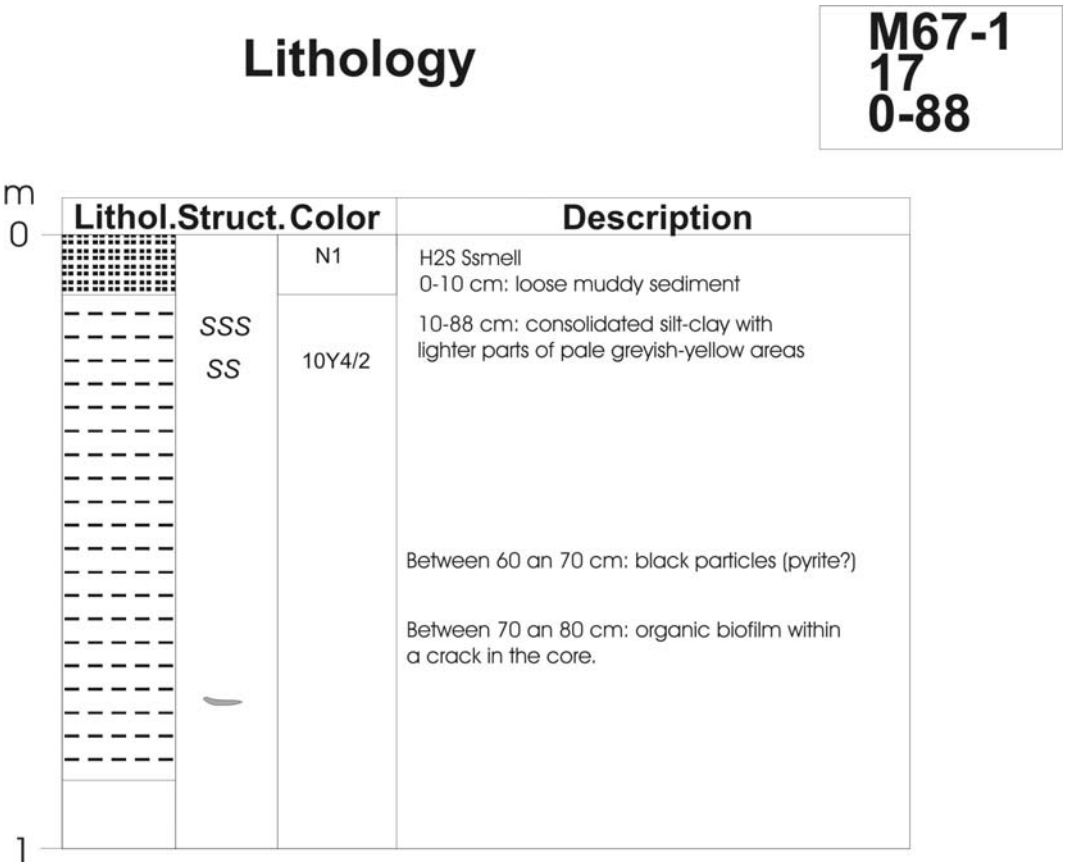

Figure 7.5.8: *Core description Station M67-1/ 17/ 0-88 cm*

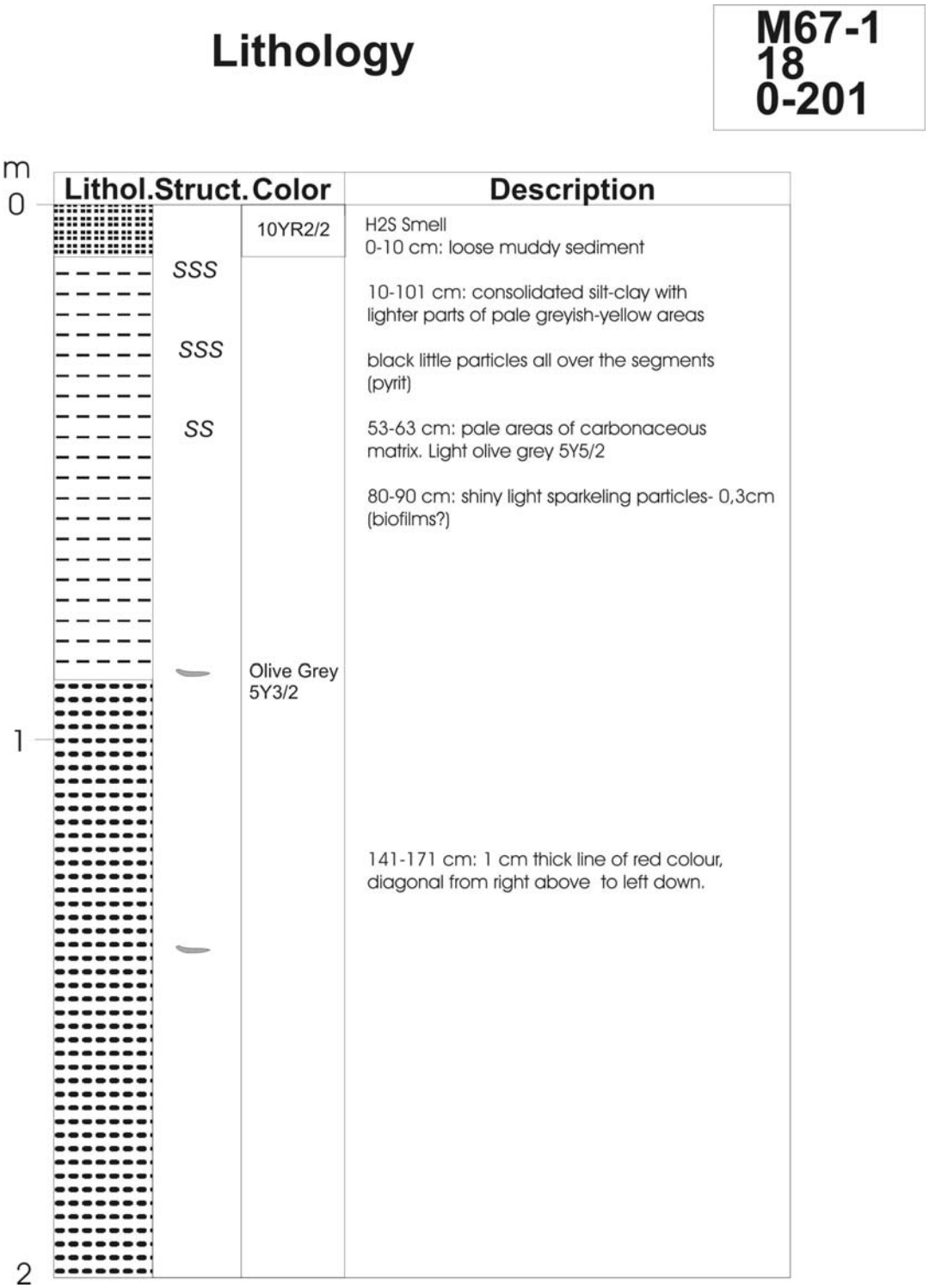

Figure 7.5.9: *Core description Station M67-1/ 18/ 0-201 cm*

-Station 19-

The core at station 19 was taken on a small mound structure similar in size to the one sampled with station 17 and 18 (Fig. 7.1.1). However, there was no pre-site information from earlier cruises and from the PARASOUND survey. The total recovery was about 260 cm of homogeneous, greyish-olive clay. There were only few bioturbation marks at the top, but strong indications for bioturbation between 60 and 90 cmbsf (Figure 7.5.12). The segment from 160 to 260 cmbsf had striae of different colours orientated perpendicular to the horizontal layering of the dense clay. Again, there were black particles indicating the precipitation of pyrite.

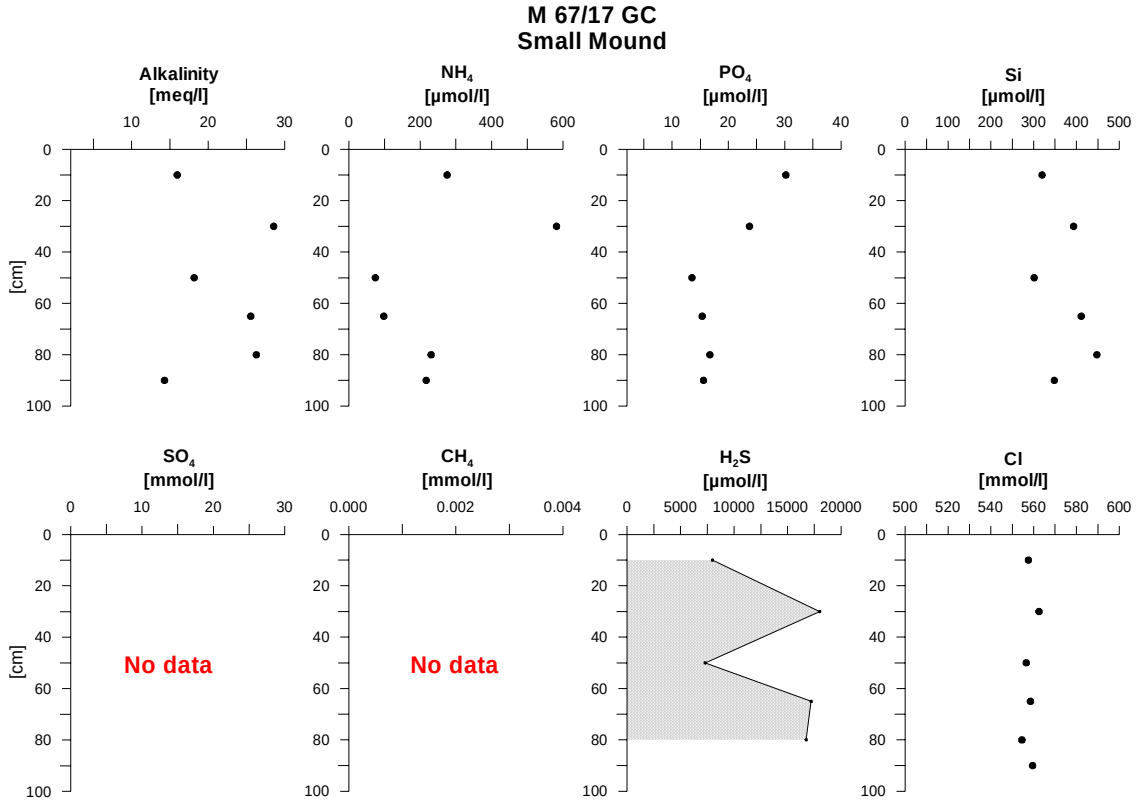

Figure 7.5.10: *Pore water geochemistry at station 17, Small Mound (Fault Prolongation)*

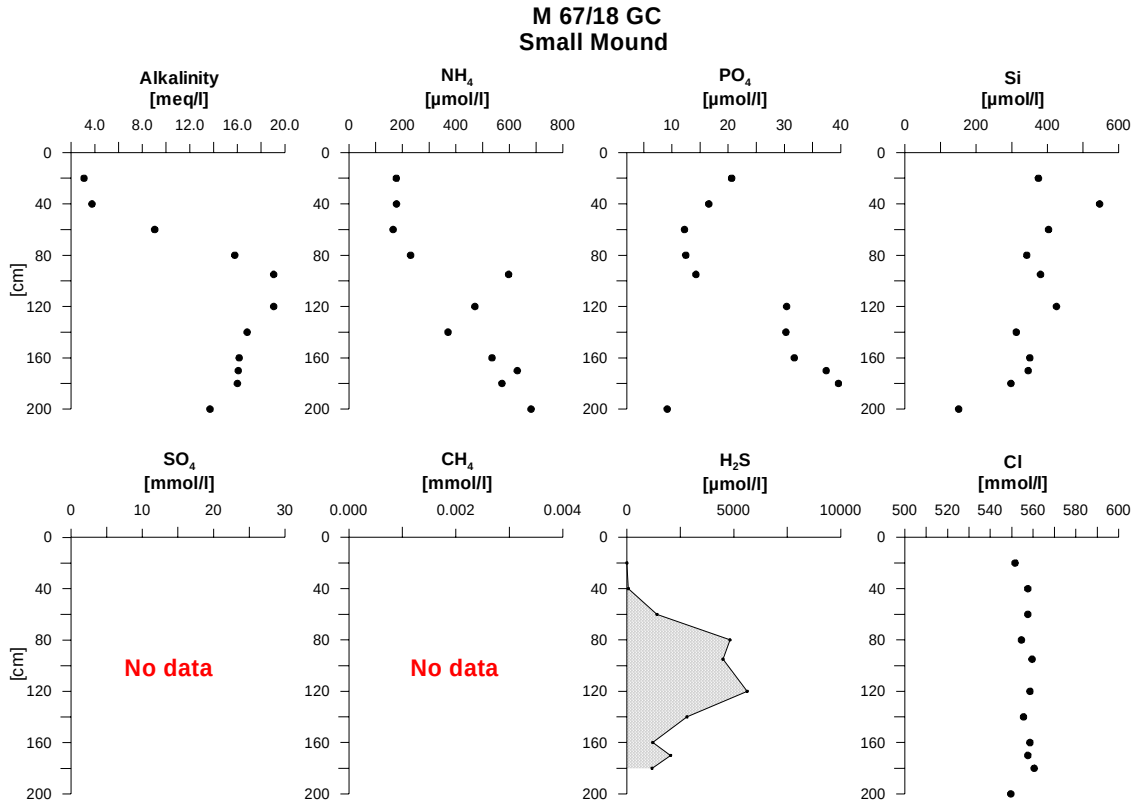

Figure 7.5.11: *Pore water geochemistry at station 18, Small Mound (Fault Prolongation)*

The pore water profiles of this nearly 3-m-long core reach slightly higher levels of alkalinity, ammonia, and phosphate than at station 16 and hence, indicate active diagenetic processes in these subsurface sediments (Figure 7.5.13). However, signs of fluid venting could not be observed and no chlorinity anomalies were detected.

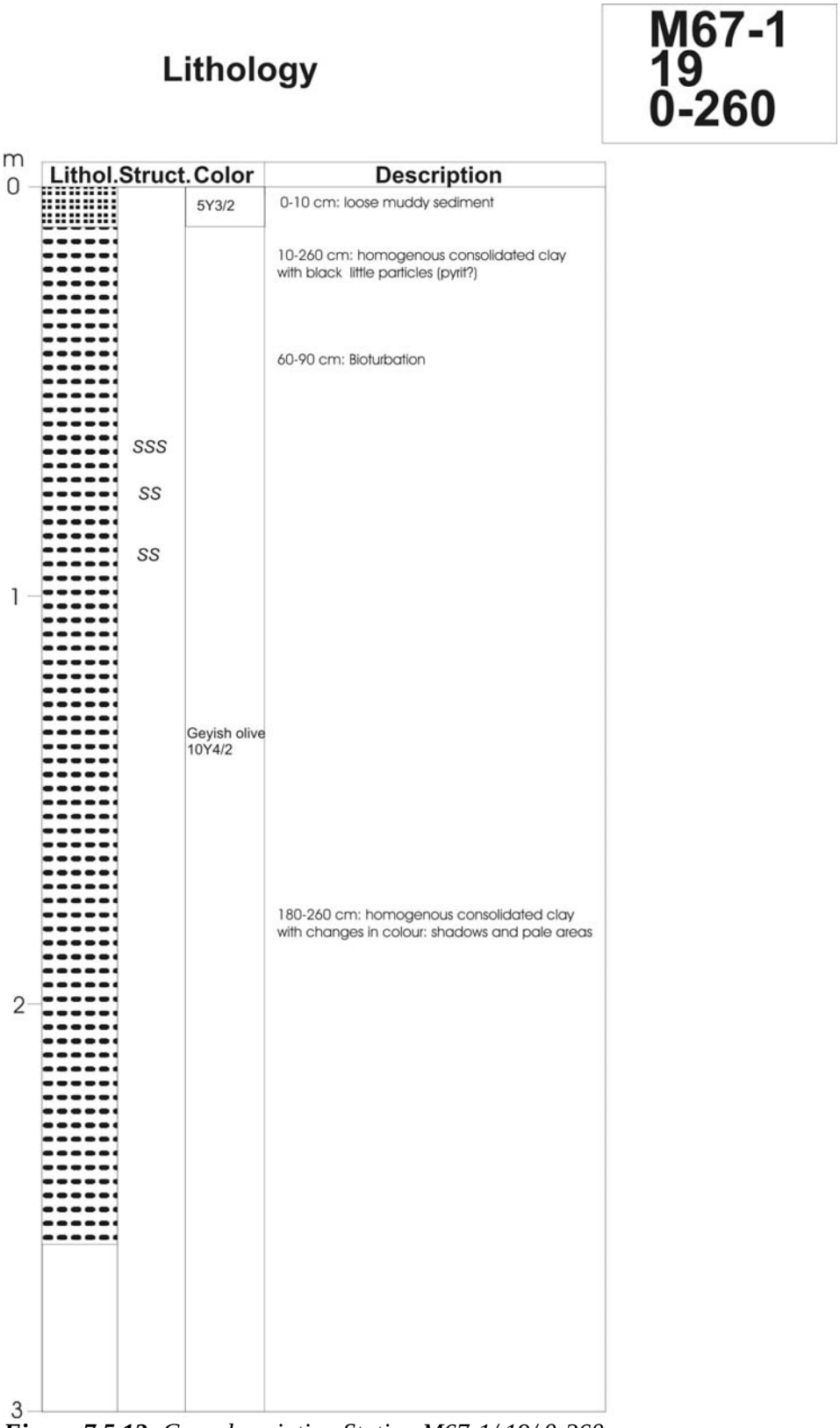

Figure 7.5.12: *Core description Station M67-1/ 19/ 0-260 cm*

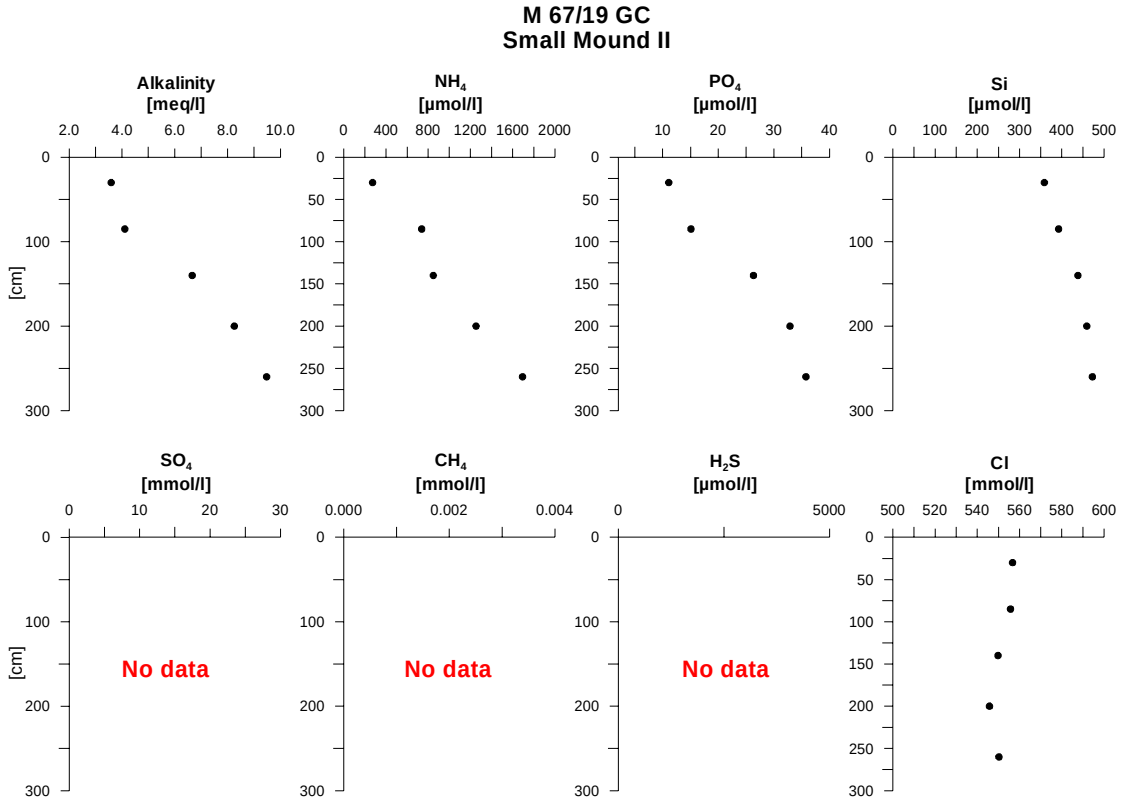

Figure 7.5.13: *Pore water geochemistry at station 19, Small Mound II*

-Station 20-

Station 20 was taken at a small, but very prominent SW-NE-trending fault (Fig. 7.1.1), which was also clearly visible in the PARASOUND survey. However, due to some problems with the navigation during deployment, it is not completely clear if the predetermined site was hit exactly. In total, 500 cm of olive-grey clay were recovered with remarkable ash lenses throughout the core (Fig. 7.5.14). Near the top, bioturbation reached down to depths of about 60 cmbsf, indicated by the downward transport of surface sediment macrofaunal activity. A prominent dark layer (probably pyrite accumulations) between 470 and 480 cmbsf gave off a slight smell of H_2S.

The pore waters of the longest core retrieved during M 67/1 are strongly enriched in nutrients and alkalinity (Fig. 7.5.15). However, especially alkalinity and phosphate exhibit linear profiles and H_2S levels are very low (H_2S could be smelt at the base of the core, but was absent in the pore water after squeezing) which is typical for intense, but normal subsurface diagenesis according to the location in a highly productive area. Hence, fluid advection can be excluded as a process affecting the geochemistry at this site. As in all other cores, chlorinity values correspond to normal sea water composition.

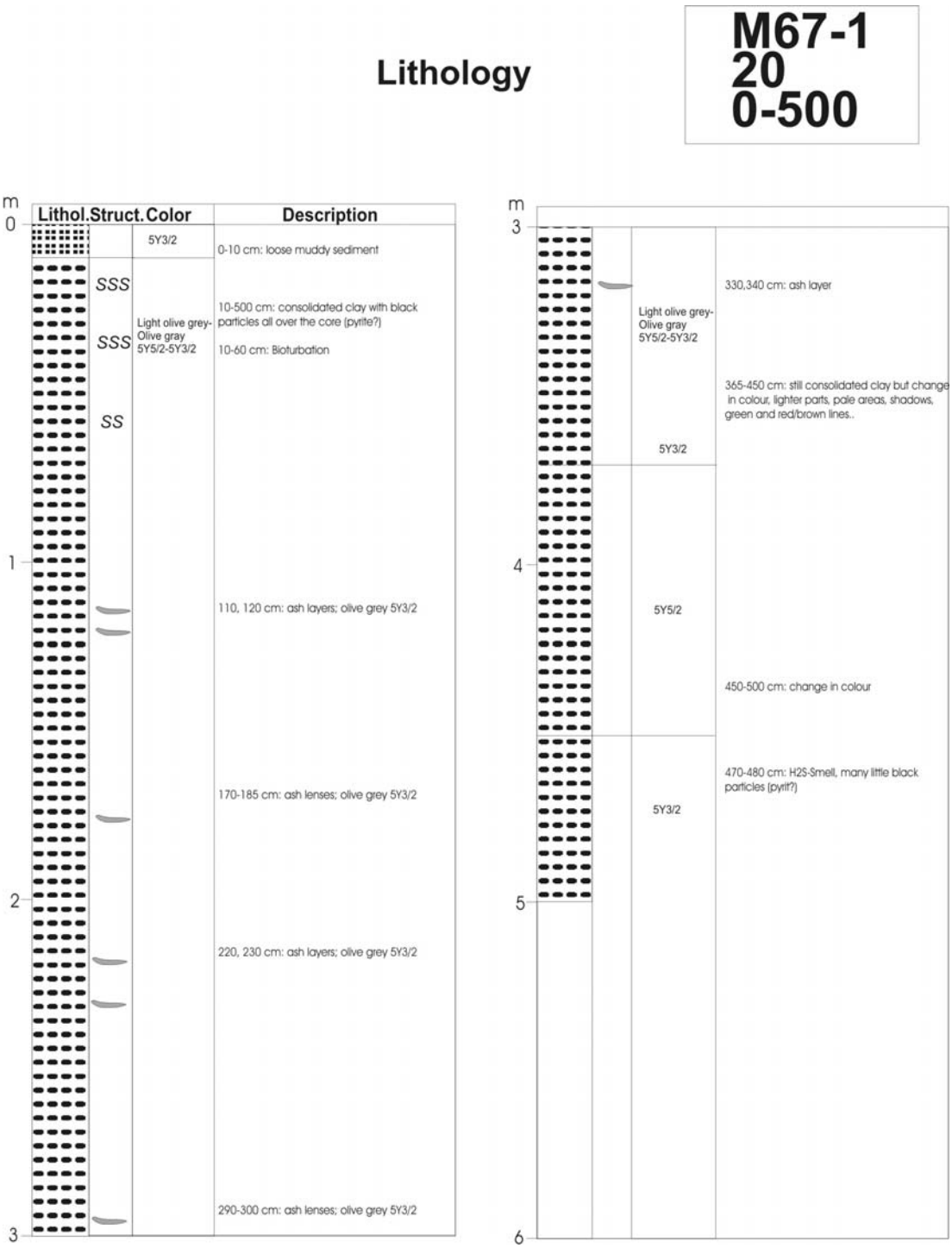

Figure 7.5.14: *Core description Station M67-1/ 20/ 0-500 cm*

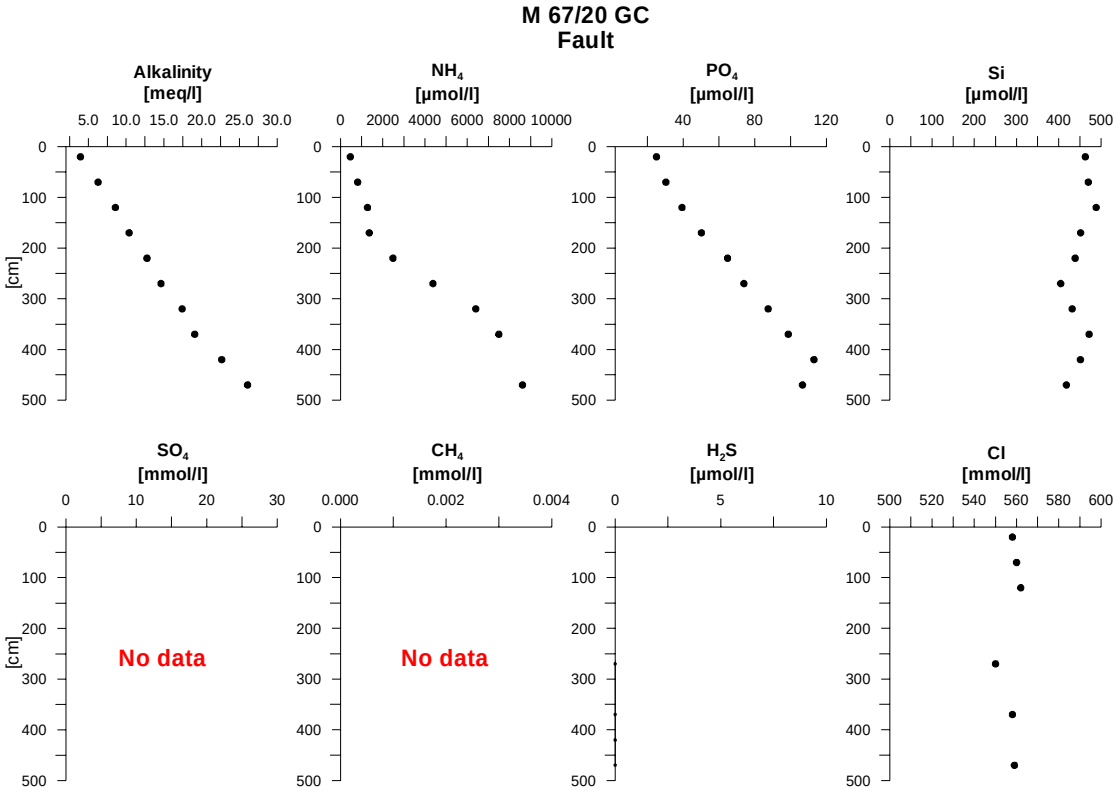

Figure 7.5.15: *Pore water geochemistry at station 20, Fault location.*

8. Acknowledgements

Expeditions with RV METEOR are sponsored by the Deutsche Forschungsgemeinschaft (DFG). The vessel is financed 70% by the DFG and 30% by the Ministry of Education and Research (BMBF). Cruise M67/1 is part of SFB-574 at Christian Albrechts University in Kiel, which is supported by the DFG. We warmly thank master Niels Jakobi and his crew for their excellent support in all the work done and for the splendid working atmosphere throughout the entire working programme.

Chapter 2.2:
Bathymetry data from central and northern Chile were collected with R/V SONNE funded by the German Ministry of Research and Education (BMBF). Jaques Bourgois kindly provided the multibeam bathymetry from the Chile Triple Junction area. The stack of R/V R. Conrad line 769 was kindly provided by J Alsop from Lamont Doherty Earth Observatory. J Laursen and D Klaeschen processed Sonne 101-15. All figures in this paper have been produced with the GMT package (Wessel and Smith, 1998).

Figures 5.1, 5.2, 6.6.2, 6.6.3 and 6.6.4 were provided by Thomas Liebe, Reederei F. Laeisz GmbH, Bremerhaven.

9. References

Ballance et al., Subduction of a large Cretaceous seamount of the Louisville ridge at the Tonga Trench: A model of normal and accelerated tectonic erosion. Tectonics 8, 953-962, 1989

Bangs N.L., S.C. Cande, S.D. Lewis, and J.J. Miller, Structural framework of the Chile margin at the Chile Ridge collision zone, Proc. Ocean Drill. Program, Initial Rep., 141, 11-21, 1992

Bangs N.L. and S. Cande, The episodic development of a convergent margin inferred from structures and processes along the southern Chile margin, Tectonics, v. 16, N° 3, 489-505,. 1997

Behrmann, J.H., et al., Proceedings of the Ocean Drilling Program, Initial Reports., vol. 141, 708 pp., Ocean Drill. Program, College Station, Tex., 1992

Behrmann, J.H., S.D. Lewis, S.C. Cande, and ODP Leg 141 Scientific Party, Tectonics and geology of spreading ridge subduction at the Chile Triple Junction: A synthesis of results from Leg 141 of the Ocean Drilling Program, Geol. Rundsch., 83, 832-852, 1994.

Behrmann, J. H. and A. Kopf, Balance or tectonically accreted andsubducted sediment at the Chile Triple Junction, International Journal of Earth Sciences, 90, 753-768, 2001

Bourgois, J., Martin, H., Lagabrielle, Y., Le Moigne, J., and Frutos Jara, J., Subduction-erosion related to spreading-ridge subduction: Taitao peninsula (Chile margin triple junction area), Geology, 24, 723-726, 1996

Bourgois, J., Guivel, C., Lagabrielle, Y., Calmus, T., Boulegue, J., Daux, V., Glacial-interglacial trench supply variation, spreading-ridge subduction, and feedback controls on the Andean margin development at the Chile triple junction area (45-48˚ S), Journal of Geophysical Research, 105, 8355-8386, 2000

Cande S.C. and R.B. Leslie, Late Cenozoic tectonics of the southern Chile trench, J. Geophys. Res., 91, 471-496, 1986

Cande, S.C., Leslie, R.B., Parra, J.C., Hobart, M., Interaction between the Chile Ridge and the Chile trench: Geophysical and geothermal evidence. J. Geophys. Res., 92, 495-520, 1987

Caress, D. W., and Chayes, D. N., Improved processing of HYDROSWEEP DS multibeam data on R/V Maurice Ewing, Mar. Geophys. Res., 18, 631-650, 1996

DeMets, C., Gordon, R. G., Argus, D. F., and Stein, S., Current plate motions, Geophys. J. Int., 101, 425-478, 1990

Diaz, J. L. Sediment subduction and accretion at the Chilean convergent margin between 35° and 40°S. PhD, Christian-Albrechts-Universität zu Kiel, 130 pp., 1999

Fisher, R.L., and R.W. Raitt, Topography and structure of the Peru-Chile trench, Deep-Sea Res. 9, 423-443, 1962

Flueh, E.R., Vidal, N., Ranero, C.R., Hojka, A., von Huene, R., Bialas, J., Hinz, K., Cordoba, D., Dañobeitia, J.J., and Zelt, C., seismic investigation of the continental margin off- and onshore Valparaiso, Chile, Tectonophysics 288, p. 251-263, 1998

Grasshoff, K., Ehrhardt, M., and Kremling, K., Methods of seawater analysis, Verlag Chemie, 1997

Kimura, G., et al., Proceedings of the Ocean Drilling Program Initial Reports, vol. 170, Ocean Drill. Program, College Station, Tex., 1997.

Lagabrielle, Y., Guivel, C., Maury, R., Bourgois, J., Fourcade, S., Martin, H., Magmatic-tectonic effects of high thermal regime at the site of active ridge subduction: the Chile triple junction model, Tectonophysics, 326, 255-268., 2000

Laursen, J., Scholl, D., von Huene, R., Neotectonic deformation of the central Chile margin: Deepwater forearc basin formation in response to hot spot ridge and seamount subduction. Tectonics, 21, 1038, doi:10,1029/2001TC901023, 2002

Polonia, A., Brancoloni, G., Torelli, L., Vera, E., Structural variability at the active continental margin off southernmost Chile. J. Geodynamics, 27, 289-307, 1999

Polonia, A., Brancoloni, G., Loreto, M.F., Torelli, L., The accretionary complex of southernmost Chile from the analysis of multichannel seismic data. Terra Antartica, 8, 87-98, 2001

Ranero, C.R. and von Huene R., Subduction erosion along the Middle America convergent margin, Nature, 404, 748-752, 2000

Ranero, C.R., R. von Huene, E. Flueh, M. Duarte, D. Baca, and K. McIntosh, A cross-section of the convergent Pacific margin of Nicaragua, Tectonics, 19, 335-357, 2000

Ranero, C. R.; von Huene, R.; Weinrebe, W. and Reichert, C., Tectonic Processes along the Chile Convergent Margin published in: The Andes – from Top to Bottom. Monography Series Frontiers in Earth Sciences, Vol. 1, Springer Verlag, Eds. O. Oncken et al. (in press, a)

Ranero, C. R.; von Huene, R.; Weinrebe, W. and Barckhausen, U., Convergent margin tectonics of Middle America: A marine perspective. Ed. G. Alvarado, Central America, Geology, Hazards and Resources.A. A. Balkema Publisher (in press, b).

Rutland, R.W.R., Andean orogeny and ocean floor spreading, Nature, 233, 252-255, 1971.

Sallares, V., Ranero, C.R., Structure of the North Chile erosional convergent margin off Antofagasta (23˚30’ S), J. Geophys. Res. 110, B06101, doi 10.1029/2004JB003418, 2005

Scholl, D.W., M.N. Christensen, R. von Huene, and M.S. Marlow, Peru-Chile trench sediments and sea-floor spreading, Geol. Soc. of Am. Bull., 81, 1339-1360, 1970.

Schweller, W.J., L.D. Kulm, and R.A. Prince, Tectonics, structure, and sedimentary framework of the Perú-Chile Trench, in Nazca Plate: Crustal formation and Andean convergence, edited by L.D. Kulm et al., Mem. Geol. Soc. Am. 154, 323-349, 1981.

Smith, W.H.F., Sandwell, D.T. Bathymetric predictions from dense altimetry and sparse shipboard bathymetry. J. Geophys. Res., 99, 21803-21824, 1994.

von Huene, R.; Corvalan, J.; Flueh, E. R.; Hinz, K.; Korstgard, J.; Ranero, C. R.; Weinrebe, W. and CONDOR Scientists. Tectonic control of the subducting Juan Fernández Ridge on the Andean margin near Valparaiso, Chile. Tectonics , vol. 16, 474-488, 1997.

von Huene, R., C.R. Ranero, W. Weinrebe, and K. Hinz, Quaternary convergent margin tectonics of Costa Rica, segmentation of the Cocos Plate, and Central American volcanism, Tectonics, 19, p. 314-334, 2000.

von Huene, R.; Ranero, C. R. Subduction erosion and basal friction along the sediment starved convergent margin off Antofagasta Chile. Journal of Geophysical Research vol 108, 2079, doi10.1029/2001JB001569, 2003.

Wessel, P., and Smith, W. H. F., New version of Generic Mapping Tools released, EOS, Trans. Amer. Geophys. U. 76, 329, 1995

Wessel, P.; and Smith, W. H. F., New improved version of generic mapping tools released, EOS, Trans. Amer. Geophys. U. 79 (47), 579, 1998.

Yañez, G. A.; Ranero, C. R.; von Huene, R. and Díaz, J. A tectonic interpretation of magnetic anomalies across a segment of the convergent margin of the Southern Central Andes (32°-34°S). Journal of Geophysical. Research. 106, 6325-6345, 2001.

Yañez, G.; Cembrano, J.; Pardo, M.; Ranero, C. R.; Selles, D. The Challenger-Juan Fernández-Maipo major tectonic transition of the Nazca-Andean subduction system at 33°-34°S: geodynamic evidences and implications. Journal of South American Earth Sciences 15, 23-38, 2002.

10. Appendices

Appendix 1: Mapping profiles

Appendix 2: Magnetic profiles

Appendix 3: Station list of gravity cores

Appendix 4: Legend for stratigraphic columns

Appendix 5: Captain's Report

Appendix 6: Scripts for processing of multibeam data

Appendix 1: Mapping profiles

profile	date	time	length	position	
number		UTC –3		latitude	longitude
MB-01	24.02.06	18:17		36°13.50 S	73°29.50 W
				35°32.00 S	73°11.50 W
				35°11.00 S	73°04.50 W
	25.02.06	10:15	126 nm	34°17.70 S	72°29.40 W
MB-02	25.02.06	10:42		34°17.70 S	72°32.90 W
				35°08.00 S	73°06.00 W
				35°28.00 S	73°12.30 W
	26.02.06	01:42	118 nm	36°02.80 S	73°27.10 W
MB-03	26.02.06	01:58		36°02.80 S	73°29.50 W
	26.02.06	07:05	43 nm	35°22.00 S	73°12.00 W
MB-04	26.02.06	07:22		35°22.00 S	73°14.40 W
	26.02.06	12:24	40 nm	36°00.00 S	73°30.80 W
MB-05	26.02.06	22:27		36°16.50 S	73°43.30 W
	27.02.06	00:21	15 nm	36°31.80 S	73°43.30 W
MB-06	27.02.06	00:31		36°31.80 S	73°41.80 W
	27.02.06	02:25	15 nm	36°16.50 S	73°41.80 W
MB-07	27.02.06	05:37		35°51.40 S	73°37.60 W
				35°29.00 S	73°27.00 W
				35°04.80 S	73°11.90 W
	27.02.06	19:39	116 nm	34°10.79 S	72°38.86 W
MB-08	27.02.06	21:28		34°10.78 S	72°56.04 W
				35°05.00 S	73°26.00 W
				35°44.00 S	73°42.50 W
	28.02.06	15:14	139 nm	36°17.00 S	73°46.00 W
MB-09	01.03.06	04:01		36°16.50 S	73°39.20 W
	01.03.06	06:08	12 nm	36°28.40 S	73°39.80 W
MB-10	01.03.06	06:15		36°28.40 S	73°38.80 W
	01.03.06	08:13	12 nm	36°16.50 S	73°38.20 W
MB-11	01.03.06	08:22		36°16.50 S	73°37.20 W
	01.03.06	09:11	5 nm	36°21.40 S	73°37.50 W
MB-12	01.03.06	09:18		36°21.40 S	73°36.70 W
	01.03.06	10:05	5 nm	36°16.50 S	73°36.30 W
MB-13	01.03.06	15:51		36°09.50 S	73°44.80 W
	01.03.06	19:32	21 nm	36°30.00 S	73°44.80 W
MB-14	02.03.06	09:13		35°45.00 S	74°02.30 W
				34°06.00 S	73°12.60 W
	03.03.06	03:06	139 nm	33°35.00 S	73°15.70 W
MB-15	03.03.06	04:00		33°35.00 S	73°24.00 W
				34°04.80 S	73°21.70 W
	03.03.06	12:14	65 nm	34°38.20 S	73°38.20 W
MB-16	03.03.06	13:10		34°33.00 S	73°45.00 W
	03.03.06	17:26	33 nm	34°02.00 S	73°29.80 W

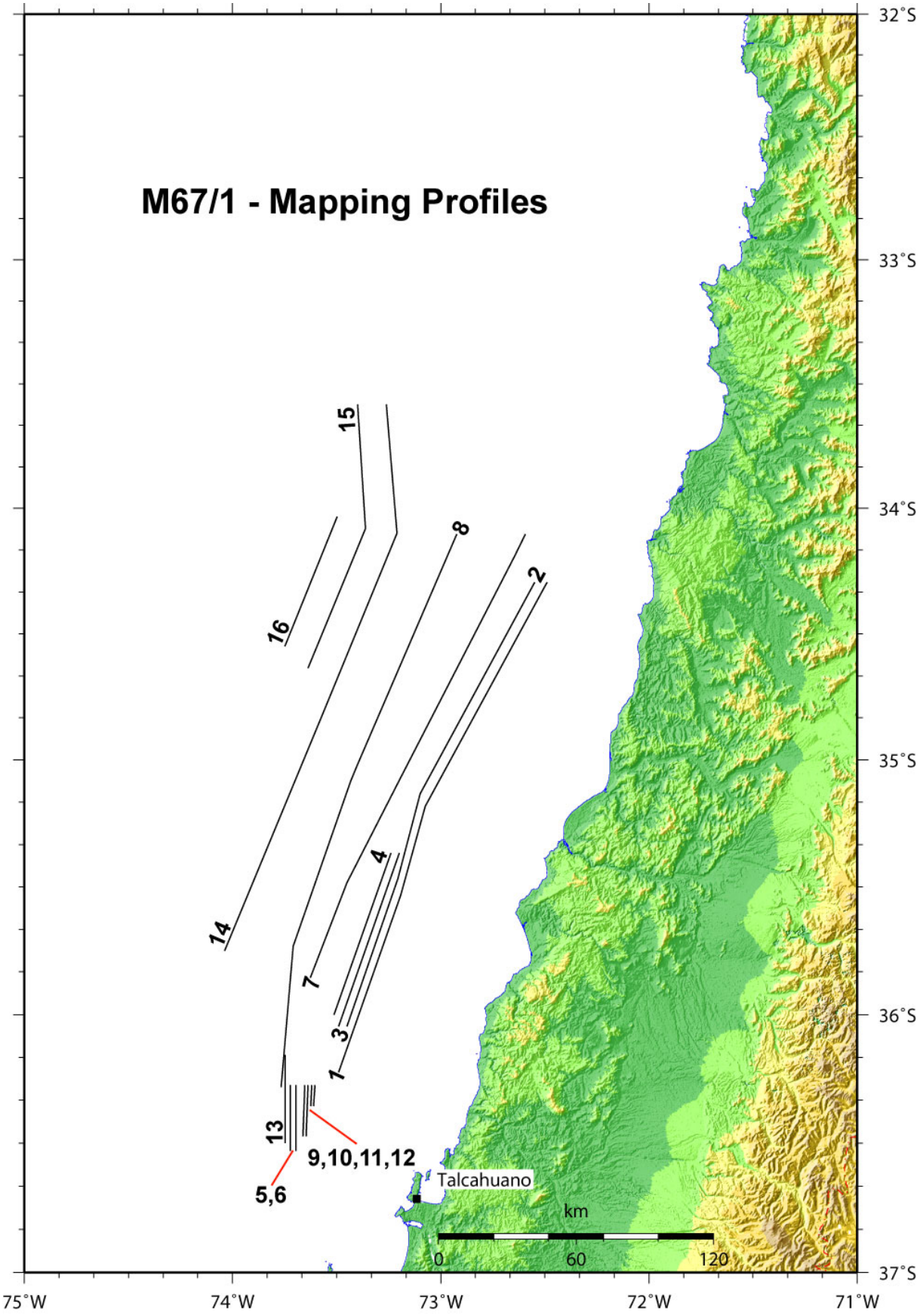
M67/1 - Mapping Profiles
32°S
33°S
34°S
35°S
36°S
37°S
75°W
74°W
73°W
72°W
71°W
15
16
8
2
14
7
4
3
1
13
9,10,11,12
5,6
Talcahuano
km
0
60
120

Appendix 2: Magnetic profiles

profile	date	time	length	position	
number		UTC –3		latitude	longitude
MAG-01	24.02.06	18:17		36°13.50 S	73°29.50 W
				35°32.00 S	73°11.50 W
				35°11.00 S	73°04.50 W
	25.02.06	10:15	126 nm	34°17.70 S	72°29.40 W
MAG-02	25.02.06	10:42		34°17.70 S	72°32.90 W
				35°08.00 S	73°06.00 W
				35°28.00 S	73°12.30 W
	26.02.06	01:42	118 nm	36°02.80 S	73°27.10 W
MAG-03	26.02.06	01:58		36°02.80 S	73°29.50 W
	26.02.06	07:05	43 nm	35°22.00 S	73°12.00 W
MAG-04	26.02.06	07:22		35°22.00 S	73°14.40 W
	26.02.06	12:24	40 nm	36°00.00 S	73°30.80 W
MAG-05	26.02.06	22:27		36°16.50 S	73°43.30 W
	27.02.06	00:21	15 nm	36°31.80 S	73°43.30 W
MAG-06	27.02.06	00:31		36°31.80 S	73°41.80 W
	27.02.06	02:25	15 nm	36°16.50 S	73°41.80 W
MAG-07	27.02.06	05:37		35°51.40 S	73°37.60 W
				35°29.00 S	73°27.00 W
				35°04.80 S	73°11.90 W
	27.02.06	19:39	116 nm	34°10.79 S	72°38.86 W
MAG-08	27.02.06	21:28		34°10.78 S	72°56.04 W
				35°05.00 S	73°26.00 W
				35°44.00 S	73°42.50 W
	28.02.06	15:14	139 nm	36°17.00 S	73°46.00 W
MAG-14	02.03.06	09:13		35°45.00 S	74°02.30 W
				34°06.00 S	73°12.60 W
	03.03.06	03:06	139 nm	33°35.00 S	73°15.70 W
MAG-15	03.03.06	04:00		33°35.00 S	73°24.00 W
				34°04.80 S	73°21.70 W
	03.03.06	12:14	65 nm	34°38.20 S	73°38.20 W
MAG-16	03.03.06	13:10		34°33.00 S	73°45.00 W
	03.03.06	17:26	33 nm	34°02.00 S	73°29.80 W

Appendix 3: Station list of gravity cores

Station No.	Latitude (S)	Longitude (W)	Water Depth	Recovery
5	S 35°55,07	73°34,40	1170 m	core catcher, consolidated mud
6	S 35°55,37	73°34,66	1172 m	85 cm, consolidated mud
7	S 36°01,45	73°35,30	780 m	146 cm, consolidated mud
8	S 36°01,94	73°35,28	746 m	core catcher, consolidated mud
15-1	S 36°26,55	73°42,14	706 m	core catcher, cemented shells
15-2	S 36°26,57	73°42,10	707 m	36 cm, mud + carbonates
16	S 36°23, 74	73°43,31	787 m	370 cm, soft sediment
17	S 36°21,90	73°43,34	848 m	88 cm, soft sediment, H_2S smell
18	S 36°22,25	73°43,35	832 m	201, soft sediment, H_2S smell
19	S 36°21,84	73°42,14	748 m	260, soft sediment
20	S 36°20, 54	73°41,87	858 m	500, soft sediment

Appendix 4:

Legend for stratigraphic columns

Lithology

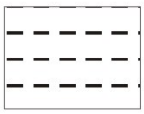
Silty clay

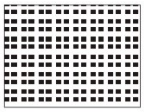
Silt

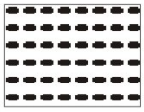
Consolidated clay

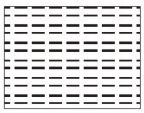
Clay

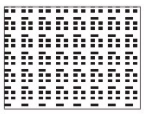
Sandy silt

Structures

SSS	bioturbated > 60% of sediment
SS	bioturbated < 30-60% of sediment
S	bioturbated < 30% of sediment

Lenses/ channels

Erosive contact

Appendix 5: Captain's Report

Reederei F. Laeisz G.m.b.H.						**FS METEOR**	
						Kapitän: Niels Jakobi	
Stationsprotokoll Reise						**M 67.1 B**	
Winden, Seile, Kabel:							
Winde	bestückt mit	RF-Nummer	aktuelle Länge	aufgelegt	Zustand	Bemerkungen	
W 01	COSA 8 8 mm	720090	5930	Sep 01	3		
W 02	Kabel 11 mm	50500433	6000	Feb 06	1	Neubelegung in Werft 02/2006	
W 03	Kabel 11 mm	723005	6000	Feb 06	1	Neubelegung in Werft 02/2006	
W 04	Seil 12 mm	11308	(1011)	Apr 04	2	auf Haspel im Laderaum	
W 05	Kurrleine 20 mm	727406	3000	Aug 98	2	Winde ausgelagert HH	
W 06	Kurrleine 20 mm	727406	3000	Aug 98	2	Winde ausgelagert HH	
W 09	Kabel 11 mm	725331	8190	Sep 01	2	Winde ausgelagert HH	
W 11	Seil 18 mm	723011	10726	Okt 03	3		
W 12	Kabel 18 mm	80400823	8005	Nov 05	1	neu aufgelegt am 20.11.2005	
W 13	Netzsondenkabel 13 mm	Erstausrüst.	2732	Feb 86	4	Winde ausgelagert HH	

Winde	Einsatzzeit			Arbeits-länge m	max. gest. Länge	Bemerkungen
	vorherige	diese Reise	gesamt			
W 01	142,9	3,1	146,0	1900	3455	Sept. 01 neu aufgelegt W 01 spult nicht optimal, Kunststoffseil ist nicht formstabil

W 02	0,0	1,0	1,0	50	50	Neubelegung in Werft 02/2006	
W 03	0,0	0,0	0,0	0	0	Neubelegung in Werft 02/2006	
W 04	4,8	0,0	4,8	0	0	Juli 04 Seil 12mm abgetrommelt, Stauraum	
(W 09)	3,6	0,0	3,6	0	5005	Sept. 01 neu aufgelegt - Winde 10/04 **ausgelagert**	
W 11	691,6	7,2	698,8	1178	10250	Okt.03 neu aufgelegt	
W 12	0,2	2,2	2,4	240	240	aufgelegt am 20.11.2005 in Corinto	
(W 13)	23,6	0,0	23,6	0	0	letzter Einsatz 30.7.00 - Winde 10/04 **ausgelagert**	

Abkürzungen im Stationsprotokoll:

a.D.	an Deck	KL	Kabellänge
z.W.	zu Wasser	PN	PARASOUND
WT	Wassertiefe PN	HS	HYDROSWEEP
Pi	Pinger Schiff	BoKo	Bodenkontakt
SL	Seil-/Kabellänge	BoSi	Bodensicht

Eingesetzte seilgebundene Geräte	**Einsätze**
Transponder (zur Kalibrierung Echolote)	6
Magnetometer (parallel zu Fächerlotprofilen)	3
Schwerelote (SL6m)	11
Side-Scan mit Deep Tow Streamer (DTS) und Airgun	1

Eingesetzte nicht seilgebundene Geräte	**Einsätze**
Transponder, 2 x aus und wieder aufgenommen, zur Kalibrierung von POSIDONIA	2
Gesamteinsätze während der M 67.1 B Reise auf 21 Stationen 23 Geräteeinsätze	
Geräteverluste: KEINE	
Insgesamt wurden 27 Fächerlotprofile mit insgesamt 1005 sm gefahren. Dabei kam bei 3 Profilgruppen das Magnetometer zum Einsatz.	
Bemerkungen:	
Zeitangaben alle in UTC, Positionen nach GPS	
Tiefenangaben: wenn nicht besonders vermerkt, wurden PARASOUND-Tiefen notiert	

		Bemerkungen	Position						Meteorologische Beobachtungen								
			Breite			Länge			Wind		Bedeckung	Luft		Wasser	Dünung		
Zeit	Beginn/Ende Station		Grad	Min	N/S	Grad	Min	E/W	dd	ff	N	Druck	Temp.	Temp.	Richt.	Periode	Höhe
[UTC]		**21 Stationen**	[°]			[°]				[Bft.]		[hPa]	[°C]	[°C]	[°]	[s]	[m]
13:12		Abfahrt Talcahuano															
17:30		Anfang der Seereise	36	39,34	S	73	1,06	W	NE	3	c	1014,1	18,4	17,0			
20:25		Beginn der Stationsarbeiten der Reise M 67.1	36	42,44	S	73	35,29	W									
20:25	Beginn	Transponder z. W. (wegen Kalibrierung Echolotanlagen)	36	42,44	S	73	35,29	W									
20:39		Transponder SL max = 278 m	36	42,46	S	73	35,28	W									
20:48	Ende	Transponder a.D.	36	42,46	S	73	35,28	W									
		anschliessend diverse Kurse zum Testen der neuen Lotanlagen nach Vorgaben der Techniker															
4:29	Beginn	Transponder z. W. (wegen Kalibrierung Echolotanlagen)	36	30,83	S	73	32,00	W	WNW	4	c	1012,9	16,4	14,9	240	8	2,0
4:33		Transponder SL max = 120 m	36	30,79	S	73	31,99	W									
4:40	Ende	Transponder a.D.	36	30,77	S	73	31,99	W									
		anschliessend diverse Kurse zum Testen der neuen Lotanlage EM 710 nach Vorgaben der Techniker															
11:36	Beginn	Transponder z. W. (wegen Kalibrierung Echolotanlagen)	36	37,65	S	74	14,94	W	SW	4	c	1014,7	16,3	16,9	240	8	1,5
12:09		Transponder SL max = 718 m	36	37,32	S	74	15,22	W									
12:50		Transponder a.D.	36	37,04	S	74	14,83	W									
13:17		Transponder z. W. (wegen Kalibrierung Echolotanlagen)	36	37,80	S	74	15,00	W									
14:02		Transponder SL max = 1900 m	36	37,31	S	74	15,00	W									

14:39	Ende	Transponder a.D.	36	37,11	S	74	14,34	W										
		anschliessend diverse Kurse zum Testen der neuen Lotanlagen nach Vorgaben der Techniker																
13:36		Ankern vor Talcahuano, 5 Personen von Bord, Ausklarierung für Panama	36	42,17	S	73	5,54	W										
14:36		Ende Ankerzeit, Fortsetzung der Reise	36	42,17	S	73	5,54	W										
17:00		Beginn der Datenaufzeichnungen Reise M67.1	36	22,30	S	73	15,07	W	SSE	5/6	c	1010,0	16,5	16,2	230	8	1,5
18:19	Beginn	Beginn Fächerlotprofil 1, rwK 019°, d = 44 sm, v = 8,0 kn	36	13,50	S	73	29,50	W										
19:56		Magnetometer z.W.	36	1,08	S	73	24,10	W										
23:51		ä.K. rw 015°, d = 22 sm	35	32,00	S	73	11,50	W	SSW	5/6	c	1011,0	23,6	15,9	230	8	2,0
2:35		ä.K. rw 029°, d = 61 sm	35	11,00	S	73	4,50	W										
10:17		Ende Profil 1	34	17,70	S	72	29,40	W										
10:43		Beginn Fächerlotprofil 2, rwK 208°, d = 58 sm, v = 8,0 kn	34	17,70	S	72	32,90	W	umlfd.	1	co	1012,6	16,8	18,0	230	8	2,0
21:11		ä.K. rw 199°, d = 37 sm	35	28,00	S	73	12,30	W	SWz S	3	o	1013,6	16,0	16,6	230	8	2,0
1:42		Ende Profil 2	36	2,80	S	73	27,10	W										
1:56		Beginn Fächerlotprofil 3, rwK 019°, d = 43 sm, v = 8,0 kn	36	2,80	S	73	29,50	W										
7:07		Ende Profil 3	35	22,00	S	73	12,00	W										
7:27		Beginn Fächerlotprofil 4, rwK 199°, d = 40 sm, v = 8,0 kn	35	22,00	S	73	14,40	W	S'l.	4	c	1013,1	14,3	15,6	230	8	2,0
12:24		Ende Profil 4	35	59,76	S	73	30,87	W										
12:24		Beginn Fächerlotprofil 5, rwK 320°, d = 5 sm, v = 8,0 kn	35	59,76	S	73	30,87	W										
13:09	Ende	Ende Profil 5, Magnetometer a.D.	35	55,58	S	73	33,76	W										
13:52	Beginn	SL6m z.W.	35	55,07	S	73	34,39	W										
14:11		SL6m BoKo bei SL = 1173 m, Zug max = 24,5 kN	35	55,07	S	73	34,40	W										
14:34	Ende	SL6m a.D.	35	55,58	S	73	33,76	W										
15:10	Beginn	SL6m z.W.	35	55,59	S	73	34,72	W	W'l.	3	o	1016,4	16,0	15,2	230	9	2,0
15:29		SL6m BoKo bei SL = 1178 m, Zug max = 25,7 kN	35	55,37	S	73	34,66	W										
15:53	Ende	SL6m a.D.	35	55,37	S	73	34,67	W										
17:04	Beginn	SL6m z.W.	36	1,43	S	73	35,31	W										
17:14		SL6m BoKo bei SL = 791 m, Zug max = 32,0 kN	36	1,45	S	73	35,30	W										

17:37	Ende	SL6m a.D.	36	1,39	S	73	35,32	W										
18:02	Beginn	SL6m z.W.	36	1,95	S	73	35,28	W										
18:15		SL6m BoKo bei SL = 752 m, Zug max = 20,4 kN	36	1,94	S	73	35,28	W										
18:35	Ende	SL6m a.D.	36	1,95	S	73	35,53	W										
18:49	Beginn	Transponder z. W. (wegen Kalibrierung POSIDONIA)	36	1,84	S	73	35,71	W										
18:52		Transponder SL max = 50 m	36	1,84	S	73	35,71	W										
19:20		Transponder a.D.	36	1,54	S	73	35,80	W										
19:44		Transponder z. W. (wegen Kalibrierung POSIDONIA)	36	2,36	S	73	35,65	W	S'l.	4	c	1017,9	17,1	15,0	230	8	2,0
19:47		Transponder SL max = 50 m	36	2,36	S	73	35,65	W										
20:11	Ende	Transponder a.D.	36	2,01	S	73	35,67	W										
20:21	Beginn	Beginn Fächerlotprofil 6, rwK 204°, d = 16 sm, v = 8,0 kn	36	1,95	S	73	35,26	W										
20:24		Magentometer z.W.	36	2,10	S	73	35,33	W										
22:27		ä.K. rw 090°, d = 15 sm	36	16,50	S	73	43,25	W	SSW	4	c	1018,8	15,3	14,4	230	8	2,0
0:20		Ende Profil 6	36	31,55	S	73	43,26	W										
0:30		Beginn Fächerlotprofil 7, rwK 360°, d = 15 sm, v = 8,0 kn	36	31,80	S	73	43,30	W										
2:26		ä.K. rw 010°, d = 19 sm	36	16,50	S	73	41,80	W										
5:41		ä.K. rw 021°, d = 24 sm	35	51,43	S	73	37,58	W										
8:37		ä.K. rw 341°, d = 4 sm	35	29,00	S	73	27,00	W	S'l.	7	c	1017,3	14,6	16,3	230	8	2,5
11:54		ä.K. rw 030°, d = 63 sm	35	4,80	S	73	11,90	W										
12:30		ä.K. rw 027°, d = 27 sm	35	0,13	S	73	13,63	W	S'l.	7	c	1017,6	17,8	17,1	230	8	2,5
19:35		Brechen Profil ab und ändern Kurs wegen Manöver der chilenischen Marine	34	11,06	S	72	38,62	W	S'l.	7	c	1016,0	18,4	17,7	230	9	3,0
19:35		Beginn Fächerlotprofil 8, rwK 270°, d = 16 sm, v = 8,0 kn	34	11,06	S	72	38,62	W										
21:40		Ende Profil 8	34	10,98	S	72	57,96	W										
21:40		Beginn Fächerlotprofil 9, rwK 203°, d = 59 sm, v = 8,0 kn	34	10,98	S	72	57,96	W										
5:32		ä.K. rw 199°, d = 41 sm	35	4,97	S	73	25,98	W	S	6	c	1015,9	15,7	16,8	230	9	3,0
10:55		ä.K. rw 184°, d = 32 sm	35	44,00	S	73	42,50	W	SSW	4/5	c	1016,7	14,7	14,8	230	9	3,0
15:10		Ende Profil 9	36	17,14	S	73	46,00	W	SSW	4	c	1017,7	15,7	14,3	230	9	3,0
15:49	Ende	Magnetometer a.D.	36	18,29	S	73	42,66	W										

16:48	Beginn	Beginn Einmessen POSIDONIA, Transponder ausgesetzt und abgetaucht	36	17,96	S	73	42,26	W									
16:50		diverse Kurse zum Einmessen POSIDONIA	36	17,96	S	73	42,26	W									
22:35		Ende Kalibrierung, Auslösung Transponder	36	17,90	S	73	42,11	W	SW'l.	3/4	c	1017,1	15,7	14,1	230	9	3,0
22:57		Transponder a.D.	36	17,88	S	73	42,41	W									
0:10		Fortsetzung Einmessen POSIDONIA, Transponder ausgesetzt und abgetaucht	36	9,47	S	73	38,92	W									
0:11		diverse Kurse zum Einmessen POSIDONIA	36	9,47	S	73	38,92	W									
2:10		Ende Kalibrierung, Auslösung Transponder	36	9,43	S	73	38,86	W									
2:23	Ende	Transponder a.D.	36	9,46	S	73	38,62	W	SW'l.	4	c	1017,2	15,1	14,7	230	9	3,0
4:08	Beginn	Beginn Fächerlotprofil 10, rwK 182°, d = 12 sm, v = 6,0 kn	36	16,50	S	73	39,20	W									
6:07		Ende Profil 10	36	28,40	S	73	39,80	W									
6:07		Beginn Fächerlotprofil 11, rwK 090°, d = 1 sm, v = 6,0 kn	36	28,40	S	73	39,80	W									
6:16		Ende Profil 11	36	28,40	S	73	38,80	W									
6:16		Beginn Fächerlotprofil 12, rwK 002°, d = 12 sm, v = 6,0 kn	36	28,40	S	73	38,80	W									
8:16		Ende Profil 12	36	16,50	S	73	38,20	W	SSW	4	c	1016,5	14,2	13,9	230	9	3,0
8:16		Beginn Fächerlotprofil 13, rwK 090°, d = 1 sm, v = 6,0 kn	36	16,50	S	73	38,20	W									
8:24		Ende Profil 13	36	16,50	S	73	37,20	W									
8:24		Beginn Fächerlotprofil 14, rwK 183°, d = 5 sm, v = 6,0 kn	36	16,50	S	73	37,20	W									
9:14		Ende Profil 14	36	21,40	S	73	37,50	W									
9:14		Beginn Fächerlotprofil 15, rwK 090°, d = 1 sm, v = 6,0 kn	36	21,40	S	73	37,50	W									
9:19		Ende Profil 15	36	21,40	S	73	36,70	W									
9:19		Beginn Fächerlotprofil 16, rwK 004°, d = 5 sm, v = 6,0 kn	36	21,40	S	73	36,70	W									
10:08		Ende Profil 16	36	16,50	S	73	36,30	W									
10:08		Beginn Fächerlotprofil 17, rwK 298°, d = 6 sm, v = 6,0 kn	36	16,50	S	73	36,30	W	SSW	2/3	c	1016,1	14,5	14,1	230	8	2,0
11:15	Ende	Ende Profil 17	36	13,31	S	73	43,93	W									
12:25	Beginn	Deep-Tow-Streamer z.W.	36	10,29	S	73	42,36	W									
12:28		Side-Scan z.W.	36	10,29	S	73	42,36	W									
12:50		Depressor z.W.	36	11,52	S	73	42,35	W									

13:53		Probleme mit Datenübertragung, Hieven Gerät a.D., SL max = 240 m	36	13,60	S	73	43,05	W									
14:14		Depressor a.D.	36	14,26	S	73	43,23	W									
14:32		Side-Scan a.D.	36	14,54	S	73	43,56	W									
14:35	Ende	Deep-Tow-Streamer a.D.	36	14,56	S	73	43,69	W									
15:40	Beginn	Beginn Fächerlotprofil 18, rwK 270°, d = 1 sm, v = 6,0 kn	36	8,50	S	73	43,60	W	SSW	3	c	1017,7	17,6	14,6	230	8	2,5
15:52		Ende Profil 18	36	9,50	S	73	44,80	W									
15:52		Beginn Fächerlotprofil 19, rwK 180°, d = 21 sm, v = 6,0 kn	36	9,50	S	73	44,80	W									
19:17		Ende Profil 19	36	30,00	S	73	44,80	W									
19:17		Beginn Fächerlotprofil 20, rwK 270°, d = 1 sm, v = 6,0 kn	36	30,00	S	73	44,80	W									
19:28		Ende Profil 20	36	30,00	S	73	46,00	W									
19:28		Beginn Fächerlotprofil 21, rwK 360°, d = 4 sm, v = 6,0 kn	36	30,00	S	73	46,00	W									
20:03		Ende Profil 21	36	26,56	S	73	46,00	W									
20:03		Beginn Fächerlotprofil 22, rwK 090°, d = 3 sm, v = 6,0 kn	36	26,56	S	73	46,00	W									
20:36	Ende	Ende Profil 22	36	26,56	S	73	42,13	W									
20:54	Beginn	SL6m z.W.	36	26,55	S	73	42,12	W									
21:08		SL6m BoKo bei SL = 706 m, Zug max = 20,5 kN	36	26,55	S	73	42,14	W	umlfd.	3	bc	1017,5	16,5	14,6	230	8	2,0
21:25		SL6m a.D.	36	26,51	S	73	42,04	W									
21:36		SL6m z.W.	36	26,54	S	73	42,12	W									
21:50		SL6m BoKo bei SL = 714 m, Zug max = 20,5 kN	36	26,57	S	73	42,10	W									
22:09	Ende	SL6m a.D.	36	26,54	S	73	42,12	W									
22:35	Beginn	SL6m z.W.	36	23,70	S	73	43,33	W									
22:52		SL6m BoKo bei SL = 793 m, Zug max = 38,3 kN	36	23,74	S	73	43,31	W									
23:12	Ende	SL6m a.D.	36	23,59	S	73	43,96	W									
23:42	Beginn	SL6m z.W.	36	21,89	S	73	43,31	W									
23:59		SL6m BoKo bei SL = 854 m, Zug max = 35,0 kN	36	21,90	S	73	43,34	W									
0:25	Ende	SL6m a.D.	36	21,91	S	73	43,49	W									
0:43	Beginn	SL6m z.W.	36	22,26	S	73	43,42	W									
0:58		SL6m BoKo bei SL = 843 m, Zug max = 32,9 kN	36	22,25	S	73	43,35	W									

1:17	Ende	SL6m a.D.	36	22,17	S	73	43,34	W										
1:51	Beginn	SL6m z.W.	36	21,84	S	73	42,09	W										
2:06		SL6m BoKo bei SL = 753 m, Zug max = 37,9 kN	36	21,84	S	73	42,14	W										
2:25	Ende	SL6m a.D.	36	21,80	S	73	42,09	W										
2:55	Beginn	SL6m z.W.	36	20,62	S	73	41,90	W	W	4	c	1017,5	15,0	13,9	230	8	2,0	
3:44		SL6m BoKo bei SL = 861 m, Zug max = 32,7 kN	36	20,54	S	73	41,87	W										
4:02	Ende	SL6m a.D.	36	20,54	S	73	41,87	W										
4:18	Beginn	Beginn Fächerlotprofil 23, rwK 335°, d = 38 sm, v = 8,0 kn	36	19,54	S	73	42,51	W										
4:18		Magnetometer z.W.	36	19,54	S	73	42,51	W										
9:15		ä.K. rw 022°, d = 107 sm	35	45,00	S	74	2,30	W	SSW	6	c	1016,5	15,1	15,4	230	8	2,0	
22:46		ä.K. rw 355°, d = 31 sm	34	6,00	S	73	12,60	W	SSW	4/5	o	1018,9	16,4	16,8	230	8	2,0	
3:10		Ende Profil 23	33	35,06	S	73	15,68	W	S'l.	3	o	1019,2	17,7	17,4	230	8	2,0	
3:10		Beginn Fächerlotprofil 24, rwK 270°, d = 7 sm, v = 8,0 kn	33	35,06	S	73	15,68	W										
4:00		Ende Profil 24	33	35,00	S	73	23,92	W										
4:00		Beginn Fächerlotprofil 25, rwK 176°, d = 30 sm, v = 8,0 kn	33	35,00	S	73	23,92	W										
7:47		ä.K. rw 202°, d = 36 sm	34	4,80	S	73	21,70	W	SSW	5	c	1017,3	15,7	17,2	230	8	2,0	
12:15		Ende Profil 25	34	38,15	S	73	38,30	W										
12:15		Beginn Fächerlotprofil 26, rwK 312°, d = 8 sm, v = 8,0 kn	34	38,15	S	73	38,30	W										
13:09		Ende Profil 26	34	33,05	S	73	44,82	W										
13:09		Beginn Fächerlotprofil 27, rwK 022°, d = 34 sm, v = 8,0 kn	34	33,05	S	73	44,82	W	S'l.	5	c	1016,1	16,8	17,0	230	8	2,0	
17:20		Ende Profil 27	34	2,00	S	73	29,80	W										
17:35	Ende	Magnetometer a.D.	34	0,82	S	73	31,25	W	SSW	5	c	1015,5	22,3	17,4	230	8	2,0	
17:35		Ende der Stationsarbeiten Reise M67.1	34	0,82	S	73	31,25	W										
22:54		Unterbrechung der Datenaufzeichnungen	33	0,00	S	73	49,00	W	SSW	6	c	1013,6	18,3	18,7	230	8	2,0	
1:50		Fortsetzung der Datenaufzeichnungen nach Verlassen EEZ Chile	27	56,60	S	75	22,40	W	SSE	3/4	o	1015,6	19,0	19,8	220	8	1,5	
12:30		Ende der Datenaufzeichnungen der Reise M67.1	17	7,40	S	78	28,44	W	SEzS	4/5	o	1013,2	23,3	23,1	220	8	1,5	

Appendix 6: Scripts for processing of multibeam data

A6-1: Script for preprocessing of multibeam data: `prepare_work.sh`

```
#!/bin/bash
################################
# Author Stefan Ladage
# BGR - Germany
#

if [ $# != 2 ]
then
      echo "Usage: `basename $0` cruise subdir"
      exit
fi

cruise=$1
subdir=`basename $2`
# Test if there is such a subdir

datapath="/data1/Chile/$cruise"
raw_dir="$datapath/raw_em120"
work_dir="$datapath/work_em120"
script_dir= "`basename $0`"

if [ ! -d $raw_dir/$subdir  ]
then
      echo " Alert: $subdir does not exist in RAW Dir $raw_dir"
      exit
fi
#


########### functions ##################
# copy and reformat to 57
function reformat () {
      outfile=`basename $1 .all`.mb57
      echo "IN: $1   OUT: $outfile   "
      if [ -r $outfile ]
            then
            echo ".... $outfile already exists ==> skipped"
      else
            echo -en "mb copying     ...\r"
            mbcopy -P1 -F56/57 -S2 -I$1 -O${outfile}
            echo -en "mb datalisting ...\r"
            mbdatalist -N -I${outfile}
            echo -en "mb svp listing ...\r"
            mbsvplist -I${outfile} -O
            echo "${outfile} 57" >> datalist.mb-1
            echo -en "mb setting metadata ...\r"
            metainfo.cmd ${outfile}
            echo -en "mb setting metadata ... mbprocessing \r"
            mbprocess -I${outfile}
      fi
}

function file_list () {
      echo creating datafile list ....
      ls -1 *.mb57 | awk ' { print $1, 57}'  > file57.mb-1
}

function new_dir () {
```

```
# creates a corresponding work-subdir to raw-dir
# initiates the datalist in the new subdir
# creates or appends this datalist to the workdir datalist of that subdir
# eg. (datalist_SO186_003.mb-1)
# creates or appends this to cruise-datalist in the workdir.
if [ ! -d $raw_dir/$subdir ]; then
                        echo " Alert: $subdir does not exist in RAW Dir
$raw_dir"
                        exit
            else
                  echo "Working on files in ==> $raw_dir/$subdir"
            fi
            if [ -d $work_dir/$subdir ]; then
                  echo "Appending  files in ==> $work_dir/$subdir"
            else
                  mkdir -pv $work_dir/$subdir
                  lastreturn=$?
                        if [ $lastreturn -gt 0 ] ; then
                              echo " Alert: could not create
$work_dir/$subdir !! exit $lastreturn"
                              exit
                        fi
                        echo "Writing    files in ==> $work_dir/$subdir"
                        make_datalist $work_dir/$subdir
                  fi
                  echo "${subdir}/datalist.mb-1"  >
$work_dir/datalist_${subdir}.mb-1
                  echo "datalist_${subdir}.mb-1"  >> $work_dir/datalist.mb-
1
}

function data_list () {
      echo executing datalist in dir ....
      mbdatalist -N -I $1
}


function SVP_out () {
      echo getting sound velocities ....
      mbsvplist -F-1 -I$1 -O

}


function make_datalist () {
datalistfile=${1}/datalist.mb-1
if [ ! -s $datalistfile ]
      then
            echo '$PROCESSED' > $datalistfile
            echo "Created $datalistfile"
      fi
}


function plot {
datlist=$1
mbm_plot -I${datlist} -G2 -PA4  -MGDDEGREE_FORMAT/3 -V
cp -p ${datlist}.cmd temp.cmd_$$
sed '/PAPER_MEDIA/s/A4+/A4/g' temp.cmd_$$ > ${datlist}.cmd
rm -f temp.cmd_$$
${datlist}.cmd
}
```

```
############ main #################
#Check and prepare subdirs as needed

new_dir


cd $work_dir/$subdir

for ifile in ${raw_dir}/${subdir}/*.all
do
      reformat $ifile
done

cd $work_dir

echo "Plotting ..."
plot datalist_${subdir}.mb-1

exit
```

A6-2: Script for grid calculation of multibeam data: `process.cmd`

```
#!/bin/csh -f
#
if ( -f .hsdefaults ) then
  source .hsdefaults
else
  echo "cannot find your .hsdefaults file \!"
  exit
endif
#
############################################################
############################################################
#
# set your parameters here...
# ===========================
# choose grid size, clip radius, and the name of
# your datalist file
#
############################################################
############################################################
#
set datalist    = datalist_all.mb-1
#
set DX          =  150    # dx in m for grid calculation with mbgrid
set DY          =  150    # dy in m for grid calculation with mbgrid
set UNIT        =  meters # units for grid cells: meters | degrees
set DAT_TYP     =  2      # datatype                check man mbgrid!
set CLIP        =  4      # interpolation radius    check man mbgrid!
set MODE        =  1      # interpolation mode      check man mbgrid!
set GRDALG      =  1      # gridding algorithm      check man mbgrid!
set GRDKIND     =  3      # gridkind                check man mbgrid!
set SPEED       =  4      # minimum ship speed in km/h - data
                          # recorded at slower speed are ignored
#
############################################################
#
############################################################
#
############################################################
#
#
# Run mbgrid
  echo Running mbgrid...
#
#
mbgrid -I$datalist -O${F_NAME}_${DX}_${DY}_z \
       -A${DAT_TYP} -C${CLIP}/${MODE} \
       -F${GRDALG} -G${GRDKIND} -N \
       -R${REGION_GRID} -S$SPEED -E${DX}/${DY}/${UNIT}
#
#
############################################################
############################################################
#
# All done
echo All done...
```

A6-3: Script for plotting of digital terrain models: `fig_bathy.cmd`

```
#!/bin/csh -f
#
##############################################################
###
### maybe you want to change these gmtdefault values?
###
##############################################################
#
gmtdefaults -D > .gmtdefaults
gmtset PAPER_MEDIA A4
gmtset PAGE_ORIENTATION LANDSCAPE
gmtset PLOT_DEGREE_FORMAT ddd:mmF
gmtset D_FORMAT %4.0f
gmtset ANOT_FONT_SIZE   10
gmtset LABEL_FONT_SIZE  10
gmtset GRID_CROSS_SIZE 0
gmtset GRID_PEN 0
gmtset BASEMAP_TYPE PLAIN
gmtset COLOR_NAN 255/255/255
gmtset WANT_EURO_FONT TRUE
#
##############################################################
###
### source default values
###
##############################################################
#
if ( -f .hsdefaults ) then
  source .hsdefaults
else
  echo "cannot find your .hsdefaults file \!"
  exit
endif
#
if ( -f .constants ) then
  source .constants
else
  echo "cannot find your .constants file \!"
  exit
endif
#
if ( -f .projectdefaults ) then
  source .projectdefaults
else
  echo "cannot find your .projectdefaults file \!"
  echo "using default values\!"
  set ship      = "RV SONNE"
  set cruise    = "SO-xyz"
  set project   = "PROJECT"
  set institute = "IFM-GEOMAR"
  set operator  = "WW"
endif
#
##############################################################
###
### choose what your script should do:
### processing steps...
### ==================
### activate by uncommenting
###
```

```
############################################################
#
#set FIG_CAPT   = 1  # make figure caption
#set CONT_PLOT  = 1  # make contour plot
#set CLIP_MASK  = 1  # masking with psclip - polygon files needed
set IMG_PLOT   = 1  # make grdimage-plot
#set PROF_PLOT  = 1  # plot profile lines
#set NAV_PLOT   = 1  # plot navigation
#set STAT_PLOT  = 1  # plot stations
#set CORL_PLOT  = 1  # plot points/symbols
set CITIES     = 1  # plot and annotate cities
#set SCALE_BAR  = 1  # include scale bar
set COL_SCALE  = 1  # include color scale
#set TEXT_BOX   = 1  # plot a text box
#set STAMP      = 1  # print GMT timestamp with add. info
#set PRINT_PLOT = 1  # print <PRINT_PLOT> copies of the plot
#
############################################################
###
### check / change these parameters and switches
###
############################################################
#
# required for any plot:
#
set B_STRING  = f10ma1/f10ma1ESwn
set X_OFFS    = 3.0  # lower left corner ...
set Y_OFFS    = 3.9  # ... of plot
set COAST_RES = f    # choose one of f[ull], h[igh], l[ow], c[rude]
#
# required for figure caption:
#
set CAPT_TEXT = " - RV METEOR Cruise M67-1 Cruise Track"
#
# required for CONT- and IMG-PLOT
#
set GRID      = ${F_NAME}_150_150_z.grd
set BGRID     = topo_37-32_200_200_z.grd
set CONT_INT  = 1000
set ANT_INT   = 5000f4
set CONT_COL  = ${BLACK}
set ANT_COL   = ${RED}
set CONT_MIN  = -10000   # minimum and ...
set CONT_MAX  = -10      # ... maximum depth to be contoured
#
# required for IMG-PLOT
#
   set CPT_FILE  = tipteq_z.cpt   # color scale file
   # if you do not want illumination, comment the next line out!
   set ILU       = 300
#
if ( ${?CLIP_MASK} ) then
#
# required if CONT- or IMG-PLOT has to be clipped
#
  set CLIP_DIR = CLIPS
  set CLIPS    = clip_
#
endif
#
# required for optional profile-, nav-, station- ... plots:
# according file names with data
#
```

```
set PROF_FILE = survey_lines.xy
set NAV_FILE  = ../../margin_37-32/chileplanung_final.xy
set STAT_FILE = /data1/Chile/VidalGormaz/stations/mudvolcano.xy
set STAT_TXT  = ../stations/cities.txt
set CORL_FILE1 = box_1.xy
set CORL_FILE2 = box_2.xy
set NAME_FILE  = ../../stations/cities
#
# required if SCALE_BAR included
#
set SCALE_X_POS =  -74.00  # position of ...
set SCALE_Y_POS =  -33.90  # ... km scale bar
set REF_LAT     =  -33.0   # reference latitude
set SCALE_LEN   =   60     # length of scale bar in km
#
# required if TEXT_BLOCK
#
set TITLE     = "MULTIBEAM Survey"
set TB_X =  0.1    # lower left corner ...
set TB_Y =  0.1    # ... of text block
#
# required if print wanted
#
set PRINTER   = qms2425-a4-8d_213
#
############################################################
###
### do not change these statements
###
############################################################
#
set CMD = $0
set FIG_NR    = `echo $CMD | sed 's%.\/fig_%%g' | sed 's%.cmd%%g'`
set PS_FILE   = "fig_${FIG_NR}.ps"
set GRID_SIZE = `grdinfo ${GRID} | grep x_inc | awk '{print $7'}`
#if ( ${?CITIES} ) then
#  #
#  # plot and annotate cities
#  set NAME_FILE = `./plot_cities.cmd`
#endif
#
############################################################
#
# now start plotting ...
#
# ====================================================================
#
if ( ${?FIG_CAPT} ) then
#
echo figure caption...
pstext -Jx0.1 -R0/90/0/90 -G${BLACK} \
                                              -K -V << END > ${PS_FILE}
10  2 12 0  5 1  Figure ${FIG_NR}:
END
pstext -Jx -R -G${BLACK} \
                                           -O -K -V << END >> ${PS_FILE}
40  2 12 0  4 1  ${CAPT_TEXT}
END
#
# ====================================================================
#
#
#
```

```
echo Running psbasemap...
psbasemap -Jm${SCALE_A4} -R${PLOT_AREA} \
          -B${B_STRING}  -Y${Y_OFFS}    \
                                              -O -K -V >> ${PS_FILE}
#
# ===================================================================
#
else    # psbasemap call is different if figure caption is included
#
# ===================================================================
#
echo Running psbasemap...
psbasemap -Jm${SCALE_A4} -R${PLOT_AREA} \
          -B${B_STRING}  -X${X_OFFS} -Y${Y_OFFS} \
                                                -K -V >  ${PS_FILE}
#
endif
#
# ===================================================================
#
if ( ${?CLIP_MASK} ) then
   #
   # Activate clipping path...
   echo Running psclip...
   psclip ${CLIP_DIR}/${CLIPS}*.b  \
           -bi  -Jm${SCALE_A4} -R${REGION} -N \
                                            -O  -K -V >>  ${PS_FILE}
endif
#
# ===================================================================
#
if ( ${?IMG_PLOT} ) then
  #
  if ( ${?ILU} ) then
  #
  # Make grdimage plot with illumination
  #
  # Get shading array
  #
    if  !( -f ilum${ILU}_${GRID} ) then
      echo Getting shading array...
      echo Running grdgradient...
      grdgradient ${GRID} -A${ILU} -G${F_NAME}.grad  -N -M
      echo Running grdhisteq...
      grdhisteq ${F_NAME}.grad -G${F_NAME}.eq -N
      echo Running grdmath...
      grdmath ${F_NAME}.eq  0.4  MUL = ilum${ILU}_${GRID}
      echo Deleting surplus files...
      /bin/rm -f ${F_NAME}.grad ${F_NAME}.eq
    endif
  #
    echo Running grdimage with illumination ...
    grdimage ${GRID} -Jm${SCALE_A4} -R${REGION} \
       -C${CPT_FILE} -Iilum${ILU}_${GRID} \
                                              -O -K -V >>  ${PS_FILE}
  else
  #
    echo Running grdimage without illumination ...
    grdimage ${GRID} -Jm${SCALE_A4} -R${REGION} \
       -C${CPT_FILE}  \
                                              -O -K -V >>  ${PS_FILE}

  endif
```

```
  #
endif
#
# ====================================================================
#
if ( ${?CONT_PLOT} ) then
#
  # Make contour map
  echo Running grdcontour...
  grdcontour ${GRID} -Jm${SCALE_A4} \
    -R${REGION} -C${CONT_INT}  -A${ANT_INT} -Q20 \
       -T   -Wa1/${ANT_COL} -Wc0/${CONT_COL} \
       -L${CONT_MIN}/${CONT_MAX} \
                                              -O  -K -V >>  ${PS_FILE}
#
endif
#
# ====================================================================
#
if ( ${?CLIP_MASK} ) then
  #
  # De-activate clipping path...
  echo Running psclip...
  psclip -C                                  -O  -K -V >>  ${PS_FILE}
  #
endif
#
# ====================================================================
#
if ( ${?PROF_PLOT} ) then
#
# Plot profile lines...
#
   echo plot track lines ...
   psxy ${PROF_FILE} -R -Jm  -M \
     -W3                      -O -K -V >> ${PS_FILE}
#
endif
#
# ====================================================================
#
if ( ${?NAV_PLOT} ) then
#
#
# Plot DVS navigation on top...
#
   psxy ${NAV_FILE} -R -Jm   \
     -W2/${RED}               -O -K -V  >> ${PS_FILE}
#
#
endif
#
# ====================================================================
#
if ( ${?STAT_PLOT} ) then
#
# Plot  stations...
#
   echo plot stations ...
   #
   set TITLE = "station positions"
   #
```

```
   psxy ${STAT_FILE} -R -Jm  -G${RED} \
            -W1/${BLACK}  -Sc0.2    -O -K -V  >> ${PS_FILE}
#
#   pstext ${STAT_TXT} -Jm -R -G${BLACK} \
#                                    -O -K -V  >> ${PS_FILE}
#
endif
#
# ================================================================
#
echo plot  land topography ...
#
pscoast -R${PLOT_AREA} -Jm -D${COAST_RES} \
        -B${B_STRING}  -Gc          -O -K -V >> ${PS_FILE}
#
# Make grdimage plot with illumination
#
# Get shading array
#
    if  !( -f ilum${ILU}_${BGRID} ) then
      echo Getting shading array...
      echo Running grdgradient...
      grdgradient ${BGRID} -A${ILU} -G${F_NAME}.grad  -N -M
      echo Running grdhisteq...
      grdhisteq ${F_NAME}.grad -G${F_NAME}.eq -N
      echo Running grdmath...
      grdmath ${F_NAME}.eq  0.35  MUL = ilum${ILU}_${BGRID}
      echo Deleting surplus files...
      /bin/rm -f ${F_NAME}.grad ${F_NAME}.eq
    endif
#
 echo Running grdimage with illumination ...
 grdimage ${BGRID} -Jm -R${REGION} \
       -C${CPT_FILE} -Iilum${ILU}_${BGRID} \
                                          -O -K -V >>  ${PS_FILE}
#
pscoast -Q -O -K -V >>  ${PS_FILE}
#
pscoast -R${PLOT_AREA} -Jm -D${COAST_RES} \
        -W1/${BLUE} \
        -Ia/2,${BLUE},solid  -N1/2/255/0/0:0t15_10_2_10:0       \
        -Lf${SCALE_X_POS}/${SCALE_Y_POS}/${REF_LAT}/${SCALE_LEN} \
        -B${B_STRING}            -O -K -V >> ${PS_FILE}
#
#
# ================================================================
#
if ( ${?CITIES} ) then
#
# include geographic names...
#
   echo "include geographic names ..."
   #
   psxy ${NAME_FILE}.xy        \
        -R      \
        -Jm     \
        -Ss0.2 -G${BLACK}                 -O -K -V  >> ${PS_FILE}
   #
#   /bin/rm ${NAME_FILE}.xy
   #
```

```
   pstext  ${NAME_FILE}.txt     \
        -R      \
        -Jm     \
        -W${WHITE} -G${BLACK}              -O -K -V  >> ${PS_FILE}
   #
#   /bin/rm ${NAME_FILE}.txt
#
endif
#
# ====================================================================
#
if ( ${?CORL_PLOT} ) then
#
# Plot  points of interest...
#
   echo plot  points ...
   #
   set TITLE = "points of interest"
   #
   psxy ${CORL_FILE1} -R -Jm    \
       -W3/${RED}                  -O -K -V  >> ${PS_FILE}
   psxy ${CORL_FILE2} -R -Jm    \
       -W3/${RED}                  -O -K -V  >> ${PS_FILE}
#
endif
#
# ====================================================================
#
if ( ${?COL_SCALE} ) then
#
gmtset ANOT_FONT_SIZE    6
gmtset LABEL_FONT_SIZE   8
#
psscale -D0.2c/4.0c/7.5c/0.5c -B:meter: -C${CPT_FILE} -L \
                                          -O -K -V  >> ${PS_FILE}
#
gmtset ANOT_FONT_SIZE   10
gmtset LABEL_FONT_SIZE  10
#
endif
#
# ====================================================================
#
# Plot text box ...
#
if ( ${?TEXT_BOX} ) then
echo plot textbox...
#
pstext -Jx0.1 -R0/90/0/40 -G${BLACK} \
       -X${TB_X} -Y${TB_Y}   \
       -C0.001   -W          -O -K -V << END >> ${PS_FILE}
1.00    7.0 10 0 31 1  ${ship} ${cruise}
1.00    5.5  8 0  0 1  ${F_NAME}
1.00    4.0  8 0  0 1  ${project} ${TITLE}
1.00    2.5  8 0  0 1  Mercator WGS84 ${SCALE_A4}
1.00    1.0  8 0  0 1  contour interval ${CONT_INT} m
END
echo textbox done...
#
endif
#
# ====================================================================
#
```

```
if ( ${?STAMP} ) then
#
  pstext -Jm${SCALE_A4} -R${PLOT_AREA} -G${BLACK} \
       -U"${CMD} / $institute / produced by $operator" \
                            -O    -V << END >> ${PS_FILE}
END
#
else
#
# ================================================================
#
  pstext -Jm${SCALE_A4} -R${PLOT_AREA} -G${BLACK} \
                            -O    -V << END >> ${PS_FILE}
END
#
endif
#
# ================================================================
#
if ( ${?PRINT_PLOT} ) then
#
# Print one copy...
#
  while ($PRINT_PLOT)
    #
    @ PRINT_PLOT --
    echo printing a copy on ${PRINTER} ...
    lp -d${PRINTER} ${PS_FILE}
    sleep 10
  end
#
endif
#
# All done
echo All done...
```

A6-4.1: ancillary files: `.hsdefaults`

```
set F_NAME = Area_1
set REGION      = -74.70/-71.00/-34.00/-32.00
set REGION_GRID = -74.70/-71.00/-34.00/-32.00
set PLOT_AREA   = -74.70/-71.00/-34.00/-32.00
set SCALE_A4    = -73.0/-34.0/1:1500000
set SCALE_A3    =
set SCALE_A0    = -73.0/-34.0/1:300000
```

A6-4.2: ancillary files: `.projectdefaults`

```
set ship      = "RV METEOR"
set cruise    = "M67-1"
set project   = "CHILE-MARGIN-SURVEY"
set institute = "IFM-GEOMAR"
set operator  = "WW"
```

A6-4.3: ancillary files: `.constants`

```
set WHITE     = 255/255/255
set BLACK     = 0/0/0
set RED       = 255/0/0
set GREEN     = 0/255/0
set BLUE      = 0/0/255
set GREY      = 150/150/150
set LIGHTGREY = 200/200/200
set DARKGREY  = 120/120/120
set LAND_COL  = 200/150/100
```